Proyecto Fin de Carrera
Ingeniería Aeroespacial

Numerical study of one-dimensional unsteady radiation problems with applications to the thermal structure of planetary lower atmospheres

Autor: Adrián Carriba Merino

Tutor: Miguel Pérez-Saborid Sánchez-Pastor

Dpto. Ingeniería Aeroespacial y Mecánica de Fluidos
Escuela Técnica Superior de Ingeniería
Universidad de Sevilla

Sevilla, 2019

Proyecto Fin de Carrera
Ingeniería Aeroespacial

Numerical study of one-dimensional unsteady radiation problems with applications to the thermal structure of planetary lower atmospheres

Autor:

Adrián Carriba Merino

Tutor:

Miguel Pérez-Saborid Sánchez-Pastor

Profesor titular

Dpto. de Ingeniería Aeroespacial y Mecánica de Fluidos

Escuela Técnica Superior de Ingeniería

Universidad de Sevilla

Sevilla, 2019

Proyecto Fin de Carrera: Numerical study of one-dimensional unsteady radiation problems with applications to the thermal structure of planetary lower atmospheres

Autor: Adrián Carriba Merino

Tutor: Miguel Pérez-Saborid Sánchez-Pastor

El tribunal nombrado para juzgar el Proyecto arriba indicado, compuesto por los siguientes miembros:

Presidente:

Vocales:

Secretario:

Acuerdan otorgarle la calificación de:

Sevilla, 2019

Agradecimientos

En primer lugar, me gustaría agradecer a mis padres todo lo que han hecho por mí, así como el apoyo recibido durante estos años, que han permitido que este trabajo sea posible. También a mi hermano pequeño que me anima siempre que lo necesito.

Por otro lado, agradecer también a mis amigos, especialmente a Penélope Asuero Llanes, Pablo Nogales Criado, Alejandro Ortega Fernández y Narciso Amador Sánchez todas las horas que hemos pasado juntos y que me han permitido seguir siempre adelante, así como a mis compañeros de ARUS, en especial al departamento de chasis por tantos buenos momentos.

Finalmente, acordarme de todos aquellos profesores a los que les estoy tan agradecido por haberme ayudado a completar este camino, y que me han ayudado a crecer no solo profesionalmente, sino también como persona. Particularmente a Miguel Pérez-Saborid Sánchez-Pastor por acogerme para este trabajo de fin de grado y ayudarme siempre que ha estado en su mano.

Muchas gracias a todos.

Adrián Carriba Merino

Ingeniería Aeroespacial

Sevilla, 2019

Abstract

This document will be concerned with the study of the radiation as a mechanism of energy transfer. Several unsteady, one-dimensional problems will be described, focusing in radiation atmospheric problems.

The governing equations are derived taking as theoretical base the general principles of the physics of radiation. In addition, a simplified, one-dimensional model of the atmosphere is described.

The governing equations are written in an appropriate form in order to solve them by a numerical collocation method which is based on a finite difference discretization of the non-linear algebraic-integro-differential unsteady radiation equations. The resulting non-linear set of algebraic equations are solved using a Newton-Raphson's method which yields the temperature field within the domain at each instant of time. The method is verified by comparing the results obtained with those of the literature.

Finally, implementation of the atmospheric model in the numerical method is checked and validated. The method is then used to study the evolution and steady state of different kinds of atmospheres. Lastly, to have a complete model of the energy transfer, convection is included and, again results for different atmospheres are calculated.

Índice

ÍNDICE DE FIGURAS

1 INTRODUCTION TO RADIATION PHYSICS

1.1. Fundamentals of thermal radiation and its applications

Every piece of matter whose temperature is greater than absolute zero emits electromagnetic energy which propagates away from it in all directions at the speed of light. This energy, when due only to the temperature of the body, is called thermal radiation. It has its origin in the rapidly varying electric and magnetic fields created by the accelerations and, in general, transitions between quantum energy levels of the body's atomic charges (electrons and protons) due to their thermal motion. A body can not only emit thermal radiation, but also absorb, scatter (deflect without absorption) or transmit that coming from other bodies. When the atomic charges absorb radiation, they tend to increase the thermal energy of the body, and it is an experimental fact that an isolated system of bodies exchanging thermal radiation eventually reach the same temperature. Observe that, because of its electromagnetic nature, radiation permits the transfer of thermal energy between two bodies at different temperatures to take place through vacuum, which is a feature that distinguish thermal radiation from thermal conduction and thermal convection, since the latter require the presence of a material medium to occur.

Electromagnetic energy can be considered to be transported by waves obeying Maxwell's equations or, from the quantum point of view, by photons. In accordance with the wave-particle duality principle of quantum mechanics, each electromagnetic wave has an associated photon. The wave and its photon travel at the speed of light, c, and are characterized by their frequency, ν. Their corresponding wavelength is defined as

$$\lambda = \frac{c}{\nu} \tag{1.1}$$

and, according to Quantum Mechanics, the energy of the photon is

$$\epsilon_\nu = h\nu = h\frac{c}{\lambda} \tag{1.2}$$

where $h = 6.627e \cdot 10^{-34}$ is the Planck's constant. Therefore, radiation can be characterized either by ν or λ, although ν has the advantage that does not change when radiation travels from a medium to another. The speed of light c and the wavelength within a given medium are related to those in vacuum, c_0 and$\lambda_0 = c_0/\nu$, by

$$c = \frac{c_0}{n} \quad and \quad \lambda = \frac{\lambda_0}{n} \tag{1.3}$$

where n is the index of refraction. In what follows radiation will be characterized by c and λ and from the photon point of view.

Thermal radiation is a volumetric phenomenon, although for bodies called *opaque* is often conveniently treated as a surface phenomenon. This is due to the fact that most photons emitted by the body are reabsorbed within its interior except those emitted in a very narrow layer adjacent to its surface, while photons received by the body are absorbed or scattered (reflected) in that layer before penetrating deep into the interior[1]. However, some other materials, such as glass, water or radiating gases, allow radiation to travel a considerable distance within them and are called *semitransparent*, or *participative*, media. Due to the random character of the thermal motions of the atomic charges within its volume, a body emits radiation by sending photons across each element of its surface with a wide range of wavelengths and traveling in all directions within the hemispherical space above the element. Therefore, the thermal radiation leaving the body through each unit surface area has both a spectral distribution and a directional distribution. If the number of photons of a given wavelength crossing per unit time a given surface element is independent of direction, the thermal radiation through that element is called *diffuse*. Some elementary aspects of the spectral distribution will be next considered, leaving a more complete characterization of the radiant energy for later in this chapter.

Consider an element of the surface of a radiating body. The amount of radiation that crosses the element's unit area per unit time within a wavelength interval $d\lambda$ and integrated over all directions within the hemisphere above the element will be denoted by $E_\lambda d\lambda$[2]. The quantity E_λ is called the *spectral (or monochromatic) emissive power* of the body through the surface element. It depends on λ, the temperature and the radiative properties of the body sufficiently near its surface[3], as well as of the index of refraction of the bounding medium[4]. The body emissive power is obtained by integrating E_λ over the whole range of walenghts as

$$E = \int_0^\infty E_\lambda \, d\lambda \tag{1.4}$$

and the emissive power in the wavelength range between λ_1 and λ_2 is given by

$$E_{\lambda_1-\lambda_2} = \int_{\lambda_1}^{\lambda_2} E_\lambda \, d\lambda \tag{1.5}$$

For a body with uniform both temperature and superficial properties and emitting to a bounding medium whose index of refraction is also uniform, the spectral emissive power is constant on the surface, and the total emitted power in a wavelength interval $d\lambda$ is $E_\lambda A$, where A is the body's surface area.

An idea of how E_λ depends on λ and the temperature for a given body can be gotten by considering the so-called *black body radiation*. A black body is an idealized opaque body that absorbs all incident radiation and emits diffusely the maximum amount of radiant power per unit surface area at a given surface temperature medium and to a given bounding[5]. The existence of black body radiation can be demonstrated by application

---

[1] The thickness of this layer is usually a few microns. This is why applying very thin coating layers on the surface of a body can change so much its radiation characteristics

[2] In this section, quantities subscripted by λ are meant to be integrated over all directions within the hemisphere above a surface element. They are also known in the literature as *hemispherical* quantities.

[3] This statement must be taken with caution. As previously mentioned, for bodies which can be considered as opaque the term "sufficiently near" usually means a very thin layer adjacent to the surface, but for a participative, or semitransparent, medium, the emissive power generally depends on the temperature distribution and the properties of the whole body. In general, the opaque or semitransparent behavior of a body may depend on the wavelength of radiation. In fact, water and glass are semitransparent to visible radiation while practically opaque to infrared radiation.

[4] For most applications the index of refraction can be taken as $n = 1$, corresponding to vacuum and low density gases such as ordinary air, but there are some other common media for which the value of n differs appreciably from unity, such as glass ($n = 1.5$) and water ($n = 1.33$).

[5] An approximate realization of a black body is a cavity with a small hole in its wall. Photons incident on the hole are absorbed or scattered (reflected) many times at the internal surfaces and they are unlikely to reemerge, so that the cavity acts as a nearly perfect absorber (this is what makes it difficult to see the interior a cave from the outside). Also, photons reaching the hole from the interior will be equally likely to arrive in any direction, making the radiation through the hole to be emitted diffusely

of the second law of thermodynamics and, using quantum statistics arguments, Planck calculated the spectral emissive power of a black body whose surface is at an absolute temperature T emitting radiation of wavelength lambda to a medium whose index of refraction equals unity as

$$E_{b\lambda} = \frac{2\pi hc^2}{\lambda^5[e^{hc/(k\lambda T)} - 1]} \tag{1.6}$$

where $k = 1.38 \cdot 10^{-23}\ J/K$ is the Boltzmann's constant. Note that, since it has been assumed $n = 1$, this expression is appropriate if the body's bounding medium is vacuum or a low density gas (i.e. ordinary air). For other mediums, such as glasses or liquids, this equation should be modified by replacing c by c_0/n and, if the index of refraction depends of the wavelength, by multiplying it by the factor $(1 + \lambda/n \cdot dn/d\lambda)$. For simplicity, in the rest of this work only the case $n = 1$ will be considered.

Figure 1 shows the spectral emissive power as a function of the wavelength for black bodies at different temperatures. Observe that the emitted radiation at a given wavelength increases with the body's temperature, while for a given temperature it presents a maximum at a certain wavelength, λ_m, and decays for wavelengths which are either large or small compared to λ_m. The dominant wavelength decreases with the absolute temperature in accordance to the Wien's displacement law

$$\lambda_m = \frac{2897.8}{T}\ \mu m \tag{1.7}$$

This law explains, for example, why when a metallic body is heated its surface color changes gradually from dull red to orange to yellow and eventually to white. It can be seen in Figure 1 that the maximun spectral emissive power of the solar radiation occurs at $\lambda_m = 0.5\ \mu m$, which is about the middle of the visible range $(0.4\ \mu m < \lambda < 0.8\ \mu m)$, while the peak of the radiation emitted by the earth - at an ambient temperature of about $300\ K$- takes place at $\lambda_m = 9.7\ \mu m$, which is well in the infrared region of the spectrum $(0.8\ \mu m < \lambda < 100\ \mu m)$.

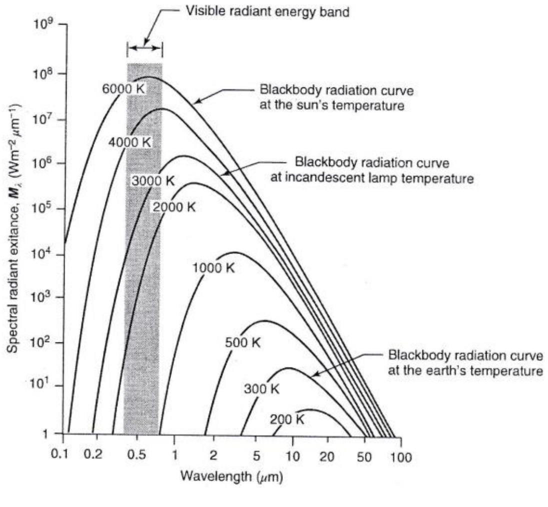

Figure 1: Blackbody spectral emissive power. Taken from [Lillesand et al. (2008)]

The total emissive power of a black body whose surface is at a given temperature T is obtained by inserting (1.6) into (1.4), which yields the Stefan-Boltzmann law

$$E_b = \sigma T^4 \tag{1.8}$$

where $\sigma = 2\pi^5 k^4/(15h^3c^2) = 5.67 \cdot 10^{-8}\ W/(m^2K^4)$ is the Stefan-Boltmann constant. From the Stefan-Boltzmann law can be inferred the strong, non-linear dependence of a body's radiated power on its temperature. By using an approximate value of $T = 6000\ K$ for the temperature of the solar surface, (1.8) yields the value $E_b = 7.35 \cdot 10^6\ W/m^2$ for the Sun's emissive power. The fractions of the emissive power in the visible, infrared and ultraviolet $(0 < \lambda < 0.4\ \mu m)$ can be found by substituting in equation (1.5) the corresponding wavelength ranges, resulting around 43%, 54% and 4% respectively.

Real bodies are not perfectly black and, therefore, their spectral emissive power is only a fraction of that of a black body at the same temperature. The emission of radiation by a real surface is characterized by its *spectral emissivity*, $\varepsilon_\lambda\ (T)$, which defined as the ratio of the spectral emissive power of the real surface at a given temperature to that of a black body at the same temperature. Therefore, the emissive power of a real surface can be expressed as

$$E_\lambda(T) = \varepsilon_\lambda(T) E_{b\lambda}(T) \tag{1.9}$$

where, for surfaces of different materials, $\varepsilon_\lambda\ (T) \leq 1$ must be determined experimentally. The *total emissivity* is defined as the ratio of the emissive power of the real body to that of a black body at the same temperature,

$$\varepsilon(T) = \frac{E(T)}{E_b(T)} = \frac{\int_0^\infty \varepsilon(T) E_{b\lambda}(T)}{\sigma T^4} \tag{1.10}$$

which, as $\varepsilon_\lambda(T)$, is also a property of the material. According to Kirchoff's law, if H_λ denotes the total power falling on a surface element of an opaque body per unit area and unit wavelength, which is called *spectral irradiance*, the surface element must absorb a fraction $\varepsilon_\lambda(T)H_\lambda$ and reflect the remaining $[1 - \varepsilon_\lambda(T)]H_\lambda$. The total radiant power per unit area and wavelength emanating from the surface element is, therefore,

$$B_\lambda = \varepsilon_\lambda(T) E_{b\lambda}(T) + [1 - \varepsilon_\lambda(T)] H_\lambda \tag{1.11}$$

a quantity which is defined as the *spectral radiosity* of the surface element. A body whose radiative properties can be considered to be independent of the wavelength is called *gray*. Thus, for a gray surface element of an opaque body one has that $\varepsilon_\lambda(T) = \varepsilon(T)$, and (1.11) can be integrated over the wavelength to yield

$$B = \varepsilon(T)\sigma T^4 + [1 - \varepsilon(T)] H \tag{1.12}$$

where $B = \int_0^\infty B_\lambda\, d\lambda$ and $H = \int_0^\infty H_\lambda\, d\lambda$ are the (total) radiosity y (total) irradiance, respectively. The relation (12) can be pictorially represented as in Figure 2.

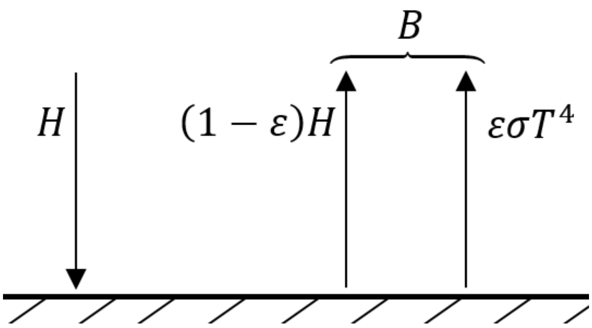

Figure 2: Pictorial representation of equation (1.12) for a Surface element.

Thermal radiation is present in numerous engineering and natural phenomena. Of special interest in this work is the study of radiation in participating media - that is, that which takes place in nontransparent media, such as gases, that can absorb, emit and scatter radiation throughout their interiors. As will be shown in the next section, the mathematical treatment of these phenomena is inherently complicated since emission, absorption and scattering of radiation occur at every point within the medium - not just near the system boundaries - and, in addition, these processes generally show very marked both directional and spectral dependencies. Therefore, the solution of the problem requires the knowledge of the temperature (from which radiant energy depends in strongly nonlinear way) and the physical properties at every point within the medium. This yields a spectral and directional dependent, nonlinear, system of integro-diferential equations whose solution is often worked out in the literature with the use of sensible approximations. A common, and often drastic, approximation - which will also be extensively employed in this work- is to assume a gray medium and use radiative properties conveniently averaged over the wavelength.

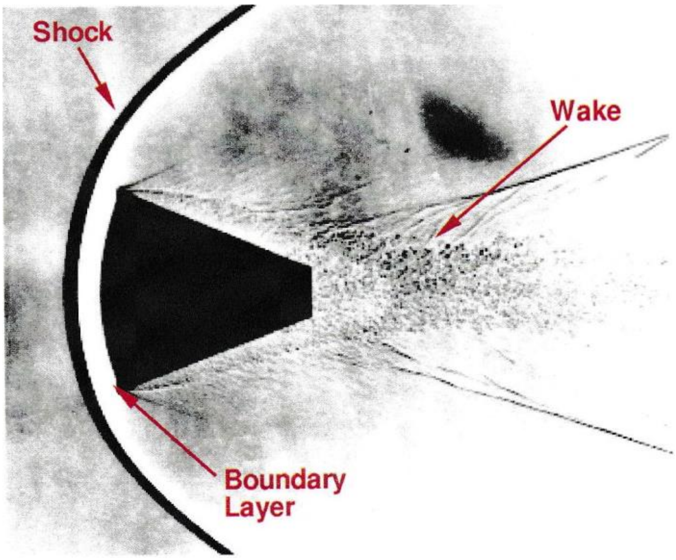

Figure 3: Hypersonic shock and boundary layers.

Important engineering applications of radiative heat transfer in participative media appear in the areas of combustion in furnaces and engine combustion chambers, where the temperatures can reach a few thousand degrees and the emission and absorption of radiation by the products of combustion - essentially carbon dioxide and water vapor- play an important role carrying the heat liberated by the combustion of the fuel to the chamber walls. Another interesting phenomenon in which thermal radiation in a participative medium plays a very important role is in the hypersonic shock layers formed during the atmospheric reentry of spatial vehicles (see Figure 3), where radiation is a very efficient mechanism in the transferring of the high thermal energy originated in the shock to the vehicle's surface which, therefore, must be protected by a radiation shield.

In nature, thermal radiation plays a great role in the structure of stellar interiors such as that of the Sun (Figure 4), where the thermal energy generated by the fusion of hydrogen in the solar core is transported outwards solely by radiation up to the convection zone, which is a convectively unstable envelope of about one third of the solar radius where the energy transport takes place by both radiation and turbulent convection.

Figure 4: Schematics of the solar interior.

Finally, another important application of thermal radiation in nature, and to which an important part of this work will be devoted, is the analysis of the global-mean thermal structure of the Earth's atmosphere. The ultimate source of all atmospheric phenomena is the solar radiant energy absorbed by the Earth's surface. As schematized in Figure 5, the global averaged amount of SW solar radiation reaching the top of the atmosphere ($341\ W/m^2$) is partly absorbed by the Earth's surface and atmosphere (due to clouds, H_2O, O_3 and aerosols) and partly reflected and scattered by the Earth's surface, clouds and air.

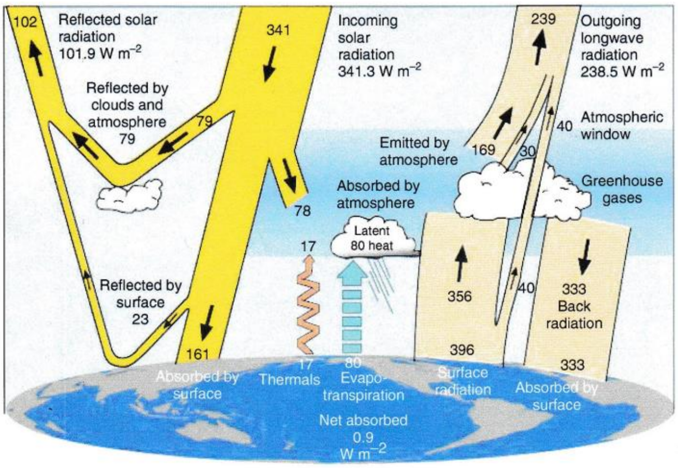

Figure 5: Schematics of the Earth's atmospheric energy budget.

For times long compared to those taken by the redistributions of the latent heat - which enters the atmosphere due to evaporation - and of the kinetic energy of the atmospheric motions, the atmosphere shows a state thermal quasi-equilibrium in a global-mean sense. This requires (see Figure 5) that the global averaged amount of SW radiant energy absorbed by the Earth's surface and atmosphere $(161 + 78 = 239\ W/m^2)$ must be equal to that of LW energy $(189 + 40 + 10 = 239\ W/m^2)$ that they emit to outer space. Observe that the Earth's surface emits $396\ W/m^2$ of LW radiation -as can be estimated from (1.8) assuming that it emits as a blackbody with a global-mean surface temperature of 288 K-, but only $40\ W/m^2$ pass directly to outer space through the atmospheric window. The rest ($356\ W/m^2$) is absorbed by the atmosphere ($108\ W/m^2$ by clouds and $248\ W/m^2$ by the greenhouse gases, mainly by water vapor and, to a lesser extent, by CO_2). The atmosphere emits 199 W/m^2 to outer space (74 W/m^2 emitted by clouds and 125 W/m^2 emitted by water vapor and other minor constituents) and 333 W/m^2 of LW radiation to the Earth's surface. The latter constitutes the well known *greenhouse effect*, which maintains the Earth's global-mean surface temperature at 288 K, well above the value 254 K which would have in the absence of clouds and greenhouse gases (mainly water vapor). The role of the greenhouse effect in determining the global-mean atmospheric thermal structure will be considered more fully in Section 1.3 and in Chapter 3.

1.2. Description of the radiation field: radiant intensity and the equation of radiative transfer

As stated in the previous section, the radiation field possesses both a spectral and a directional distribution. Thus, a complete description of the thermal radiation field requires to specify at each point of space the number of photons per unit volume, wavelength and solid angle and to establish the law that governs the changes of this quantity changes in space and time. In this section the radiant intensity will be first defined, and the radiative heat flux vector field expressed in terms of it. Next, the so-called radiative transfer equation for the radiant intensity will be formulated.

1.2.1 Radiant intensity

Consider the volume element dV around the point $\boldsymbol{r}$ shown in Figure 6. Let $n_P(\boldsymbol{r},t)$ be the number of photons per unit of volume at $\boldsymbol{r}$ at time t and $f(r,t,\lambda,\boldsymbol{n})$ the fraction of that number whose wavelengths are contained within a unit interval around λ and whose directions are contained within a unit solid angle around direction defined by the unit vector $\hat{s}(\theta,\phi)$, where θ and ϕ are the angular spherical coordinates shown in Figure 6. Then, the numbers of photons in dV with wavelengths in the interval $(\lambda,\lambda+d\lambda)$ and whose directions are contained within the solid angle $d\Omega = sin\theta d\theta d\phi$ around $\hat{s}$- such as the directions of the two photons schematized in Figure 6- is given by

$$n_P(\boldsymbol{r},\boldsymbol{t})\, f(\boldsymbol{r},t,\lambda,\hat{s})\, d\lambda\, d\Omega\, dV \tag{1.13}$$

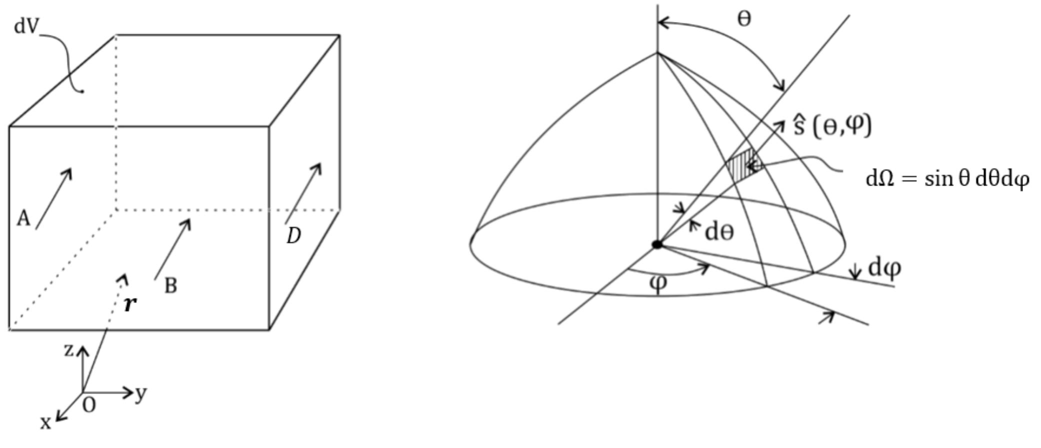

Figure 6: Schematics of a volume element dV around a point $\boldsymbol{r}$ (left) showing photons A, B and C whose directions are contained within the solid angle $d\Omega = \sin\theta\, d\varphi\, d\theta$ around the unit vector $\hat{s}(\theta,\varphi)$ (right).

Consider next the energy carried by photons crossing a surface element of area dA and unit normal $\boldsymbol{n}$ around the point $\boldsymbol{r}$. It is clear from Figure 7 that the photons with wavelengths in the interval $(\lambda,\lambda+d\lambda)$ and directions within the solid angle $d\Omega$ around $\hat{s}$ that cross the element in a small time dt are, to first approximation, contained in the oblique prism of volume $cdtcos\theta dA$, where θ is the angle between $\hat{s}$ and $\boldsymbol{n}$. This number can be obtained by simply replacing dV by the prism's volume as

$$cn_P(\boldsymbol{r},t)f(\boldsymbol{r},t,\lambda,\hat{s})\cos\theta\, dA\, d\lambda\, d\Omega\, dt \tag{1.14}$$

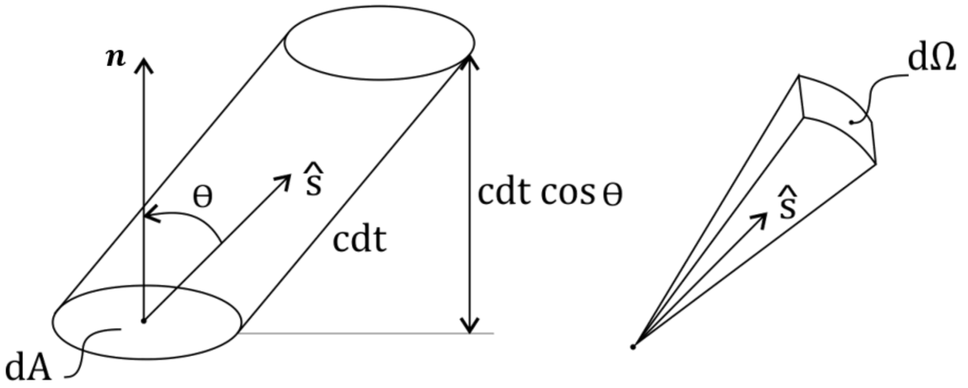

Figure 7: Photons crossing during a time interval dt a surface element dA (left) with directions contained with the solid angle $d\Omega$ around the unit vector $\hat{s}$ (right) are, to first approximation, contained in an oblique cylinder of base dA, generatrix parallel to $\hat{s}$ and volume $cdt\ cos\ \theta$.

The radiant energy that crosses the surface element per unit time due to photons with wavelengths in the interval $(\lambda, \lambda + d\lambda)$ and directions within the solid angle $d\Omega$ around $\hat{s}$ follows by multiplying (1.14) by hc/λ and dividing the result by dt as

$$\frac{hc^2}{\lambda} n_P(\boldsymbol{r},t)f(\boldsymbol{r},t,\lambda,\hat{s})\cos\theta\, dA\, d\lambda\, d\Omega \tag{1.15}$$

In thermal radiation studies, the *spectral radiant intensity*, defined as

$$I_\lambda(\boldsymbol{r},t,\hat{s}) \equiv \frac{hc^2}{\lambda} n_P(\boldsymbol{r},t)f(\boldsymbol{r},t,\lambda,\hat{s}) \tag{1.16}$$

is taken as the fundamental quantity to describe the radiation field. As can be inferred from (1.15) and (1.16) the spectral radiant intensity represents the radiant energy in the direction $\hat{s}$ that crosses per unit time, unit wavelength and unit solid angle the unit surface normal to $\hat{s}$. The *radiant intensity* is obtained by integrating the spectral radiant intensity over the wavelength as

$$I_\lambda(\boldsymbol{r},t,\hat{s}) = \int_0^\infty I_\lambda(\boldsymbol{r},t,\hat{s})\, d\lambda \tag{1.17}$$

Photons crossing an infinitely small surface element dA whose directions are within an infinitesimal solid angle $d\Omega$ around a unit vector $\hat{s}$ (see Figure 7) constitute what is called a *ray* in the direction $\hat{s}$ through dA. Pictorically, a ray of photons of wavelength λ through a surface element and its associated energy transport is usually represented in the literature as in Figure 8. On using (1.16) in (1.15), the radiant heat flux per unit wavelength, or *spectral radiant heat flux*, through dA is obtained in term of the spectral radiant intensity by integrating over the unit sphere centered at $\boldsymbol{r}$ as

$$dQ_{R\lambda}(\boldsymbol{r},t) = dA \int_{4\pi} \cos\theta \, I_\lambda(\boldsymbol{r},t,\hat{s}) \, d\Omega = dA \, \boldsymbol{n} \cdot \boldsymbol{q}_{R\lambda}(\boldsymbol{r},t) \tag{1.18}$$

where has been taken into account that $\cos\theta = \boldsymbol{n} \cdot \hat{s}$ and *spectral radiative heat flux density vector*, has been defined as

$$\boldsymbol{q}_{R\lambda}(\boldsymbol{r},t) = \int_{4\pi} \hat{s} \, I_\lambda(\boldsymbol{r},t,\hat{s}) \, d\Omega \tag{1.19}$$

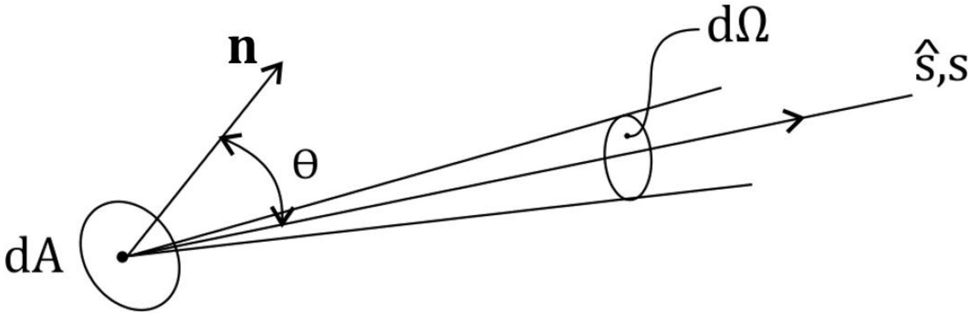

Figure 8: Schematic representation of a ray in the direction represented by the unit vector $\hat{s}$ through a surface element of unit normal $\boldsymbol{n}$. The path length along the ray is denoted by s.

The *radiative heat flux vector* field is obtained in term of the radiant intensity by integrating (1.19) over the wavelength as

$$\boldsymbol{q}_R(\boldsymbol{r},t) = \int_{4\pi} \hat{s} \, I(\boldsymbol{r},t,\hat{s}) \, d\Omega \tag{1.20}$$

Observe that, on integrating (1.18) over the wavelength, the total radiant heat flux through any surface element centererd at $\boldsymbol{r}$ of unit normal $\boldsymbol{n}$ is obtained from the field $\boldsymbol{q}_R(\boldsymbol{r},t)$ as

$$dQ_R(\boldsymbol{r},t) = dA \, \boldsymbol{n} \cdot \boldsymbol{q}_R(\boldsymbol{r},t) \tag{1.21}$$

Also, by integrating (1.21) over the surface of small volume element dV centered at $\boldsymbol{r}$ and applying Gauss's theorem, the radiant heat leaving the unit volume located at $\boldsymbol{r}$ per unit time can be obtained as

$$\nabla \cdot \boldsymbol{q}_R(\boldsymbol{r},t) = \int_{4\pi} \hat{s} \cdot \nabla I(\boldsymbol{r},t,\hat{s}) \, d\Omega \tag{1.22}$$

which is the quantity representing thermal radiation effects in the energy conservation equation of a continuum medium.

It is often convenient to separate in (1.19) the contribution from photons through dA passing to the hemispherical space above the element ($\theta \leq \pi/2$ in Figure 8) from that due to photons passing to the hemispherical space below it ($\theta \geq \pi/2$). Thus, if $\hat{s}(\theta,\phi)$ is restricted to vary on the upper hemisphere ($\theta \leq \pi/2\,, 0 \leq \phi \leq 2\pi$) and $\int_{2\pi} d\Omega$ denotes $\int_0^{2\pi}\int_0^{\pi/2} d\phi d\theta \sin\theta$, (1.19) can be written as

$$\boldsymbol{q}_{R\lambda}(\boldsymbol{r},t) = \boldsymbol{q}_{R\lambda}^{+}(\boldsymbol{r},t) - \boldsymbol{q}_{R\lambda}^{-}(\boldsymbol{r},t) \tag{1.23}$$

where we have defined the spectral heat flux density vectors for the upper and the lower hemispheres as

$$\boldsymbol{q}_{R\lambda}^{+}(\boldsymbol{r},t)=\int_{2\pi}\hat{s}\,I_\lambda(\boldsymbol{r},t,\hat{s})\,d\Omega \qquad and \qquad \boldsymbol{q}_{R\lambda}^{-}(\boldsymbol{r},t)=\int_{2\pi}\hat{s}\,I_\lambda(\boldsymbol{r},t,-\hat{s})\,d\Omega \tag{1.24}$$

respectively. Observe that spectral radiant heat flux per unit area entering the hemisphere above the element is given by

$$\boldsymbol{n}\cdot\boldsymbol{q}_{R\lambda}^{+}(\boldsymbol{r},t)=\int_{2\pi}\cos\theta\;I_\lambda(\boldsymbol{r},t,\hat{s})\,d\Omega \tag{1.25}$$

In particular, if the radiation emanating from the element towards the upper hemisphere is diffuse, $I_\lambda=I_\lambda(\boldsymbol{r},t)$, the RHS of (1.25) yields $I_\lambda(\boldsymbol{r},t)\int_{2\pi}\cos\theta\,d\Omega=\pi I_\lambda(\boldsymbol{r},t)$. Therefore, for the important case of a black body on has from (1.25) and (1.6) provide the relationship between its spectral emissive power and the spectral radiant intensity as

$$I_{b\lambda}(T)=\frac{E_{b\lambda}}{\pi}=\frac{2\pi hc^2}{\pi\lambda^5\left[e^{hc/(k\lambda T)}-1\right]} \tag{1.26}$$

And, integrating (1.26) over the wavelength using (1.8), the relationship between the radiant intensity and temperature

$$I_b(T)=\frac{\sigma T^4}{\pi} \tag{1.27}$$

is obtained. In general, the heat flux density vectors for the upper and the lower hemispheres are obtained in terms of the radiant intensity by integrating (1.24) over the wavelength as

$$\boldsymbol{q}_{R}^{+}(\boldsymbol{r},t)=\int_{2\pi}\hat{s}\,I(\boldsymbol{r},t,\hat{s})\,d\Omega \qquad and \qquad \boldsymbol{q}_{R}^{-}(\boldsymbol{r},t)=\int_{2\pi}\hat{s}\,I(\boldsymbol{r},t,-\hat{s})\,d\Omega \tag{1.28}$$

1.2.2 The equation of radiative transfer

According to (1.22), the heat leaving by radiation the unit volume per unit time depends on the radiant intensity, which, in turn, depends on the spectral radiant intensity through (1.17). Therefore, in order to solve the energy equation for a continuum medium in the presence of radiation, it is necessary to know how $I_\lambda(\boldsymbol{r},t)$ depends on the temperature field $T(\boldsymbol{r},t)$. This is achieved by solving the so-called *equation of radiative transfer* to be considered next.

The equation of radiative transfer essentially states that the variations of the spectral radiant intensity along a ray is due to the emission, absorption and scattering of radiation. In order to establish this equation, consider the ray of spectral radiant intensity $I_\lambda(\boldsymbol{r},t,\hat{s})$ schematized in Figure 9. Then, the variation of I_λ along a ray path length ds can symbolically be written as

$$(dI_\lambda)_{abs}=(dI_\lambda)_{abs}+(dI_\lambda)_{emis}+(dI_\lambda)_{scat} \tag{1.29}$$

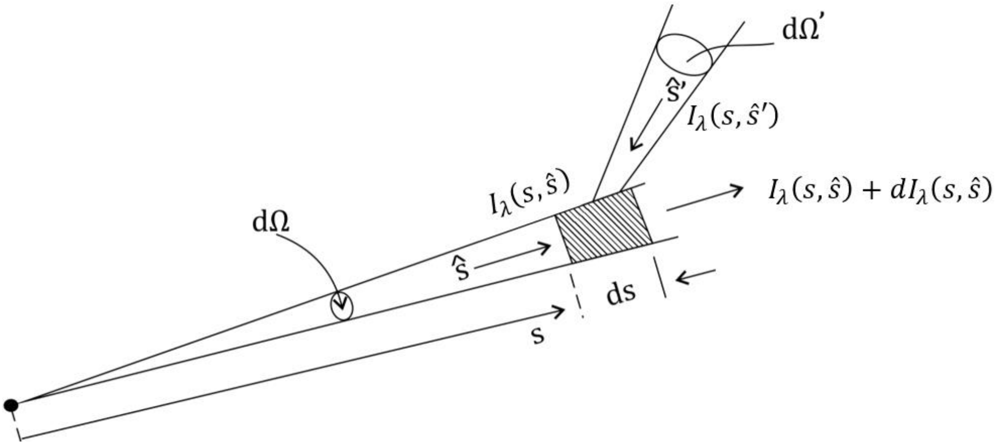

Figure 9: Emission, absorption and scattering of radiation along a ray.

It will be assumed that the attenuation experienced by the ray intensity across ds follows the Beer-Lambert law

$$(dI_\lambda)_{abs} = -\kappa_\lambda(\boldsymbol{r},t)I_\lambda(\boldsymbol{r},t,\hat{s})ds \tag{1.30}$$

where $\kappa_\lambda(\boldsymbol{r},t)$ is the *monochromatic volumetric absorption coefficient*. A medium in local thermodynamic equilibrium -in which the energy transitions are controlled by molecular collisions- will be considered throughout this work and, therefore κ_λ can be taken as a property of the medium which may depend on $\boldsymbol{r}$ and t through the local pressure a temperature. For such a medium, Kirchoff's law shows that the attenuation of radiant intensity by absorption is given by

$$(dI_\lambda)_{abs} = \kappa_\lambda I_{b\lambda}(T)ds \tag{1.31}$$

where $I_{b\lambda}(T)$ is the blackbody spectral radiant intensity introduced in (1.26) which may depend on $\boldsymbol{r}$ and t through the local temperature.

Finally, in order to compute the variation of spectral radiant intensity due to scattering one must take into account both the attenuation of the ray intensity due to scattering into directions $\hat{s}'$ different from $\hat{s}$ as well as its augmentation due to scattering of radiation from rays in directions $\hat{s}'$ into the direction $\hat{s}$ (see Figure 9). Analogously to absorption, the ray attenuation due to scattering into other directions contribution can be modelled as $-\gamma_\lambda(\boldsymbol{r},t)I_\lambda(\boldsymbol{r},t,\hat{s})ds$, where γ_λ is the *monochromatic volumetric scattering coefficient.* Since rays in other directions also attenuate according to this law, the augmentation of the intensity of the ray in the direction $\hat{s}$ due to scattering from a ray in the direction $\hat{s}'$ can be modelled as $\gamma_\lambda I_\lambda(\boldsymbol{r},t,\hat{s}')P(\hat{s},\hat{s}')d\Omega'/4\pi$, where $P(\hat{s},\hat{s}')$ is called the *scattering function* and $P(\hat{s},\hat{s}')d\Omega'/4\pi$ represents the fraction of the total energy which arrives to the ray in the direction $\hat{s}$ from other directions which is due to the scattering from rays within the solid angle $d\Omega'$ around $\hat{s}'$. Observe that $P(\hat{s},\hat{s}')$ must be symmetric, $P(\hat{s},\hat{s}') = P(\hat{s}',\hat{s})$ and satisfy that$1 = \int_{4\pi} P(\hat{s},\hat{s}')/4\pi\, d\Omega'$. The variation of radiant intensity due to scattering can be written as

$$(dI_\lambda)_{scat} = -\gamma_\lambda I_\lambda(\boldsymbol{r},t,\hat{s})ds + \gamma_\lambda ds \int_{4\pi} \frac{1}{4\pi} P(\hat{s},\hat{s}')I_\lambda(\boldsymbol{r},t,\hat{s}')\, d\Omega' \tag{1.32}$$

On substituting (1.30) -(1.32) into (1.29) and dividing by ds, one obtains the radiative transfer equation

$$\frac{dI_\lambda}{ds} = -\kappa_\lambda I_\lambda\,(\boldsymbol{r}, t, \hat{s}') + \kappa_\lambda I_{b\lambda}(T) - \gamma_\lambda I_\lambda(s, t, \hat{s}) + \gamma_\lambda \int_{4\pi} \frac{1}{4\pi} P(\hat{s}, \hat{s}') I_\lambda(\boldsymbol{r}, t, \hat{s}')\, d\Omega' \quad (1.33)$$

where, since along a ray starting at $\boldsymbol{r}_0$ one has $\boldsymbol{r} = \boldsymbol{r}_0 + \hat{s}$, the dependence $\boldsymbol{r}$ of I_λ has been replaced by a dependence on the path length, s. Defining the *total monochromatic extinction coefficient* and the *monochromatic scattering albedo coefficient* as

$$\beta_\lambda = \kappa_\lambda + \gamma_\lambda \quad and \quad \omega_\lambda = \frac{\gamma_\lambda}{\beta_\lambda} \quad (1.34)$$

Respectively, (1.33) can be written as

$$\frac{dI_\lambda}{ds} = -\beta_\lambda I_\lambda(s, t, \hat{s}) + \beta_\lambda S_\lambda(s, t) \quad (1.35)$$

where S_λ is the so-called *spectral source function* -which accounts for the processes of emission and scattering - defined as

$$S_\lambda = (1 - \omega_\lambda) I_{b\lambda}(T) + \omega_\lambda \int_{4\pi} \frac{1}{4\pi} P(\hat{s}, \hat{s}') I_\lambda(\boldsymbol{r}, t, \hat{s}')\, d\Omega' \quad (1.36)$$

For the case of a gray medium and isotropic scattering to be considered in this work, the extinction and scattering albedo coefficients can be considered independent of the wavelength and $P(\hat{s}, \hat{s}') = 1$. Then, (1.35) and (1.36) can be integrated over the wavelength to yield the equations for the radiant intensity and the (total) source function

$$\frac{dI}{ds} = -\beta I(s, t, \hat{s}') + \beta S(s, t) \quad (1.37)$$

and

$$S = (1 - \omega) I_b(T) + \frac{\omega G}{4\pi} \quad (1.38)$$

where $I_b(T) = \sigma T^4/\pi$, as given by (1.27), and the function G is the radiant intensity over the unit sphere,

$$G(s, t) = \int_{4\pi} I(s, t, \hat{s}') d\Omega \quad (1.39)$$

By taking into account that $dI/ds = \hat{s} \cdot \nabla I$, one obtains from (1.22) and (1.37) -(1.39) that the radiant heat leaving the unit voume per unit time is given by

$$\nabla \cdot \boldsymbol{q}_R(\boldsymbol{r}, t) = 4\pi\beta(1 - \omega)\left[I_b(T) - \frac{G}{4\pi}\right] \quad (1.40)$$

1.3 Fundamentals of atmospherics physics

Among the numerous physical processes involving thermal radiation, those which involve solar radiation are particularly important for astrophysics and for the study of the structure and evolution of planetary atmospheres, in particular that of Earth.

1.3.1 General features of Earth's atmosphere

Solar radiation constitutes the main energy source of our planet. This energy reaches the Earth's atmosphere carried by photons of wavelengths ranging from the infrared to the ultraviolet and interacts with the different layers of the atmosphere trough many physical mechanisms such as absorption, reflection, scattering, dissociation, ionization, etc., and provides the conditions which make life possible in this planet.

As for any other star, solar energy has its origin in the nuclear fusion processes which take place in the sun's core, where temperatures of around 15 million kelvin degrees are probably reached. From all the energy produced, only a small fraction of it reaches the Earth. This fraction, called solar irradiance (G_s), has an experimentally measured value of

$$G_s = 1373\ {}^{W}\!/_{m^2}\ . \qquad (1.41)$$

This value, also known as the *solar constant*, represents the amount of energy emitted by the Sun which reaches the Earth per unit normal surface per unit time. Its knowledge permits to determine the so called *Sun effective temperature*, which is defined as the surface temperature that a spherical black body of a radius equal to the solar radius, r_s, should have in order to radiate the same energy per unit time as the Sun. In effect, the conservation of energy demands that the total energy which per unit time abandons the Sun equals that passing through a sphere of radius equal to the mean Sun-Earth distance,

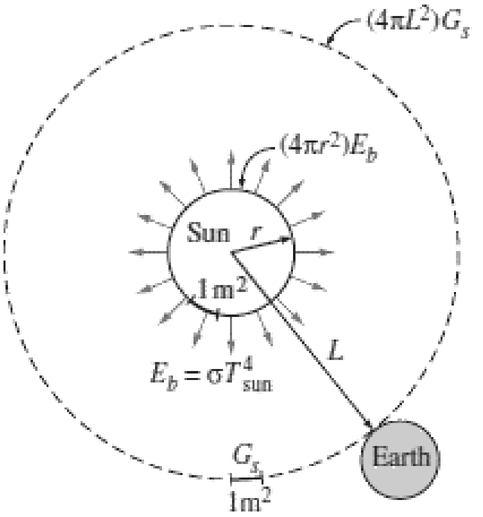

Figure 10: Energy balance between Sun and the terrestrial sphere (taken from [Cengel, 2002])

$$4\pi L^2 G_s = 4\pi r_s^2 \sigma T_s^4 \qquad (1.42)$$

where L is the astronomical unit, that is, the mean distance in the Sun-Earth orbit, r_s is the solar radius, and T_s

is the surface solar temperature. Substituting the values of each parameter, is obtained

$$T_s = 5780\ K \tag{1.43}$$

which is very close to the experimentally measured value of 5800 K. Therefore, it can be inferred that, due to the small difference between the effective and the observed solar surface temperatures, the Sun can be considered as a black body radiator which emits in a wide range of wavelengths and whose spectral emissive power has a maximum at a wavelength of approximately $0.5\ \mu m$.

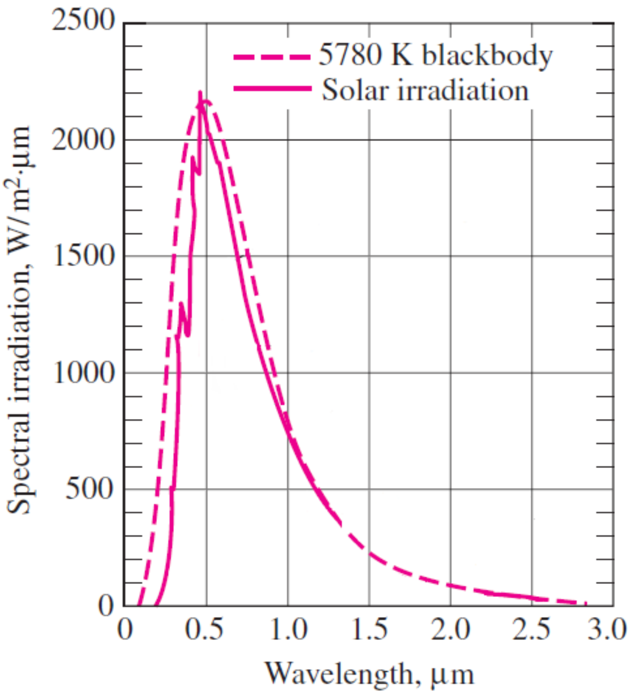

Figure 11: Comparison between real and black body emission of the Sun (taken from [Cengel, 2002])

Once some of the main characteristics of the solar radiation have been introduced, those of the second element intervening in the problem, the terrestrial atmosphere, will be next reviewed.

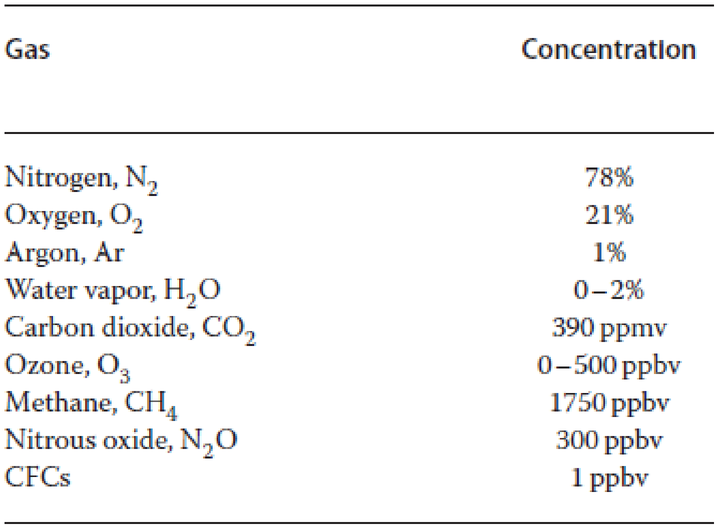

Gas	Concentration
Nitrogen, N_2	78%
Oxygen, O_2	21%
Argon, Ar	1%
Water vapor, H_2O	0–2%
Carbon dioxide, CO_2	390 ppmv
Ozone, O_3	0–500 ppbv
Methane, CH_4	1750 ppbv
Nitrous oxide, N_2O	300 ppbv
CFCs	1 ppbv

Figure 12: Concentration of the gaseous components in the atmosphere (taken from [Coakley & Yang, 2014])

The atmosphere is formed by a mixture of different substances is gaseous state which compose the air. Its two main components are the nitrogen and the oxygen, which constitute about 99% of the atmosphere.

However, the concentration of these substances greatly depends on the location within the atmosphere. Since the atmosphere is very thin, it can be assumed in a first approximation that the composition and the concentration of the different components of the air vary only with height, so that the atmosphere can be considered as divided in uniform adjacent horizontal layers. This is not really so, as, in addition to the height, it both longitudinal and horizontal variations are also present in the distribution and production of greenhouse effect gases, water evaporation, air streams which redistribute the air components, etc. However, these complications will not be taken into account in the simple atmospheric model considered in this document.

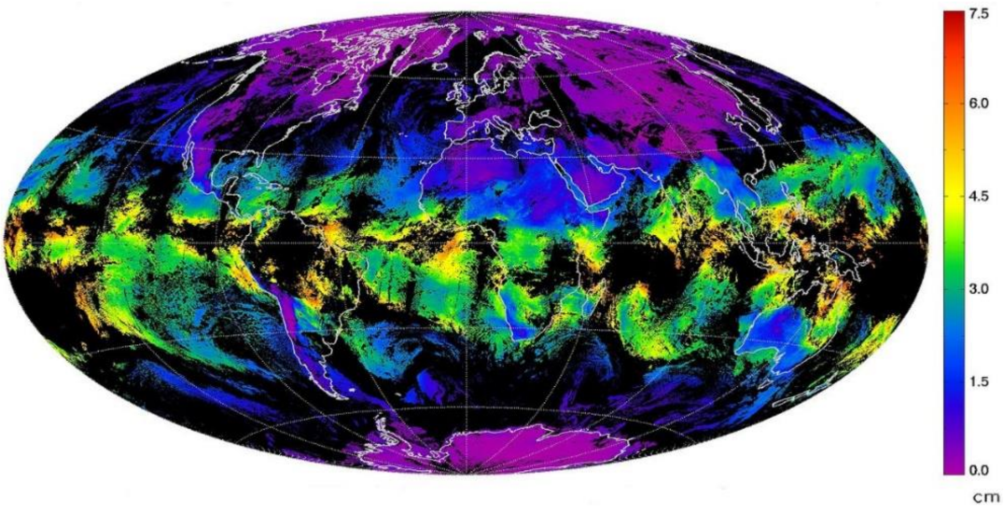

Figure 13: Mean water vapor concentration in the atmosphere, measured in cm

Within the layer model, several characteristic levels can be distinguished (see Figure 14):

Troposphere: It is the lowest level of the atmosphere, which is in contact with the Earth's surface and extends up to a height of approximately 10 km. Its mass is about 80% of that of the whole atmosphere and contains about 99% of the water vapour and most of the aerosols. In this level the temperature increases with height. The final layers of the troposphere constitute the tropopause, a region which is characterized by the fact that the temperature remains approximately constant with height.

Stratosphere: It extends from 10 Km to 30 km. It is very dry and contains the ozone layer, located at a height of 20 km, which protects the Earth's surface from harmful solar emissions. The troposphere and the stratosphere contain about 99% of the mass of the whole atmosphere. In the stratosphere the temperature decreases with height.

Mesosphere: This level, which extends from 50 to 85 km, is characterised by its low temperature - the lowest of the atmosphere -, with a distribution which decreases with height. The characteristic value of the pressure in it is only a 1% of that of Earth's surface (approximately 1 bar). As a curiosity, is in the mesosphere is where most meteorites disintegrate into small, incandescent particles due to the frictional heating.

Thermosphere: In this last level, the solar heating has a very important influence. As a consequence, the upper limit is quite diffuse, and is located at height which ranges between 500 and 1000 km. The air is rarefied, and its temperature tends to increase steeply, reaching values above 1000 K. Boreal aurores take place at this part of the atmosphere.

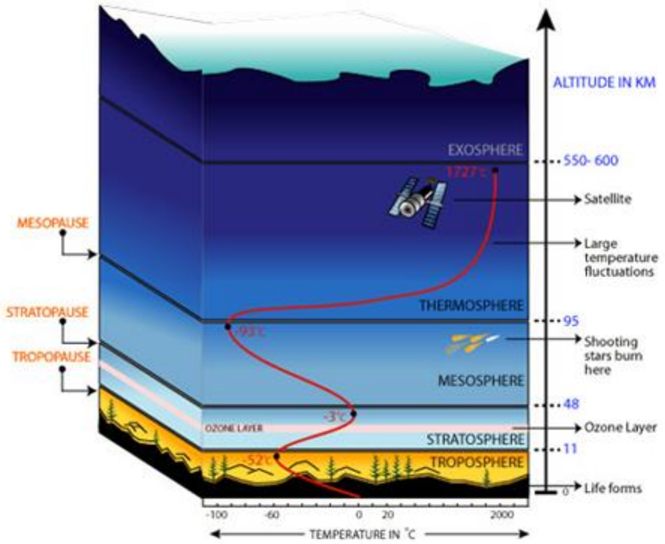

Figure 14: Schematics of the temperature distribution in the different levels of the Earth's atmosphere.

It is important to point out that the upper and lower limits established above are just approximate and must be taken only as averages, since both the climate and local atmospheric conditions can make them vary considerably.

After the introduction of some of the principal elements involved in the physics of the atmosphere, some of the relations among them will be next briefly described.

When solar radiation reaches the atmosphere and interacts with the air particles, many processes, which mainly depend on the radiation wavelength and the nature of the particles that receive it, may take place. Processes like molecules dissociation or ionization are frequent. For instance, the ozone located in the stratosphere, absorbs the ultraviolet radiation and gets divided into molecular and atomic oxygen, what protects the biosphere from these harmful radiative beams. However, in this project only the lower levels of the atmosphere - particularly the troposphere- will be considered, so that the most interesting processes will be the absorption, the emission and the scattering of radiation. As mentioned at the end of Section 1, not all the radiation which arrives to the Earth reaches its surface, but the intensity of the solar rays weakens in clear days and, much more, in foggy or cloudy days. Part of the incoming solar radiation is absorbed by the gases which compose the troposphere, which increases their thermal energy. In general, each constituent is more sensitive to the absorption of radiation within a particular (narrow) band of wavelengths. Thus, the ozone absorbs the totality of radiation which is under $\lambda = 0.3\ \mu m$ (ultraviolet), the oxygen in a narrow band around $\lambda = 0.76\ \mu m$ and the CO_2 absorbs in the infrared band – what makes it an important greenhouse gas. Nevertheless, the water vapour constitutes somewhat an exception, since it absorbs infrared radiation in a wide range of wavelengths as shown in Figure 15. This fact makes water vapor the most important component of the greenhouse gases, as will be discussed in the next subsection.

Finally, in addition to absorption, there exists another mechanism which weakens, although to a smaller extent, the intensity of the incoming solar radiation: the scattering. This mechanism consists on a reflexion process in which the radiative beams which collide with the particles bounce and get redirected randomly, yielding a diffuse radiation in every direction of the space. This implies that part of this radiation is returned to the hemisphere from which it comes, thus reducing the downwards radiative flux. The scattering is mainly governed by the particles size in relation with the incident wavelength. Thus, the oxygen and the nitrogen scatter wavelength radiation in the visible range (see Figure 15), in particular the colours blue and violet, respectively. This, together with the fact that these two gases are the most abundant in the atmosphere is what gives the sky its characteristic blue colour in clear days. The effect of the scattering in the visible range is particularly evident at sunrise and sunset, when the Sun is low on the horizon. At these times of the day, sunlight has to travel through more of the atmosphere to reach us and, therefore, the shortest wavelengths get scattered in greater amount along the paths of the rays. As a consequence, the light reaching the Earth's surface at those moments of the day mainly consists of red, orange and yellow wavelengths.

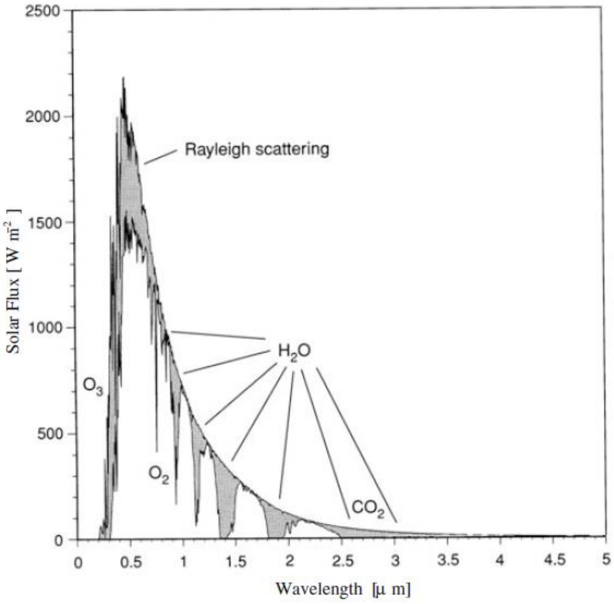

Figure 15: Absorption and scattering in the terrestrial atmosphere. The upper graph is the solar radiation which reaches the atmosphere and the lower one, the radiation which reaches the surface (taken from [Satoh, 2014])

1.3.2 Simplified atmospheric model

Once some important atmospheric physical processes have been introduced, it will be presented in this subsection a simplified model of the lower atmosphere which, in first approximation, permits to analyse the main features of its structure and evolution. Only the troposphere is considered in this work, and it is modelled as a slab which is infinite in the plane perpendicular to the direction of gravity - which will be taken along the z-axis - and is limited by lower and upper surfaces representing the Earth's surface and the top of the troposphere, respectively. It will be assumed that the problem is one-dimensional, so that quantities depend only on the z-coordinate (and, possibly, on time), which greatly simplifies the equations and is and assumption widely used in the literature dealing with global-mean properties of the atmosphere. Another commonly used assumptions, which will also be made in this work, are that the atmosphere is in local thermodynamic equilibrium (LTE) as well as in hydrostatic quasi equilibrium.

Concerning the characteristics of the thermal radiation, it will be assumed that the Earth's surface is a black body which emits at a certain temperature and that the top of the troposphere is transparent, so that it allows to escape the radiation to free space without neither absorption nor reflexion. In addition, the troposphere will be assumed to be a grey medium, an assumption which, admittedly not realistic, is often made in the literature dealing with simple atmospheric models in order to achieve a first approximation to the problem with simplified equations. Consistently with the approximate character of the model, scattering will be either neglected or considered to be isotropic and characterized by a uniform scattering albedo.

Finally, it will be taken into account that, according to Figure 12 and 15, water vapor is the atmospheric component which, besides being the most abundant infrared absorber, it is the one which absorbs in a larger number of infrared bands and that the troposphere contains 99% of the water vapor. Thus, it will be assumed that water vapor is the only absorber of radiation in the troposphere. This permits to model the absorption coefficient will be as a magnitude dependent on the height (z-coordinate) through pressure and density.

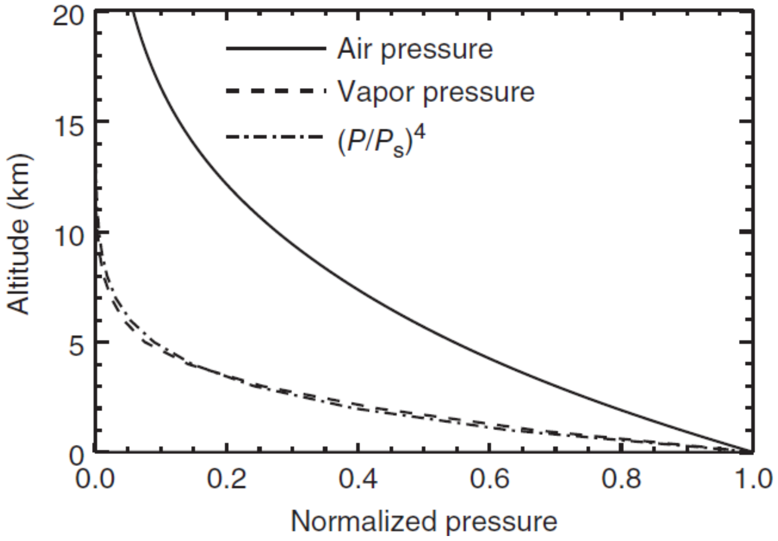

Figure 16: Total and partial pressures of air and water vapour (taken from [Coakley & Yang, 2009])

In effect, starting from the definition of the absorption coefficient,

$$\frac{\partial \tau}{\partial z} = \beta(z) = \chi \rho_a(z), \tag{1.44}$$

where β has been expressed in terms of the so called extinction coefficient per unit mass, χ , which is a constant for a given substance, and of the mass of water vapor per unit volume of air, ρ_a. Observe that the dimensions of χ are those of surface per unit mass. Since the mass fraction of water vapor is

$$q_a(z) = \frac{\rho_a(z)}{\rho(z)}, \tag{1.45}$$

one has that

$$\beta(z) = \chi \rho(z) q_a(z) \,. \tag{1.46}$$

As is usual in the literature, it will be assumed that the water vapor depends on height through a power of the nondimensional pressure defined as the local pressure divided by the sea level value in the form

$$q_a(z) = q_{as} \left(\frac{p(z)}{p_s}\right)^{\alpha}, \tag{1.47}$$

where q_{as} is the seal level water vapor mass fraction and α is a constant which must be properly chosen. According to Figure 16, (1.47) reproduces quite well the experimental data for α = 4. Thus, the absorption coefficient may be expressed as follows

$$\beta(z) = \underbrace{q_{as}\chi\rho_e}_{\beta_s}\left(\frac{\rho}{\rho_e}\right)\left(\frac{p}{p_s}\right)^4 = \beta_s\bar{\rho}\,\bar{p}^4, \tag{1.48}$$

where ρ_e is a conveniently chosen reference density that will be defined in Chapter 3. Equation (1.48) shows the β decreases with height as a consequence of the reduction in both density and pressure.

The existence of water vapor - and, to a lesser extent, of CO2 - in the atmosphere is responsible for the greenhouse effect, which consists in the heating of the Earth's surface and its surroundings due to the asymmetric properties of the terrestrial atmosphere, which is relatively transparent to solar radiation but opaque to planetary radiation. The simplest model to explain how the greenhouse effect takes place consists on a one-layer model in which the atmosphere is represented as a sheet of glass. The glass is transparent to short wave (solar) radiation $\left(q_{r_s}\right)$, but opaque to infrared (planetary) radiation, and emits in both directions as a blackbody of temperature T_e. Outward radiation from the glass corresponds to outgoing radiation at the top of the atmosphere.

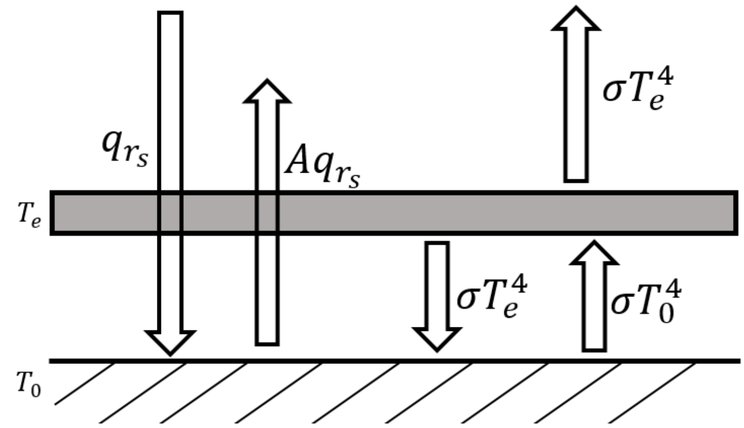

Figure 17: Schematic exchange of radiative fluxes from the surface, sun and sheet of glass which models the atmosphere.

Energy balances at the top of the atmosphere, the glass and at the lower surface yield

$$(1-A)q_{r_S} - \sigma T_e^4 = 0\,, \tag{1.49}$$

$$\sigma T_0^4 - 2\sigma T_e^4 = 0\,, \tag{1.50}$$

$$(1-A)q_{r_S} + \sigma T_e^4 - \sigma T_0^4 = 0\,, \tag{1.51}$$

respectively, where A is the Earth's albedo and represents the fraction of the total incident solar radiation absorbed by the Earth's surface. From these three equations, effective temperature and the Earth's surface temperature can be calculated as

$$T_e = \left[\frac{(1-A)q_{r_S}}{\sigma}\right]^{\frac{1}{4}}, \tag{1.52}$$

$$T_0 = \left[2\frac{(1-A)q_{r_S}}{\sigma}\right]^{\frac{1}{4}} = 2^{\frac{1}{4}}\,T_e\,. \tag{1.53}$$

As previously mentioned, the greenhouse effect makes the surface temperature is higher than the effective one - in this model by a factor of $2^{1/4}$ - the latter being be the one the Earth's surface would have in the absence of a participative atmosphere. Then, it can be concluded that the existence of an atmosphere will have an associated greenhouse effect, whose magnitude will depend on characteristics of the atmosphere such as its height, the fraction of constituents or the relative importance of radiation and conduction.

Considering the total atmosphere as a single sheet of glass is equivalent to assume that the absorption coefficient is constant with height, which will be one of the preliminary simplifications that will be made in the Chapter 2. However, this is not a realistic assumption, since the amount of water vapor decreases with height. In Chapter 3, the absorption coefficient from equation (1.48) will be considered, what would be equivalent to divide the atmosphere in many sheets of glass, each one with its own effective temperature.

2 UNSTEADY ONE-DIMENSIONAL CONDUCTION-RADIATION PROBLEMS

2.1. Introduction

As a first application of the theory of radiative transfer exposed in Section 2 of Chapter 1, the combined radiation conduction problem in the simple situation of a one-dimensional, incompressible, gray medium will be considered in this chapter. The equation governing the one-dimensional temperature field, $T(z,t)$, within the slab infinite in the horizontal directions, x and y of Figure 1 is

$$\rho c_p \frac{\partial T}{\partial t} = k \frac{\partial^2 T}{\partial z^2} - \frac{\partial q_R}{\partial z}, \tag{2.1}$$

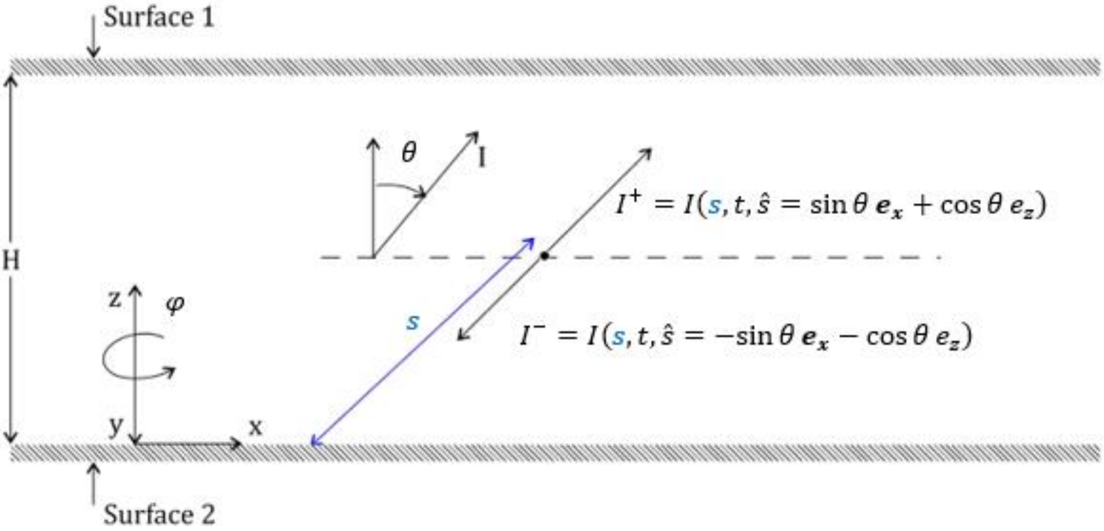

Figure 18: Schematics illustrating the radiant intensities I^+ and I^-.

where the density, ρ, the specific heat, c_p, and the thermal conductivity, k, of the medium are assumed to be uniform. According to equation (1.40), the radiant heat leaving the unit volume per unit time is

$$\frac{\partial q_R}{\partial z} = 4\pi\beta(1-\omega)\left(\frac{\sigma T^4}{\pi} - \frac{G}{4\pi}\right), \tag{2.2}$$

where $G = \int_{4\pi} I(s,t,\hat{s})\, d\Omega$ is the radiant intensity over a spherical solid angle (hemispherical radiant intensity), and $G/(4\pi)$ is the average over the unit sphere. Observe that in order to solve (2.1), the expression for G in (2.2) in terms of the temperature field within the slab must first be found. This requires solving the integro-diferential equation (1.37) of Chapter 1, which written explicitly in terms of $I(s,t,\hat{s})$ and T is

$$\frac{dI}{ds} = -\beta I + \frac{\beta\omega}{4\pi}\int_{4\pi} I(s,t,\hat{s})\,d\Omega + \frac{\beta(1-\omega)}{\pi}\sigma T^4\,, \tag{2.3}$$

to express the radiant intensity in terms of T and the boundary conditions at the slab lower and upper surfaces. Since $I(s,t,\hat{s})$ -and, therefore, $G(s,t)$- depend in a nonlinear way on the values of T at all points in the domain, (2.1) yields a partial nonlinear integro-differential equation for the temperature field.

Observe in Figure 1 that, due to the symmetry of the problem, all planes containing the z-axis are equivalent and, therefore, the radiant intensity does not depend on the angle ϕ around the z-axis, but only on the polar angle θ shown in the figure. If what follows, and for the sake of brevity, the explicit time dependence will be often suppressed from the arguments of the radiant intensity and its θ -dependence will be characterized by $\mu = \cos\theta$. Note also in Figure 1 that only the range $0 \leq \theta \leq \pi/2$ $(1 \geq \mu \geq 0)$ needs to be considered if for each value of θ in this range the intensities $I^{+}(s,\mu) \equiv I(s, \hat{\boldsymbol{s}} = \cos\theta\,\boldsymbol{e_x} + \sin\theta\,\boldsymbol{e_z})$ and $I^{-}(s,\mu) \equiv I(s, \hat{\boldsymbol{s}} = -\cos\theta\,\boldsymbol{e_x} - \sin\theta\,\boldsymbol{e_z})$ travelling in the positive and negative \$z\$-directions, respectively, are defined.

In this chapter, the equation (2.3) will be solved in Section 2 and a numerical method to solve the equation (2.1) will be proposed in Section 3 and validated in Section 4 with known results existing in the literature. The Matlab code used to implement the numerical method is detailed in the appendix.

2.2. The radiant intensity field in a one-dimensional slab

In order to solve (2.3) for the slab shown in figure 1, it is convenient to use as independent variable the *optical depth*, defined as

$$\tau = \int_0^z \beta(z')\,dz', \tag{2.4}$$

and to take into account that, the path length element ds for a ray travelling in the direction defined by an angle θ is related to the vertical coordinate element by $ds = dz/\mu = d\tau/(\beta\mu)$. Then, according to (2.3), the equation for the radiant intensity for a ray travelling in the positive *z-direction* can be written as

$$\frac{dI^+}{d\tau} = -\frac{I^+(\mu,\tau)}{\mu} + \frac{S(\tau)}{\mu}\,, \tag{2.5}$$

where $S = (1-\omega)I_b(T) + \omega G/4\pi$ is the source function introduced in equation (1.38), which represents the augmentation of radiant intensity due to the effects of both emission and scattering into the ray direction. Equation (2.5) is a first order, linear, ordinary differential for $I^+(\mu,\tau)$ which, with the help of the integrating factor $e^{\tau/\mu}$, can be immediately integrated to yield

$$I^+(\tau,\mu) = I^+(0,\mu)e^{-\frac{\tau}{\mu}} + \int_0^\tau e^{\frac{\tau'-\tau}{\mu}}\frac{S(\tau')}{\mu}\,d\tau'. \tag{2.6}$$

The first term on the RHS of (2.6) represents the attenuation -due to both absorption and scattering- of the ray intensity as it travels from the lower boundary $z = \tau = 0$ -where its value is $I^{+}(0,\mu)$ -up to a level z where the optical depth is τ, while the second term represents the augmentation of the ray intensity due to the accumulated contributions of the source functions of the elementary optical paths $d\tau'$ from $\tau' = 0$ up to $\tau' = \tau$ -note that the contribution of each $d\tau'$ is affected by weight function $e^{\frac{\tau'-\tau}{\mu}}$,which decreases as the optical distance $\tau - \tau'$ increases. Analogously, and taking into account that for rays propagating in the negative z-direction $ds = -dz/\mu = -d\tau/(\beta\mu)$, (2.3) provides the equation for $I^{-}(\tau,\mu)$ as

$$\frac{dI^{-}}{d\tau} = \frac{I^{-}(\mu,\tau)}{\mu} - \frac{S(\tau)}{\mu}. \tag{2.7}$$

By making use of the integrating factor $e^{\tau/\mu}$, equation can be immediately integrated between $\tau_0 = \tau(z = H)$ and τ to yield

$$I^{-}(\tau,\mu) = I^{-}(\tau_0,\mu)e^{\frac{-(\tau_0-\tau)}{\mu}} + \int_{\tau}^{\tau_0} e^{\frac{\tau-\tau'}{\mu}} \frac{S(\tau')}{\mu} d\tau' , \tag{2.8}$$

which is an expression with the same physical meaning as (2.6) if one takes into account that now the ray starts at the upper surface and travels towards regions of decreasing optical depth.

Since $d\Omega = d\phi d\theta \sin\theta = -d\phi d\mu$, the radiant intensity over the unit sphere can be written in terms of I^{+} and I^{-} as

$$G(\tau) = \int_0^{2\pi} d\phi \int_0^{\pi} \sin\theta \, I(\tau,\hat{\mathbf{s}}) \, d\theta = 2\pi \int_0^1 [I^{+}(\tau,\mu) + I^{-}(\tau,\mu)] \, d\mu \, . \tag{2.9}$$

In what follows only the case of diffuse boundaries will be considered, in which case the radiant intensities at the domain surfaces are independent of μ. Thus, if B_1 and B_2 denote the radiosities of the lower and the upper surfaces of the slab, one has that $I^{+}(0,\mu) = B_1/\pi$ and $I^{-}(\tau_0,\mu) = B_2/\pi$, and equations (2.6) and (2.8)-(2.9) yield

$$G(\tau) = 2[B_1 E_2(\tau) + B_2 E_2(\tau_0 - \tau)] + 2\pi \left[\int_0^{\tau_0} S(\tau') E_1(|\tau' - \tau|) \, d\tau' \right], \tag{2.10}$$

where the well known definition of the *n-th exponential integral* function

$$E(\chi) = \int_0^1 \mu^{n-2} e^{\frac{\chi}{\mu}} \, d\mu \quad (n \geq 1) \tag{2.11}$$

has been employed.

The radiative heat flux in the z-direction $q_R(z)$, can be obtained from equation (1.25) and (1.28) as

$$q_R = \boldsymbol{e_z} \cdot \boldsymbol{q_R} = \int_{2\pi} \mu I(s,\hat{\mathbf{s}}) \, d\Omega - \int_{2\pi} \mu I(s,-\hat{\mathbf{s}}) \, d\Omega \, , \tag{2.12}$$

where it has been taken into account that $\boldsymbol{e_z} \cdot \hat{\mathbf{s}} = \mu$. For the one-dimensional case, (2.12) can be expressed in terms of I^{+} and I^{-} as

$$q_R(\tau) = 2\pi \int_0^1 \mu I^+(\tau,\mu)\, d\mu - 2\pi \int_0^1 \mu I^-(\tau,\mu)\, d\mu = q_R^+ - q_R^- \,, \tag{2.13}$$

which can be obviously interpreted as the difference between the upwards heat flux carried by rays traveling in the positive z-direction, q_R^+, and that carried downwards by rays traveling in the negative z-direction, q_R^-. On sustituting (2.6) and (2.8) in (2.13) respectively, there results

$$q_R(\tau) = 2B_1E_3(\tau) - 2B_2E_3(\tau_0 - \tau) + 2\pi \int_0^{\tau_0} sign(\tau - \tau')S(\tau')E_2(|\tau - \tau'|)\, d\tau', \tag{2.14}$$

On taking into account that $E_3(0) = 1/2$, equation (2.14) particularized for $\tau = 0$ and $\tau = \tau_0$ yields respectively

$$q_R(0) = B_1 - \left[2B_2E_3(\tau_0) + 2\pi \int_0^{\tau_0} S(\tau')E_2(\tau')\, d\tau'\right] \tag{2.15}$$

and

$$q_R(\tau_0) = -B_2 + \left[2B_1E_3(\tau_0) + 2\pi \int_0^{\tau_0} S(\tau')E_2(\tau_0 - \tau')\, d\tau'\right]. \tag{2.16}$$

Observe that the quantities within the brackets in (2.15)-(2.16) can be identified as the irradiances H_1 and H_2 on the lower and upper surfaces, respectively, which where introduced in section 1 of Chapter 1. In this work, only surfaces for which the relation $B = \sigma\varepsilon T^4 + (1 - \varepsilon)\, H$ applies -where ε is the surface emissivity- will be considered. Thus, by substituting in this relation the expressions for the irradiances obtained from (2.15)-(2.16), on obtains that at the lower and upper surfaces the boundary conditions

$$B_1 - 2B_2(1 - \varepsilon_1)E_3(\tau_0) - 2\pi(1 - \varepsilon_1) \int_0^{\tau_0} S(\tau')E_2(\tau')\, d\tau' = \sigma\varepsilon_1T_1^4 \tag{2.17}$$

and

$$-2B_1(1 - \varepsilon_2)E_3(\tau_0) + B_2 - 2\pi(1 - \varepsilon_2) \int_0^{\tau_0} S(\tau')E_2(\tau_0 - \tau')\, d\tau' = \sigma\varepsilon_2T_2^4 \tag{2.18}$$

must be satisfied.

If the expression for the source function $S = (1 - \omega)I_b(T) + \omega G/4\pi$ -where $I_b(T) = \sigma T^4/\pi$ is the black body radiant intensity- is introduced in equations (2.10) and (2.17)-(2.18) the following system of three integro-algebraic equations is obtained

$$\begin{aligned} G(\tau) - \frac{\omega}{2} \int_0^{\tau_0} G(\tau')E_1(|\tau - \tau'|)\, d\tau' - 2B_1E_2(\tau) - 2B_2E_2(\tau_0 - \tau) \\ = 2\pi(1 - \omega) \int_0^{\tau_0} I_b(\tau')E_1(|\tau - \tau'|)\, d\tau' \,, \end{aligned} \tag{2.19}$$

$$-\frac{\omega}{2}(1-\varepsilon_1)\int_0^{\tau_0} G(\tau')E_2(\tau')\,dt + B_1 - 2(1-\varepsilon_1)E_3(\tau_0)B_2 = \varepsilon_1 I_{b1}\pi + 2\pi(1-\omega)(1-\varepsilon_1)\int_0^{\tau_0} I_b(\tau')E_2(\tau')\,dt\,, \tag{2.20}$$

$$-\frac{\omega}{2}(1-\varepsilon_2)\int_0^{\tau_0} G(\tau')E_2(\tau_0-\tau')\,d\tau' + B_2 - 2(1-\varepsilon_2)E_3(\tau_0)B_1 = \varepsilon_2 I_{b2}\pi + 2\pi(1-\omega)(1-\varepsilon_2)\int_0^{\tau_0} I_b(\tau')E_2(\tau_0-\tau')\,d\tau', \tag{2.21}$$

where, for the sake of simplicity in the presentation, it has been assumed that ω is uniform within the slab. Equations (2.19)-(2.20), whose discretization and numerical solution will be explained in the next section, permit to obtain simultaneously $G(\tau)$, B_1 and B_2 in terms of the distribution of $I_b(\tau)$ -or which is the same, in terms the temperature field $T(\tau)$- within the slab.

2.3. Numerical method

After the equations have been written in a proper form, they must be solved numerically and, therefore, the values of the quantities, $G(\tau)$ and $I_b(\tau)$ in this case, will be needed at discrete points.

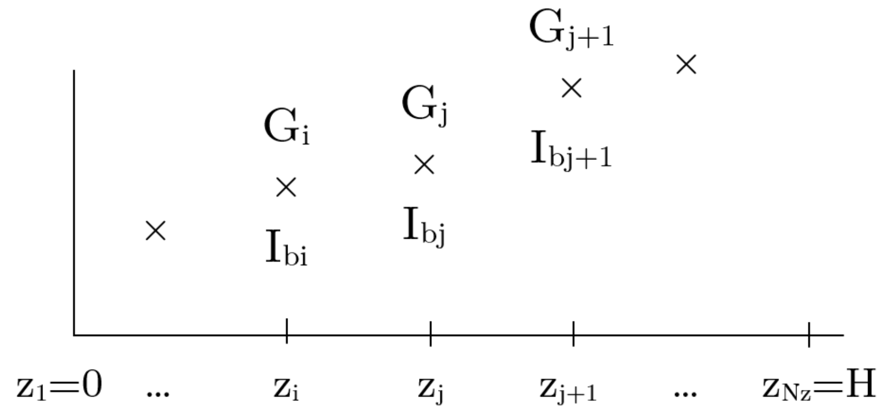

Figure 19: Schematics of the discretization and the unknown values of the function G and I_b at each point.

Therefore, the first objective is to discretize equations (2.19)-(2.21) in order to arrive to a solution of the form

$$\begin{bmatrix} \boldsymbol{G} \\ B_1 \\ B_2 \end{bmatrix} = M_{GJ}\cdot \boldsymbol{I_b}, \tag{2.22}$$

where $\boldsymbol{G} = \left[G_1, \dots, G_i, \dots, G_{N_z}\right]^T$ and $\boldsymbol{I_b} = \left[I_{b1}, \dots, I_{bi}, \dots, I_{bN_z}\right]^T$ are the values of $G(\tau)$ and $I_b(\tau)$ at the nodes, that is, $G_i = G(\tau_i)$ and $I_{bi} = I_b(\tau_i)$.

Firstly, equation (2.19) is considered with integrals with exponential integral functions ($E_1(|t-\tau|)$). For this purpose, consider any function of the form

$$F(\tau) = \int_0^{\tau_0} f(\tau')\, E_1(|\tau - \tau'|)\,, \tag{2.23}$$

which, once discretized, may be written as

$$\begin{bmatrix} F_1 \\ \vdots \\ F_i \\ \vdots \\ F_{N_z} \end{bmatrix} = \begin{bmatrix} & A_{ij} & \end{bmatrix} \begin{bmatrix} f_1 \\ \vdots \\ f_j \\ \vdots \\ f_{N_z} \end{bmatrix}. \tag{2.24}$$

Note that the contribution to the integral (2.23) at $\tau = \tau_i$ from each interval $[\tau_j, \tau_{j+1}]$, where $j = (1, \ldots, N_z)$, can be approximate by

$$\frac{f_j + f_{j+1}}{2} \int_{\tau_j}^{\tau_{j+1}} E_1(|\tau_i - \tau'|)\, d\tau' \equiv \frac{f_j + f_{j+1}}{2} g_{ij}\,. \tag{2.25}$$

Since $E_1(\tau)$ has a logarithmic singularity at the origin $\tau \to 0$, it is preferable to use the following property

$$\frac{dE_n(\chi)}{d\chi} = -E_{n-1}(\chi) \tag{2.26}$$

of the exponential integrals and write the integral in (2.25) in terms of $E_2(\tau)$. Since there is an absolute value in the function argument, two cases are distinguished. The first case is that $\tau_i \geq \tau_{j+1}$, as in Figure 20, which yields

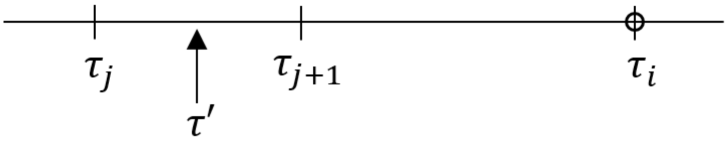

Figure 20: Schematics of the case $\tau_i \geq \tau_{j+1}$ in which τ' is between τ_j and τ_{j+1} for the integration.

$$E_1(|\tau_i - \tau'|) = E_1(\tau_i - \tau') = \frac{dE_2}{d\tau'}(\tau_i - \tau')\,, \tag{2.27}$$

and the integral becomes

$$g_{ij} = \int_{\tau_j}^{\tau_{j+1}} E_1(\tau_i - \tau')\, d\tau' = E_2(\tau_i - \tau_{j+1}) - E_2(\tau_i - \tau_j)\,. \tag{2.28}$$

The second case corresponds to $\tau_i \leq \tau_j$, which yields

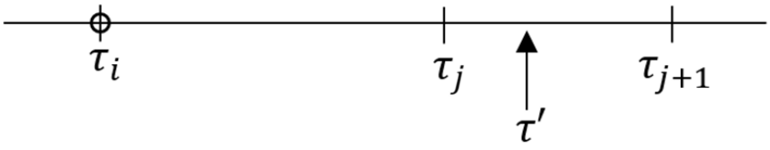

Figure 21: Schematics of the case $\tau_i \leq \tau_j$ in which τ' is between τ_j and τ_{j+1} for the integration.

$$E_1(|\tau_i - \tau'|) = E_1(\tau' - \tau_i) = -\frac{dE_2}{d\tau'}(\tau' - \tau_i) \tag{2.29}$$

And, therefore,

$$g_{ij} = -E_2(\tau_{j+1} - \tau_i) + E_2(\tau_i - \tau_j) \tag{2.30}$$

Observe that expressions (2.28) and (2.30) can be combined into the single one

$$\begin{aligned} g_{ij} &= sign(\tau_i - \tau_{j+1} + 10^{-12})E_2(|\tau_i - \tau_{j+1}|) \\ &\quad - sign(\tau_i - \tau_j - 10^{-12})E_2(|\tau_i - \tau_j|) \end{aligned} \tag{2.31}$$

which is very useful for numerical purposes. The terms $\pm 10^{-12}$ are included so that the sign functions yield the proper values when $\tau_i = \tau_{j+1}$ or $\tau_i = \tau_j$. Thus, equations (2.23) and (2.25) yield

$$\begin{aligned} F_i &= \sum_{j=1}^{N_z-1} \frac{f_j + f_{j+1}}{2} g_{ij} \\ &= \frac{f_1}{2} g_{i1} + \frac{f_2}{2}(g_{i1} + g_{i2}) + \cdots + \frac{f_j}{2}(g_{ij-1} + g_{ij}) + \cdots + \frac{f_{N_z}}{2} g_{iN_z-1} \end{aligned} \tag{2.32}$$

or, in the form of equation (2.24),

$$F_i = \sum_{j=1}^{N_z} A_{ij} f_j$$

where

$$A(i,1) = \frac{1}{2} g_{i1}\,, \quad A(i,j) = \frac{g_{ij-1} + g_{ij}}{2}\,, \quad A(i,N_z) = \frac{g_{iN_z-1}}{2}$$

Then, equation (2.19) can be discretized as

$$\left(\underline{I} - \frac{\omega}{2}\underline{A}\right) \cdot \boldsymbol{G}(\tau) - 2B_1\boldsymbol{E_2}(\tau) - 2B_2\boldsymbol{E_2}(\tau_0 - \tau) = 2\pi(1-\omega)\underline{A} \cdot \boldsymbol{I_b}(\tau) \tag{2.33}$$

where $\boldsymbol{G}(\tau)$ and $\boldsymbol{I_b}(\tau)$ have the same meaning as in (2.22) and $\boldsymbol{E_2}(\tau_0 - \tau) = [E_2(\tau_0 - \tau_1), \dots, E_2(\tau_0 - \tau_i), \dots, E_2(\tau_0 - \tau_{N_z})]^T$ and $\boldsymbol{E_1}(\tau) = [E_2(\tau_1), \dots, E_2(\tau_i), \dots, E_2(\tau_{N_z})]$ are the exponential integral function vectors.

Next the equations (2.20) and (2.21) for the radiosities will be discretized. For this purpose, observe in equation (2.20) that the expression $I_1 = \int_0^{\tau_0} G(\tau')E_2(\tau')\,d\tau'$ may be written using the trapezoidal rule as

$$
\begin{aligned}
I_1 &= \sum_{j=1}^{N_z-1} \frac{E_2(\tau_j)G_j + E_2(\tau_{j+1})G_{j+1}}{2}(\tau_{j+1}-\tau_j) \\
&= \left(\frac{E_2(\tau_1)}{2}(\tau_2-\tau_1), \dots, \frac{E_2(\tau_{N_z-1})}{2}(\tau_{N_z}-\tau_{N_z-1}), 0\right)\cdot \boldsymbol{G} \\
&\quad + \left(0, \frac{E_2(\tau_2)}{2}(\tau_2-\tau_1), \dots, \frac{E_2(\tau_{N_z-1})}{2}(\tau_{N_z}-\tau_{N_z-1})\right)\cdot \boldsymbol{G} = \boldsymbol{a}\cdot\boldsymbol{G}\,,
\end{aligned}
\tag{2.34}
$$

where the vector $\boldsymbol{a}$ is defined as

$$
\boldsymbol{a} = \left(\frac{E_2(\tau)}{2}(\tau_2-\tau_1), \dots, 0\right) + \left(0, \dots, \frac{E_2(\tau_{N_z})}{2}(\tau_{N_z}-\tau_{N_z-1})\right). \tag{2.35}
$$

Analogously, the expression $I_2 = \int_0^{\tau_0} G(\tau')E_2(\tau_0-\tau')\,d\tau'$ from equation (2.21) is discretized as

$$
I_2 = \sum_{j=1}^{N_z-1} \frac{E_2\left(\tau_0-\tau_j\right)G_j + E_2(\tau_0-\tau_{j+1})G_{j+1}}{2}(\tau_{j+1}-\tau_j) = \boldsymbol{b}\cdot\boldsymbol{G}\,, \tag{2.36}
$$

where $\boldsymbol{b}$ is the analogous to $\boldsymbol{a}$ in (2.34)

$$
\boldsymbol{b} = \left(\frac{E_2(\tau_0-\tau_1)}{2}(\tau_2-\tau_1), \dots, 0\right) + \left(0, \dots, \frac{E_2(\tau_0-\tau_{N_z})}{2}(\tau_{N_z}-\tau_{N_z-1})\right).
$$

Then, equations (2.20) and (2.21) can be written in a form similar to that of equation (2.33) as

$$
\begin{aligned}
-\frac{\omega}{2}(1-\varepsilon_1)\boldsymbol{a}\cdot\boldsymbol{G} + B_1 - 2(1-\varepsilon_1)E_3(\tau_0)B_2 \\
= \varepsilon_1 I_{b1}\pi + 2\pi(1-\omega)(1-\varepsilon_1)\boldsymbol{a}\cdot\boldsymbol{I_b}
\end{aligned}
\tag{2.37}
$$

$$
\begin{aligned}
-\frac{\omega}{2}(1-\varepsilon_2)\boldsymbol{b}\cdot\boldsymbol{G} + B_{\mathbf{2}} - 2(1-\varepsilon_2)E_3(\tau_0)B_1 \\
= \varepsilon_2 I_{bN_z}\pi + 2\pi(1-\omega)(1-\varepsilon_2)\boldsymbol{b}\cdot\boldsymbol{I_b}
\end{aligned}
\tag{2.38}
$$

Finally, equations (2.33), (2.37) and (2.38) are written in matrix form as

$$
\left[\begin{array}{c|c|c}
 & -2E_2(\tau_1) & -2E_2(\tau_0-\tau_1) \\
 & \vdots & \vdots \\
\underline{I}-\frac{\omega}{2}\underline{A} & -2\boldsymbol{E_2}(\tau) & -\boldsymbol{E_2}(\tau_0-\tau) \\
 & \vdots & \vdots \\
 & -2E_2\left(\tau_{N_z}\right) & -2E_2\left(\tau_0-\tau_{N_z}\right) \\
\hline
-\frac{\omega}{2}(1-\varepsilon_1)\boldsymbol{a} & 1 & -2(1-\varepsilon_1)E(\tau_0) \\
-\frac{\omega}{2}(1-\varepsilon_2)\boldsymbol{b} & -2(1-\varepsilon_2)E_3(\tau_0) & 1
\end{array}\right]
\left[\begin{array}{c}
G(\tau) \\ \vdots \\ \boldsymbol{G}(\tau) \\ \vdots \\ G\left(\tau_{N_z}\right) \\ \hline B_1 \\ B_2
\end{array}\right]
\tag{2.39}
$$

$$
=\left[\begin{array}{c}
2\pi(1-\omega)\underline{A} \\
\hline
2\pi\boldsymbol{a}(1-\omega)(1-\epsilon_1)+(\pi\epsilon_1\boldsymbol{e_1}) \\
2\pi\boldsymbol{b}(1-\omega)(1-\epsilon_2)+\left(\pi\epsilon_2\boldsymbol{e_{N_z}}\right)
\end{array}\right]
\left[\begin{array}{c}
I_{b1} \\ \vdots \\ \boldsymbol{I_b} \\ \vdots \\ I_{bN_z}
\end{array}\right],
$$

where $\boldsymbol{e_1} = [1, 0, \dots, 0]$ and $\boldsymbol{e_2} = [0, \dots, 0, 1]$, with N_z components in both vectors. Thus, denoting the left member by L_{GB} ,which is a $(N_z + 2) \times (N_z + 2)$ matrix, and right member by R_{Ib}, which is a $(N_z + 2)xN_z)$ matrix, equation (2.39) can be compactly simply written as

$$
\underline{L_{GB}} \cdot \begin{bmatrix} \boldsymbol{G}(\tau) \\ B_1 \\ B_2 \end{bmatrix} = \underline{R_{Ib}} \cdot \boldsymbol{I_b}(\tau) \tag{2.40}
$$

Although this system is defined to satisfy the boundary conditions $T(0) = T_1$ and $T(\tau_0) = T_2$, it can be easily modified if there are different ones. Thus, if, for example, $B_2 = 0$, last row in L_{GB} should be replaced by a vector of 0 except the last term which would be 1 and last row of R_{Ib} would be a 0 vector :

$$
\begin{gathered}
L_{GB}(N_z + 2, 1\!:\!N_z + 1) = 0\,, \quad L_{GB}(N_z + 2, N_z + 2) = 1\,, \\
R_{Ib}(N_z + 2, :) = 0.
\end{gathered} \tag{2.41}
$$

Then, in order to calculate both the radiosities and the hemispherical radiant intensity function, L_{GB} may be invert and obtain

$$
\begin{bmatrix} \boldsymbol{G}(\tau) \\ B_1 \\ B_2 \end{bmatrix} = \underline{L_{GB}}^{-1} \cdot \underline{R_{Ib}} \cdot \boldsymbol{I_b}(\tau) = \underline{M_{GB}} \cdot \boldsymbol{I_b}(\tau)\,, \tag{2.42}
$$

where M_{GB} is of the form

$$
\underline{M_{GB}} = \left[\begin{array}{c} M_G \\ \hline \boldsymbol{a_{B1}} \\ \boldsymbol{a_{B2}} \end{array}\right], \tag{2.43}
$$

M_G being a $(N_z \times N_z)$ matrix, both a_{B1} and a_{B2} are $(1 \times N_z)$ vectors, and the quantities $\boldsymbol{G}, B_1$ and B_2 are

$$\boldsymbol{G} = \underline{M_G} \cdot \boldsymbol{I_b}\,, \qquad B_1 = \boldsymbol{a_{B1}} \cdot \boldsymbol{I_b}\,, \qquad B_2 = \boldsymbol{a_{B2}} \cdot \boldsymbol{I_b}\,. \tag{2.44}$$

The (Nz x 1) vector $\boldsymbol{I_b}$ results from solving the energy equation for the temperature. In effect, that equation can be written after combining equations (2.1) and (2.2) as

$$\rho c_p \frac{\partial T}{\partial t} = k \frac{\partial^2 T}{\partial z^2} - \beta(1-\omega)(4\sigma T^4 - G)\,. \tag{2.45}$$

In order to numerically solve (2.45), it is convenient to introduce the dimensionless variables

$$z = H\bar{z}\,, \qquad T = T_1\bar{T}\,, \qquad t = \frac{k}{4\alpha\beta\sigma T_1^3}\bar{t}\,, \tag{2.46}$$

where $\alpha = k/(\rho C_p)$ is the thermal diffusivity coefficient and the bar on the top of each variable means that it is nondimensional. In terms of the new variables, equation (2.45) reads

$$\frac{\partial \bar{T}}{\partial \bar{t}} = \frac{N_{cr}}{\tau_0^2}\frac{\partial^2 \bar{T}}{\partial \bar{z}^2} - (1-\omega)\left(\bar{T}^4 - \frac{G(\tau)}{4\sigma T_1^4}\right), \tag{2.47}$$

where N_{cr} is the conduction to radiation ratio parameter and τ_0 is the optical depth, which are defined as

$$N_{cr} = \frac{k\beta}{4\sigma T_1^3}\,, \qquad \tau_0 = \beta H\,. \tag{2.48}$$

Observe that N_{cr} controls the energy transfer regime, that is, if this parameter is large the problem is dominated by conduction, while if it is small, radiation is the principle mechanism of transfer. Analogously to (2.19)-(2.22), equation (2.47) must be discretized. This will be done in terms of the mesh $\left(z_1 = 0, \ldots, z_j, \ldots, z_{N_z} = 1\right)$ and the vector $\boldsymbol{T_n} = \left[T_{1n}, \ldots, T_{jn}, \ldots, T_{N_z}\right]^T$, defined at those points at instant t_n. The discretization yields

$$\boldsymbol{T_n} = \boldsymbol{T_{n-1}} + dt\left(\frac{N_{cr}}{\tau_0^2} D_{zz} \cdot \boldsymbol{T_n} - (1-\omega)\left(1 - \frac{1}{4\pi}\underline{M_G}\right) \cdot \boldsymbol{T_n^4}\right), \tag{2.49}$$

where D_{zz} is the matrix resulting from the discretization of the operator $d^2/d\bar{z}^2$, obtained through the finite differences method, based on the Lagrange polynomials, as it is implemented in the Matlab code detailed in the appendix. The preceding equation may be written in compact form as

$$\underline{B} \cdot \boldsymbol{T_n} + \underline{c} \cdot \boldsymbol{T_n^4} = \boldsymbol{b}\,, \tag{2.50}$$

where

$$\underline{B} = \underline{I} - \frac{N_{cr}}{\tau_0^2} D_{zz} dt\,, \quad \underline{c} = (1-\omega)\left(\frac{1}{4\pi}\underline{M_G} - \underline{I}\right) dt\,, \qquad \boldsymbol{b} = \boldsymbol{T_{n-1}}\,. \tag{2.51}$$

The first and last rows of $\underline{B}$, $\underline{c}$ and $\boldsymbol{b}$ should be appropriately modified dependently on the boundary conditions. For example, if $T(z=0)=T_1(t)$ and $T(z=H)=T_2$, one should have

$$\begin{gathered} B(1,:)=0\,,\quad B(1,1)=1\,,\ c(1,:)=0\,,\ b(1)=T_1(t_n)\,, \\ B(N_z,:)=0\,,\quad B(N_z,N_z)=1\,,\ c(N_z,:)=0\,,\ b(N_z)=T_H\,. \end{gathered} \tag{2.52}$$

If, on the other hand, the boundary conditions are $T(z=0)=T_1$ and ${}^{dT}/_{dz}\,(z=H)=0$, the modifications are

$$B(N_z,:)=D_z(N_z,:)\,,\qquad c(N_z,:)=0\,,\qquad b(N_z)=0\,. \tag{2.53}$$

The system of equations (2.50) can be solved with the classical Newton-Raphson method. That is, if the guessed value of $\boldsymbol{T_n}$ for the k-th iteration is $\boldsymbol{T_k}$ and $\Delta\boldsymbol{T}$ denotes the correction for the next iteration, then

$$\underline{B}\cdot(\boldsymbol{T_k}+\Delta\boldsymbol{T})+\underline{c}\cdot(\boldsymbol{T_k^4}+4\boldsymbol{T_k^3}*\Delta\boldsymbol{T})=\boldsymbol{b} \tag{2.54}$$

where the operator $*$ means that the product is made component by component (Hadamard product), instead of a common vector product. This can also be written as

$$\Delta\boldsymbol{T}=\underline{S}^{-1}\cdot\boldsymbol{F_k}\,, \tag{2.55}$$

where $\underline{S}$ and $\boldsymbol{F_k}$ are defined as

$$\underline{S}=\underline{B}+4\underline{c}\cdot\begin{bmatrix} \boldsymbol{T_1^3} & \cdots & 0 \\ & \ddots & \\ \vdots & \boldsymbol{T_k^3} & \vdots \\ & \ddots & \\ 0 & \cdots & \boldsymbol{T_{N_z}^3} \end{bmatrix},\qquad \boldsymbol{F_k}=\boldsymbol{b}-\left(\underline{B}\cdot\boldsymbol{T_k}+\underline{c}\cdot\boldsymbol{T_k^4}\right). \tag{2.56}$$

Once the vector $\boldsymbol{T_n}$ is known, the quantities $\boldsymbol{G}(\tau)$, B_1 and B_2 can be found using the relation given by (2.44). Thus, all the quantities are known and therefore the problem is closed, since the temperature field has been found and the conductive and radiative fluxes may be calculated with the corresponding equations of section 2.

2.4. Verification and comparison of results

Up to now, in section 1, governing equations of the problem were derived while in section 2 a numerical method to solve these equations was developed. Thus, this section will be concerned with proving that the obtained results are both accurate and physically plausible.

For this purpose, a comparison with [Sparrow & Cess (1978)] results for the conduction-radiation problem will be made first for some particular cases, such as radiative equilibrium and pure scattering or non-scattering media. The results obtained are quite similar, since the same governing equations have been used. After this, the results will be contrasted with those by [Aston et al. (2000)]. In this case, the equations are different since they introduced a simplification in the model - the so called Eddington approximation to be discussed later - so that their results , although similar, differ somewhat from the ones obtained with the method proposed in this work. Finally, results corresponding to several unsteady problems will be given.

2.4.1 Validation of the method

First, the behaviour of the proposed numerical model will be tested for several cases with different values of the parameters $\boldsymbol{N_{cr}}$, $\boldsymbol{\tau_0}$, $\boldsymbol{\varepsilon_1}$, $\boldsymbol{\varepsilon_2}$ and $\boldsymbol{\omega}$. Figure 22 represents the total (radiative plus conductive) non-dimensional heat flux as a function of the parameter $\boldsymbol{N_{cr}}$ for different values of the optical thickness $\boldsymbol{\tau_0}$ and for a non-scattering media $(\boldsymbol{\omega = 0})$. As can be seen, the numerical results obtained by the method are very similar to those given by Sparrow & Cess. The figure shows how the increase of the optical depth (opaque medium) reduces the heat transfer, while the augmentation of $\boldsymbol{N_{cr}}$ increases the heat flux as the problem tends to be dominated by heat conduction. In addition, it may be observed that the graphs have an asymptotic behaviour when $\boldsymbol{N_{cr}}$ reaches either very high or very low values.

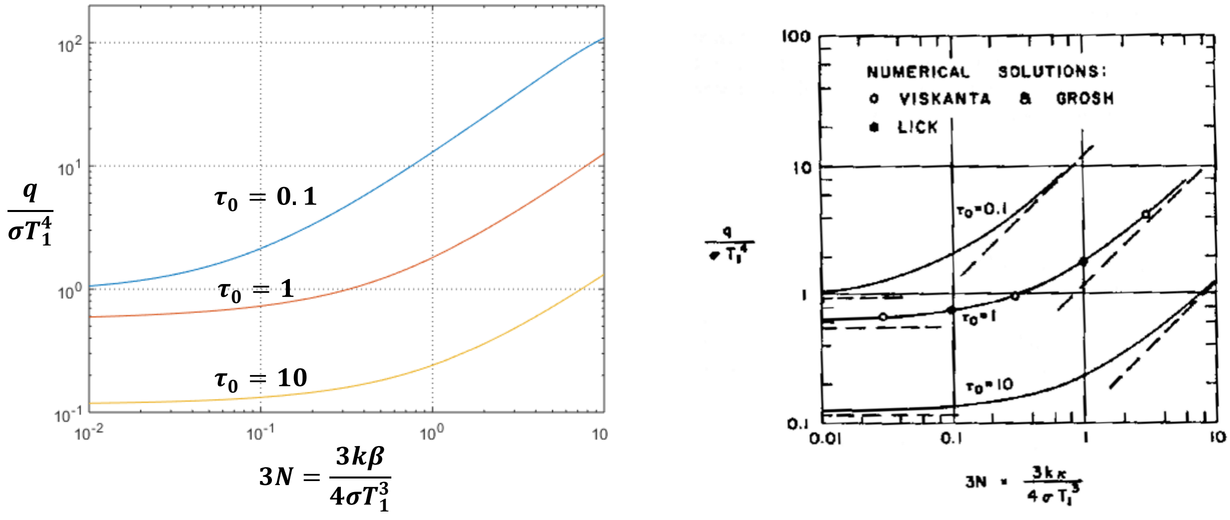

Figure 22: Heat transfer results for $\varepsilon_1 = \varepsilon_2 = 1$ and $T_2 = 0.1$

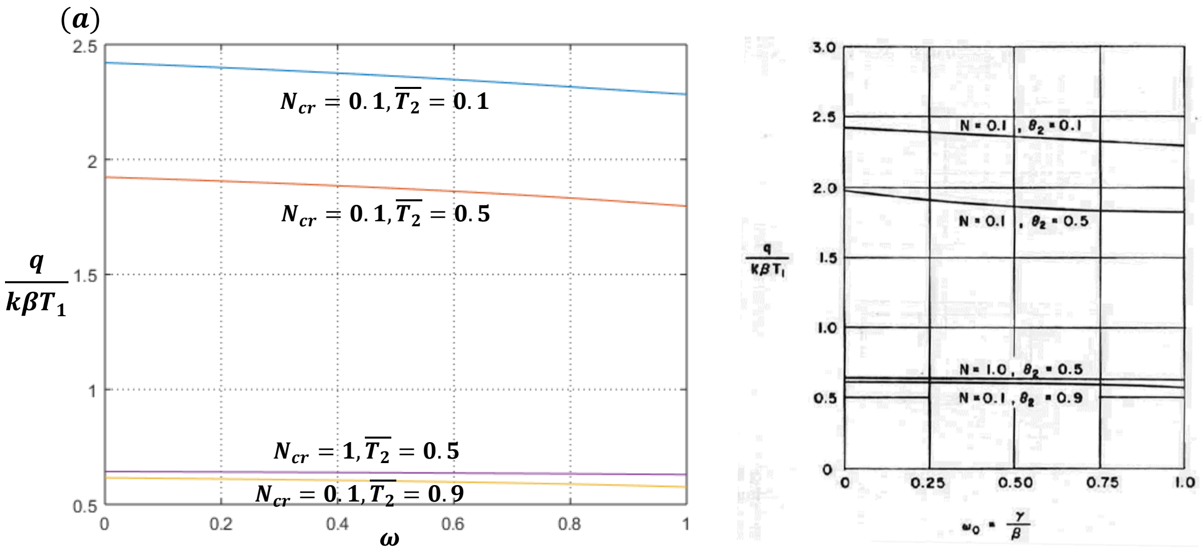

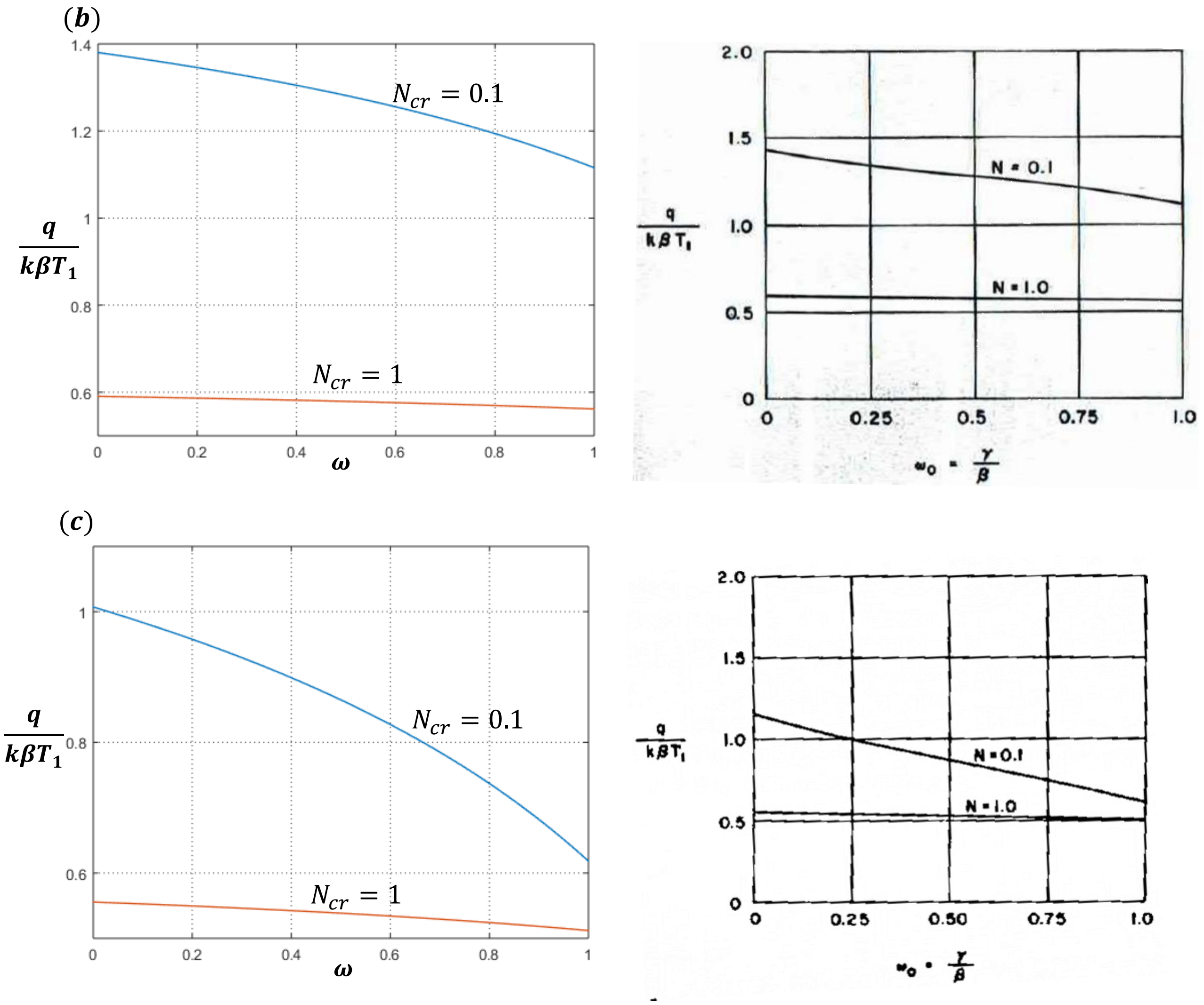

Figure 23: Effect of albedo on heat transfer for **(a)** $\tau_0 = 1, \varepsilon_1 = \varepsilon_2 = 1$; **(b)** $\tau_0 = 1, \varepsilon_1 = \varepsilon_2 = 0.5$, $T_2 = 0.5$; **(c)** $\tau_0 = 1, \varepsilon_1 = \varepsilon_2 = 0.1, T_2 = 0.5$

Figure 23 shows the effect of the scattering albedo on the total heat flux. Again, the results match properly with those of Sparrow and Cess. As the Figure 23 (a) shows, the heat flux has a very weak dependence on ω when the emissivities of the surfaces are unity, so that both surfaces are black bodies. Figures 23 (b) and (c) show that this dependence increases when the emissivity decreases and that the effect is stronger as radiation gets more important.

2.4.2 Radiative equilibrium

Next the case radiative equilibrium case will be considered. In this case, radiation is the only mechanism of energy transfer and the temperature distribution within the medium, which is steady in equilibrium, results from a balance between the absorption and the emission of radiation. The energy equation then yields

$$\frac{\partial q_R}{\partial z} = 0 \implies q_R = c\,, \tag{2.57}$$

where c is a constant. Therefore, in order to have the condition of radiative equilibrium it is necessary that the radiative heat flux is the same at every point in the domain, its value being determined by the boundary conditions. Although this consideration allows to simplify the equations, the same numerical method exposed previously will be applied to solve the problem. In order to compare with the existing literature, it is convenient to introduce the following dimensionless variable which it is independent of the boundary condition of the top surface:

$$\phi(\tau) = \frac{\sigma T^4(\tau) - B_2}{B_1 - B_2} = \frac{\overline{T^4} - \overline{B_2}}{\overline{B_1} - \overline{B_2}}. \tag{2.58}$$

This quantity is represented in Figure 24 is as a function of the optical coordinate for different values of the optical depth. Again, the agreement with the results reported by Sparrow and Cess is very good.

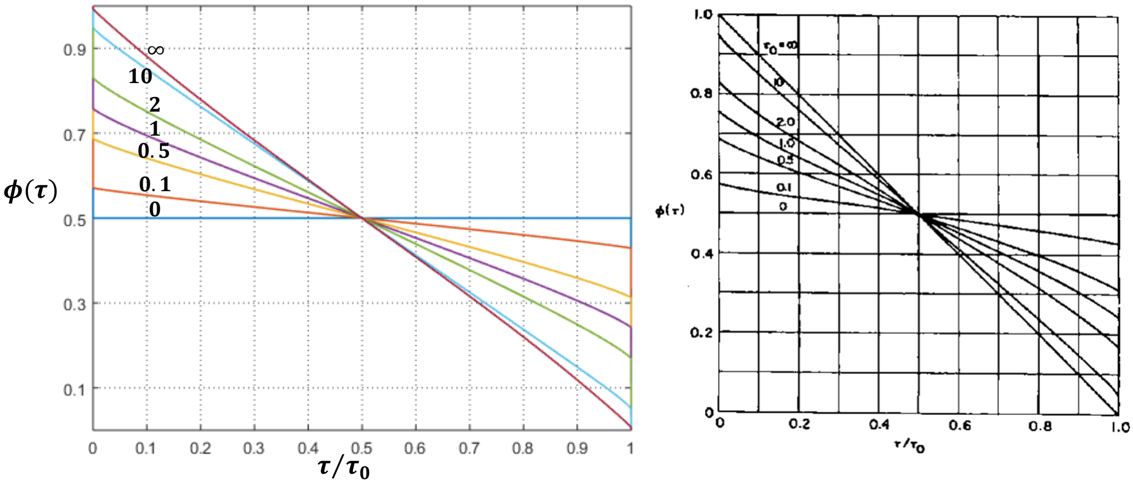

Figure 24: Temperature function for $N_{cr} = 0$, $\varepsilon_1 = \varepsilon_2 = 1$, and boundary condition $T_H = 0.5$. The values for τ_0 are the ones written in the left picture $(0, 0.1, 0.5, 1, 2, 10, \infty)$.

In addition, the temperature profile for two very different values of the optical depth is showed in Figure 25.

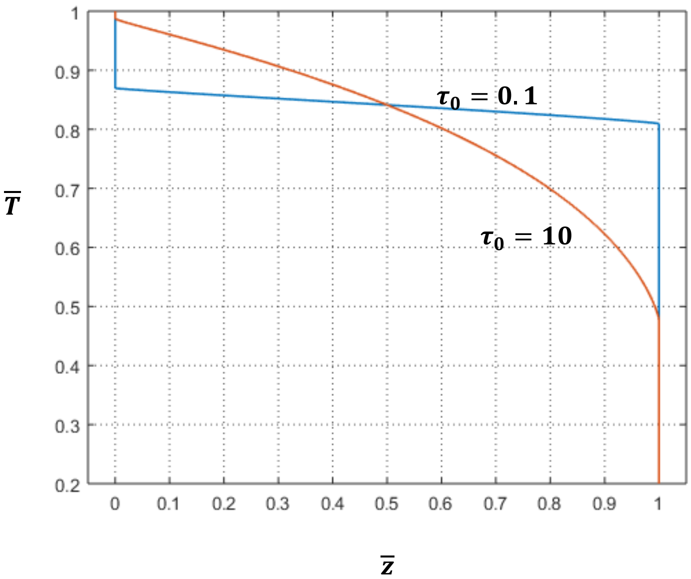

Figure 25: Temperature profiles for radiative equilibrium with values $\varepsilon_1 = \varepsilon_2 = 1$, $N_{cr} = 0$, $\tau_0 = 0.1$ (blue line) and $\tau_0 = 10$ (red line), and boundary condition $T_H = 0.2$.

It is observed that the temperature decreases more rapidly within the medium as it gets opaquer and that there exists a discontinuity in the temperature field at the boundaries. Then, it may be concluded that heat conduction must play here an analogous roll to that of viscosity in the boundary layer, so that the temperature distribution is smooth near the boundaries if heat conduction is taken into account.

2.4.3 Milne-Eddington approximation

The Eddington approximation is based on the assumption that the intensity of radiation is a linear function of μ. It may be used in a "slab medium", that is, a medium in which variables are considered to be constant in planes. Then the intensity would be described by

$$I(\mu, z) = a(z) + \mu b(z) \tag{2.59}$$

where z is the coordinate normal to the slab horizontal planes. This simplification makes use of the moment method, where the m-*th* moment of the intensity is defined by

$$m = \int_{\Omega} I\, \boldsymbol{n_{i1}} \boldsymbol{n_{i2}} \ldots \boldsymbol{n_{im}}\, d\omega \tag{2.60}$$

Thus, the first three moments are denoted as

$$J = \frac{1}{4\pi} \int_{\Omega} I\, d\omega; \qquad H_i = \frac{1}{4\pi} \int_{\Omega} I\, \boldsymbol{n_i}\, d\omega; \qquad K_{ij} = \frac{1}{4\pi} \int_{\Omega} I\, \boldsymbol{n_i} \boldsymbol{n_j}\, d\omega \tag{2.61}$$

so, the Eddington approximation would be equivalent to setting

$$K_{ij} = \frac{1}{3} J \delta_{ij} \tag{2.62}$$

with the assumption that K_{ij} is isotropic.

Introducing these terms into the equations and boundary conditions of the intensity of radiation yields the following system of equations (for a detailed derivation it can consulted the paper by [Aston et al. (2000)])

$$\frac{d\overline{T}}{d\bar{t}} = \frac{d^2\overline{T}}{d\bar{z}^2} - \frac{3\tau_0^2 \chi}{4} \left(\overline{T}^4 - \bar{J} \right), \tag{2.63}$$

$$\frac{d^2\bar{J}^2}{d\bar{z}^2} = -3\tau_0^2 \left(\overline{T}^4 - \bar{J} \right), \tag{2.64}$$

subject to the boundary conditions

$$\bar{J} - \frac{1}{\sqrt{3}\tau} \frac{d\bar{J}}{d\bar{z}} = f^4(\bar{t}), \quad \overline{T} = f(\bar{t}), \quad at\ z = 0, \tag{2.65}$$

$$\bar{J} + \frac{1}{\sqrt{3}\tau} \frac{d\bar{J}}{d\bar{z}} = 0, \qquad \frac{d\overline{T}}{d\bar{z}} = 0, \qquad at\ z = 1, \tag{2.66}$$

where the parameter χ has an opposite meaning to that of N_{cr} in the equations of section 2. Thus, when χ tends to infinity the problem is radiation-dominated, while if it tends to 0, conduction would be the principal mechanism of heat transfer. Both parameters are related by

$$N_{cr} = \frac{4}{3\chi}. \tag{2.67}$$

The temperatures a heat flux profiles obtained by solving numerically equations (2.63)-(2.66) are shown for different parameters of the medium are shown in Figure 26. This figure shows that, despite of the different equations and numerical methods used; the results are quite similar for most of the cases. However, it can be observed that the higher the optical depth is, the more important become the differences between both procedures. This fact is due to numerical issues, so increasing the number of mesh points would improve the results. Thus, we may conclude that the method developed works better for low values of the optical depth has low values, as it the case for most planetary atmospheres.

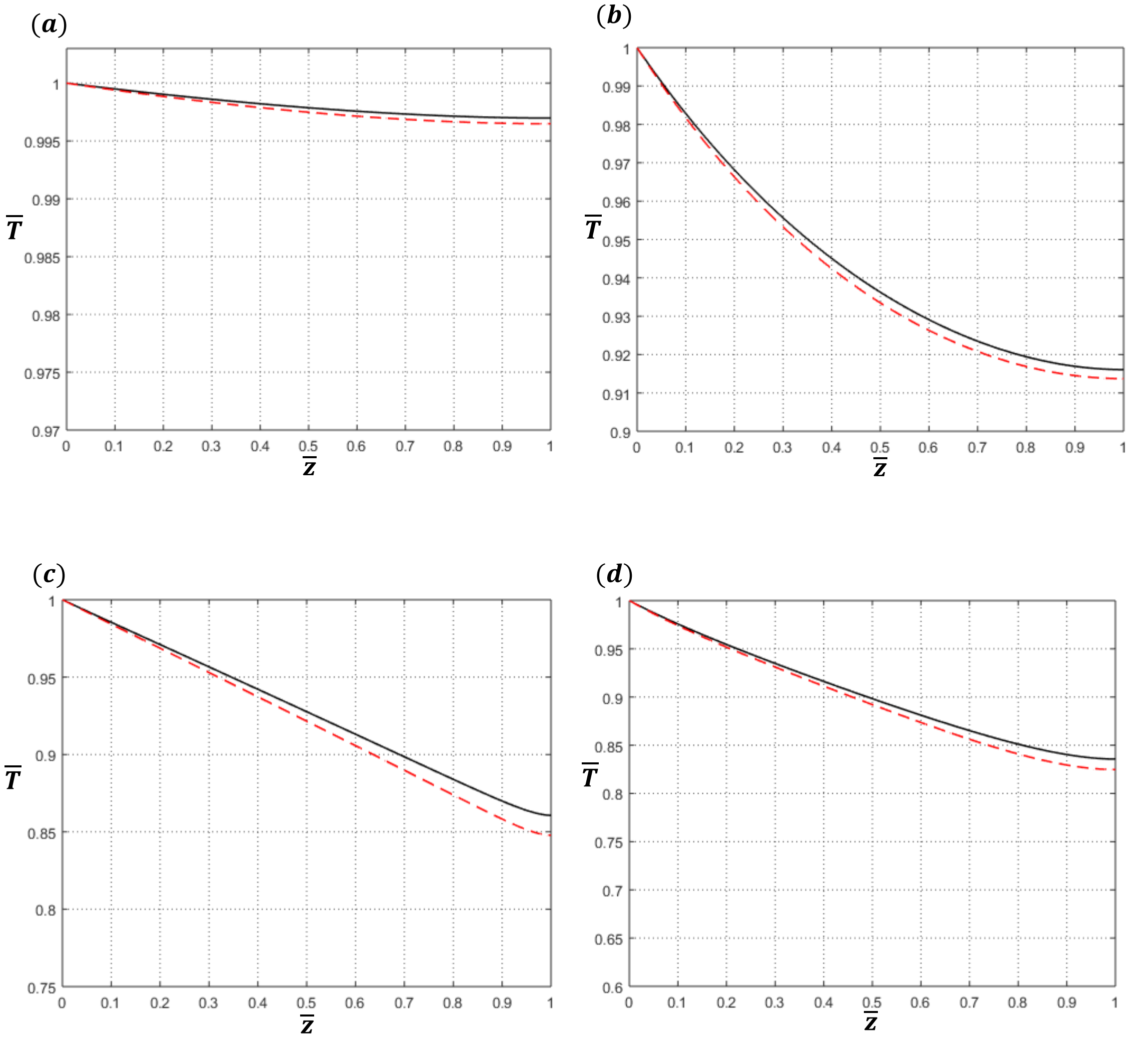

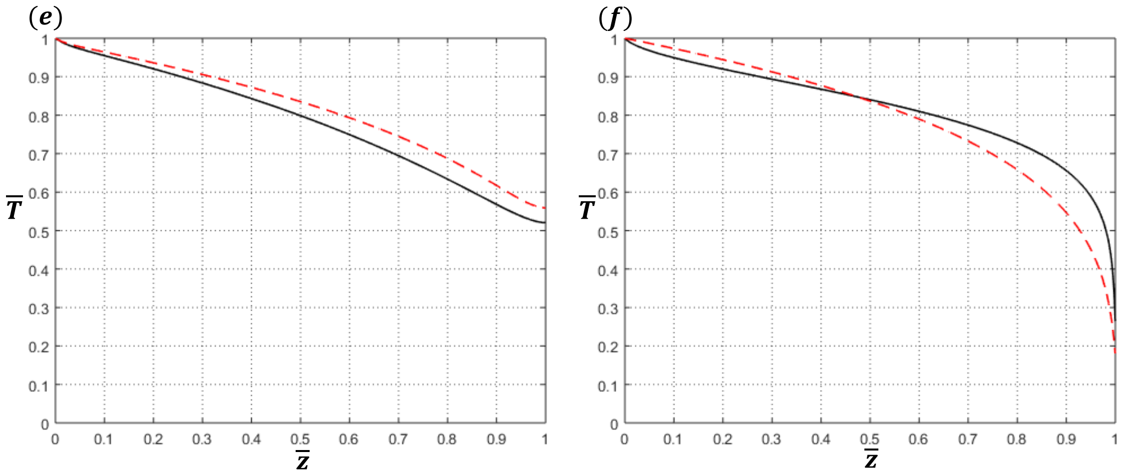

Figure 26: Comparison between the results given by [Aston et al. (2004)] (dashed lines) and the ones obtained by the numerical method (solid lines) for **(a)** $\chi = 0.1$ and $\tau_0 = 0.5$, **(b)** $\chi = 100$ and $\tau_0 = 0.1$, **(c)** $\chi = 0.1$ and $\tau_0 = 15$, **(d)** $\chi = 2$ and $\tau_0 = 2$, **(e)** $\chi = 10$ and $\tau_0 = 10$, **(f)** $\chi = 100$ and $\tau_0 = 1000$.

2.4.4 Transient state

Many applications of thermal radiation require the study of a transient state since, in general, the boundary conditions change with time. That is the case of planetary atmospheres, where the incident radiation, and therefore the surface temperature, depends cyclically on time. In these cases, the transient state acquires great important, as it is the predominant regime.

Although this topic will be treated in depth later, here the unsteady state will be validated by proving that there only exists a unique steady solution for certain boundary conditions. Then, in this section the boundary conditions will be fixed for the different cases, what fixes the unique steady state, and, for each case, give several initial conditions. In this way it can observed that for the steady state, the temperature profile is the same regardless of the starting state. However, the initial conditions will affect the time evolution at each point of the atmosphere, since the increments of temperature will change depending on the difference between the initial and final values.

As can be seen in the figures 27 and 28 the instantaneous temperature which is reached at a given point depends strongly on the initial state, and so does the tendency of the evolution. For instance, figures 27 (a) and 28 (a) show that the temperature near $z = 0.8$ tend to decrease with time, as the initial value of the temperature was higher than the final one, while for 27 and 28 (b) the opposite occurs. However, it can be noted that for all cases, the final state (steady state) is exactly the same. Thus, it can be finally concluded that, although the evolution of the temperature profile does depend on the initial condition, this is not the case for the steady state, which is unique for given parameters and boundary conditions.

To sum up, in this section it has been proved that, as expected, the numerical method developed is reliable enough, since the obtained results match properly those of the literature, and gives an unique solution for the steady state, independently of the initial temperature profile.

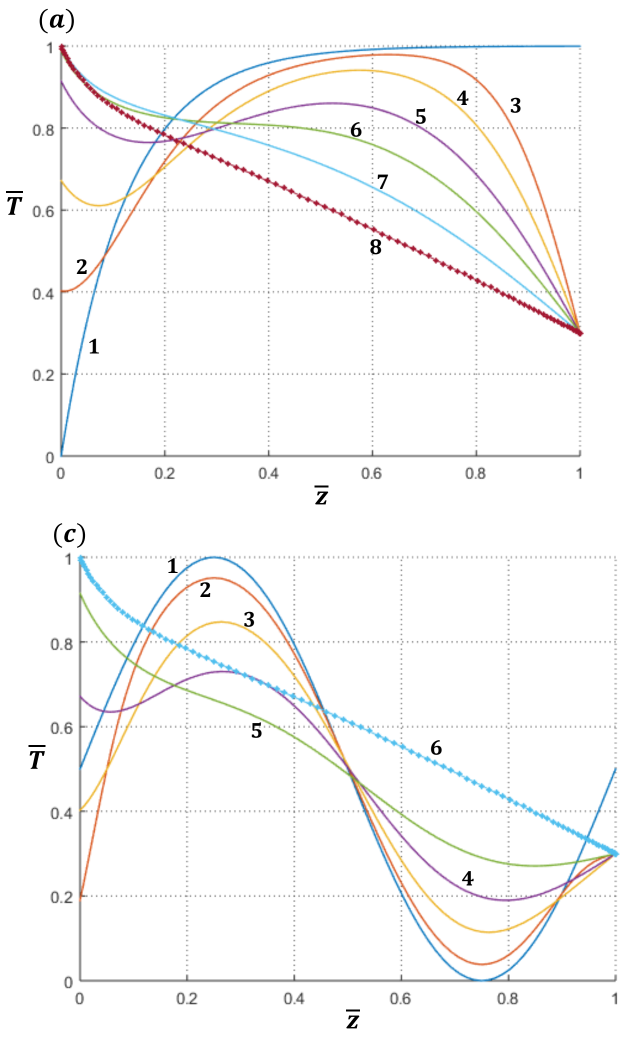

	$\overline{t}$
exp	60.43
constant	65.83
sine	59.35

Figure 27: : Temperature evolution with time for **(a)** an inverted exponential $(\overline{T}_0(\overline{z}) = 1 - e^{-8\overline{z}})$, **(b)** flat $(\overline{T}_0(\overline{z}) = 0)$ and **(c)** sine $(\overline{T}_0(\overline{z}) = 0.5 + \sin(2\pi\overline{z}))$ initial condition with parameters values $N_{cr} = 2$ and $\tau_0 = 10$. The numbers represent the order of the evolution. $\overline{t}$ is the characteristic dimensionless time to reach the steady state.

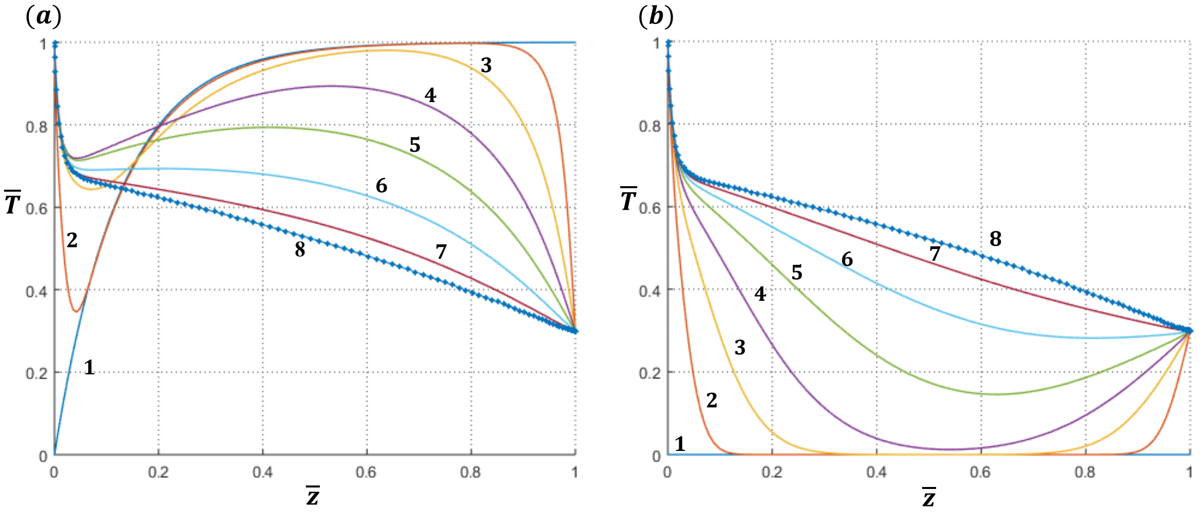

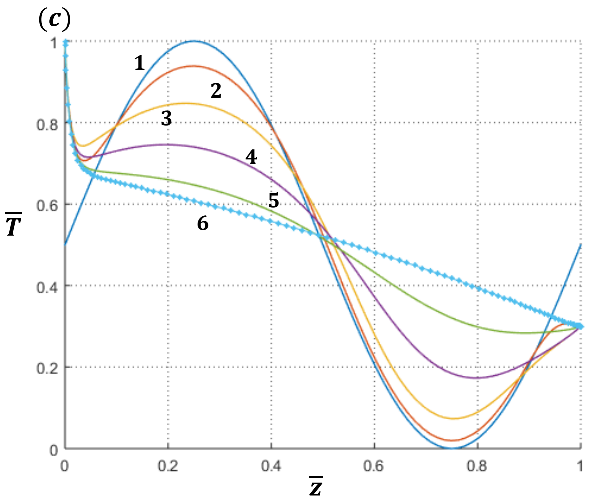

	$\bar{t}$
exp	3254
constant	3622
sine	2485

Figure 28: Temperature evolution with time for **(a)** an inverted exponential $\left(\overline{T}_0(\overline{z}) = 1 - e^{-8\overline{z}}\right)$, **(b)** flat $\left(\overline{T}_0(\overline{z}) = 0\right)$ and **(c)** sine $\left(\overline{T}_0(\overline{z}) = 0.5 + \sin(2\pi\overline{z})\right)$ initial condition with parameters values $N_{cr} = 0.5$ and $\tau_0 = 50$. The numbers represent the order of the evolution. $\bar{t}$ is the characteristic dimensionless time to reach the steady state.

3 RADIATION-CONDUCTION-CONVECTION PROBLEMS APPLIED TO THE ATMOSPHERIC THERMAL STRUCTURE

3.1. Introduction

Once the numerical method has been developed and tested in the previous chapter, it will be applied in this chapter to some practical cases related to the thermal structure of the Earth's atmosphere, whose physics was introduced in section 3 of chapter 1. Firstly, a simple atmospheric model with a uniform absorption coefficient and an atmosphere without convection will be considered and the results obtained will tested with those of the literature [Satoh (2014), Visconti (2001)]. After this, the unrealistic hypotheses of a constant absorption coefficient is replaced by that of a height dependent coefficient, which will improve the veracity of the solutions, and the transient responses of the non-convective atmosphere to several types of changes in the solar radiative flux incident on the Earth's surface are analysed. Finally, the effects of convection are included and the transient evolution of a convective-radiative atmosphere towards the current steady state – the Standard Atmosphere - is computed and the results compared with those of the literature [Manabe & Stikcler (1963)]

It is important to say that in this chapter equations and magnitudes are not expressed in terms of z , as in the previous ones, but in terms of the optical thickness, τ. When β is constant, the optical thickness and the height have a similar physical meaning, as they represent exactly the same thing but scaled by the absorption coefficient However, when β is variable, the relation between z and τ becomes complicated and unknown a priori. In this case, the optical thickness is the natural variable to use in the formulation of the radiation problem as it takes into account both the height and the absorption coefficient value at that height.

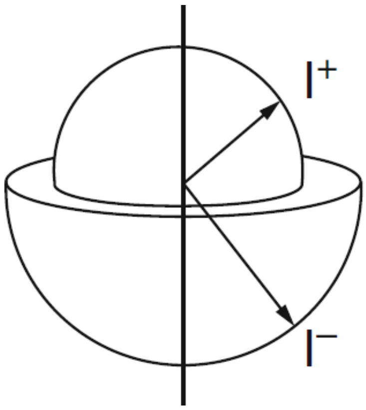

Figure 29: Pictorial representation of the isotropic hemispheres of the intensity of radiation

3.2. Radiative atmosphere with constant absorption coefficient

In this section the numerical method developed in the previous chapter will be applied to determine the thermal structure of an atmosphere in radiative equilibrium and with a constant absorption coefficient. The results will be compared with those obtained by the use of the so called "two stream" approximation [Satoh (2014)], in which the equation of radiative transfer (1.35) is solved assuming that the radiant intensity is uniform in each hemisphere (see figure 29). The two-stream approximation provides an analytical solution for the temperature field which will be reviewed next - more detailed presentations can be found in Satoh (2014) or Visconti (2001). If I^+ and I^- denote the (assumed uniform) radiant intensities in the upper and lower hemispheres (see figure 29), the upwards and downwards heat fluxes are respectively $q_R^+ = \pi I^+$ and $q_R^- = \pi I^-$, respectively. Thus, multiplying equations (2.5) and (2.7) by $2\pi\mu$ and integrating with respect to μ between 0 and 1 yield

$$-\frac{2}{3}\frac{dq_r^+(\tau)}{d\tau} = q_r^+(\tau) - \pi S\big(T(\tau)\big)\,, \tag{3.1}$$

$$\frac{2}{3}\frac{dq_r^-(\tau)}{d\tau} = q_r^-(\tau) - \pi S\big(T(\tau)\big), \tag{3.2}$$

and the net radiative flux of planetary radiation is given by

$$q_r(\tau) = q_r^+(\tau) - q_r^-(\tau). \tag{3.3}$$

Throughout this chapter it will be assumed that the Earth's surface emits as a black body and that the top of the atmosphere is transparent to radiation, so that all radiation incident upon escapes to free space. Thus, the boundary conditions for (3.1)-(3.2) are

$$q_r^+(0) = \sigma T_0^4, \quad q_r^-(\tau_0) = 0, \tag{3.4}$$

where τ_0 is the optical depth at the top of the atmosphere. In order to simplify the model as much as possible, it will be assumed that the total radiative flux in the atmosphere is formed by the sum of the fluxes from just two sources: planetary and solar radiation (see figure 30). Thus,

$$\overline{q_r} = q_r - (1-A)q_{r_S}\,, \tag{3.5}$$

where q_{r_S} is the solar flux, A is the albedo of the planet and $\overline{q_r}$ is the horizontal mean upward radiative flux. The albedo is defined as the ratio between the amount of solar flux which is reflected in the surface and the total solar flux which reaches it.

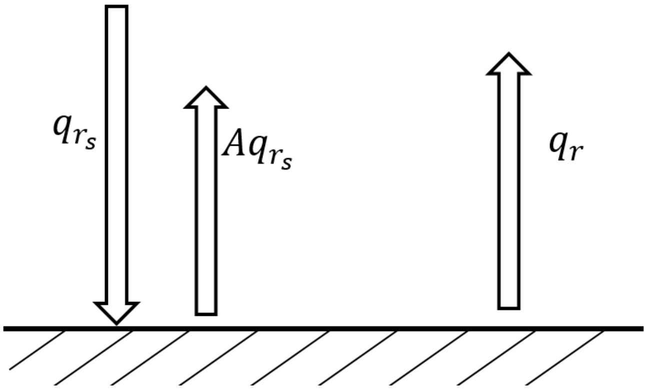

Figure 30: Representation of the sources reaching and leaving the Earth.

Since the atmosphere is assumed to be in radiative equilibrium, equation (2.57) must be satisfied, so that equation (3.5) yields

$$\overline{q_r} = c\,. \tag{3.6}$$

In particular, if there is not a radiative heat source neither in the atmosphere nor in the solid planetary system, the horizontal mean upward radiative flux must be zero $(c = 0)$, and (3.5) and (3.6) yield

$$\overline{q_r} = 0 \implies q_r = (1 - A)q_{r_S}\,. \tag{3.7}$$

Taking into account (3.3) and (3.7) together with the boundary conditions (3.4), equations (3.1)-(3.2) can be easily solved for the upward and downward fluxes to yield

$$q_r^+(\tau) = \frac{q_r}{2}\left(\frac{3}{2}(\tau_0 - \tau) + 2\right), \tag{3.8}$$

$$q_r^-(\tau) = \frac{q_r}{2}\frac{3}{2}(\tau_0 - \tau). \tag{3.9}$$

Finally, taking into account that for a non-scattering atmosphere ($\omega = 0$), the source function is $S = \sigma T^4/\pi$, and combining equations (3.1)-(3.2) and (3.7) -(3.9), the temperature profile can be obtained as a function of the optical thickness as

$$T(\tau) = \left[\frac{(1 - A)q_{r_S}}{2\sigma}\left(\frac{3}{2}(\tau_0 - \tau) + 1\right)\right]^{\frac{1}{4}}. \tag{3.10}$$

Observe that the surface temperature, T_0, obtained from equation (3.8) and the boundary condition (3.4) is higher than the temperature at $\tau = 0$ given by (3.10), so that

$$T_0 = \left[\frac{q_r}{2\sigma}\left(\frac{3}{2}\tau_s + 2\right)\right]^{\frac{1}{4}} > \left[\frac{q_r}{2\sigma}\left(\frac{3}{2}\tau_0 + 2\right)\right]^{\frac{1}{4}} = T(\tau = 0), \tag{3.11}$$

which indicates that there exists a jump in the temperature profile near the ground surface. As explained in chapter 2, this non-physical fact stems from the fact that heat conduction has been neglected in the analysis. Also note that in case the absorption coefficient does not vary with height $\big(\beta \neq \beta(z)\big)$, the relation between τ and z is linear $(\tau = \beta z)$, so that

$$(\tau_0 - \tau) = \tau_0(1 - \overline{z}) \tag{3.12}$$

where $\overline{z} = z\beta/\,\tau_0$, and equation (3.10) can be written as

$$T(\overline{z}) = \left[\frac{(1 - A)q_{r_S}}{2\sigma}\left(\frac{3}{2}(1 - \overline{z})\tau_0 + 1\right)\right]^{\frac{1}{4}} \tag{3.13}$$

which yields the temperature as a function of height.

After an analytical solution for the temperature profile has been found, it will be compared with the solution provided by the numerical method developed in chapter 2. In order to do this, first the temperature will be nondimensionalized using the effective temperature, $T_e = \left[(1-A)q_{r_S}/\sigma\right]^{\frac{1}{4}}$, instead of the surface temperature. The last row of the matrix (2.39) must be modified according to equation (2.41) to satisfy the zero radiosity condition at the upper surface imposed by de second equation in (3.4), and the emissivity of the lower surface will be set equal to one in order to satisfy the black body condition of the Earth's surface. In addition, since, the known solar heat flux absorbed by the ground surface, $(1-A)q_{r_S}$, will be imposed as boundary condition instead of the value of the surface temperature,, the first rows of the matrices B, C and vector **b** in (2.50) must be modified as follows:

$$B(1,:) = 0, \qquad b(1) = 1,$$
$$C(1,:) = \underbrace{\frac{1}{\pi}\left(\boldsymbol{a}_{\boldsymbol{B1}} - 2\pi\boldsymbol{a}(1-\omega) - \frac{\omega}{2}\boldsymbol{a}\underline{M_G}\right)}_{\overline{q_{r0}}}. \qquad (3.14)$$

Finally, at the top of the atmosphere a null variation with height of the temperature will be assumed since, as mentioned in chapter 1, in the upper layers of the troposphere –the tropopause– the temperature remains practically constant with height, as can be seen in figure 31 corresponding to the International Standard Atmosphere (ISA). This condition is achieved by (2.53).

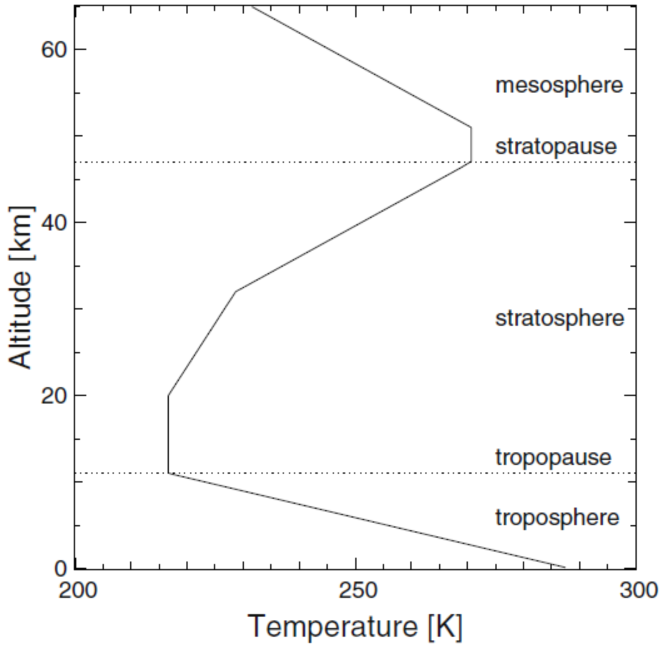

Figure 31: ISA temperature profile.

The good agreement of the results obtained with the two-stream approximation [Satoh (2014)] and with the numerical method are shown in Figure 32 for the cases of atmospheres with low τ_0 (transparent), intermediate τ_0 and high τ_0 (opaque), respectively. Note that the lower the optical depth, the flatter becomes the temperature profile. In fact, in the opaque case, the temperature gradient is quite high at the top of the atmosphere yielding an unstable thermal equilibrium which may induce convection (see section 3). The augmentation of the temperature gradient with the optical depth takes place because of the increase of the absorption coefficient, which reduces the efficiency of radiation as a mechanism of energy transport.

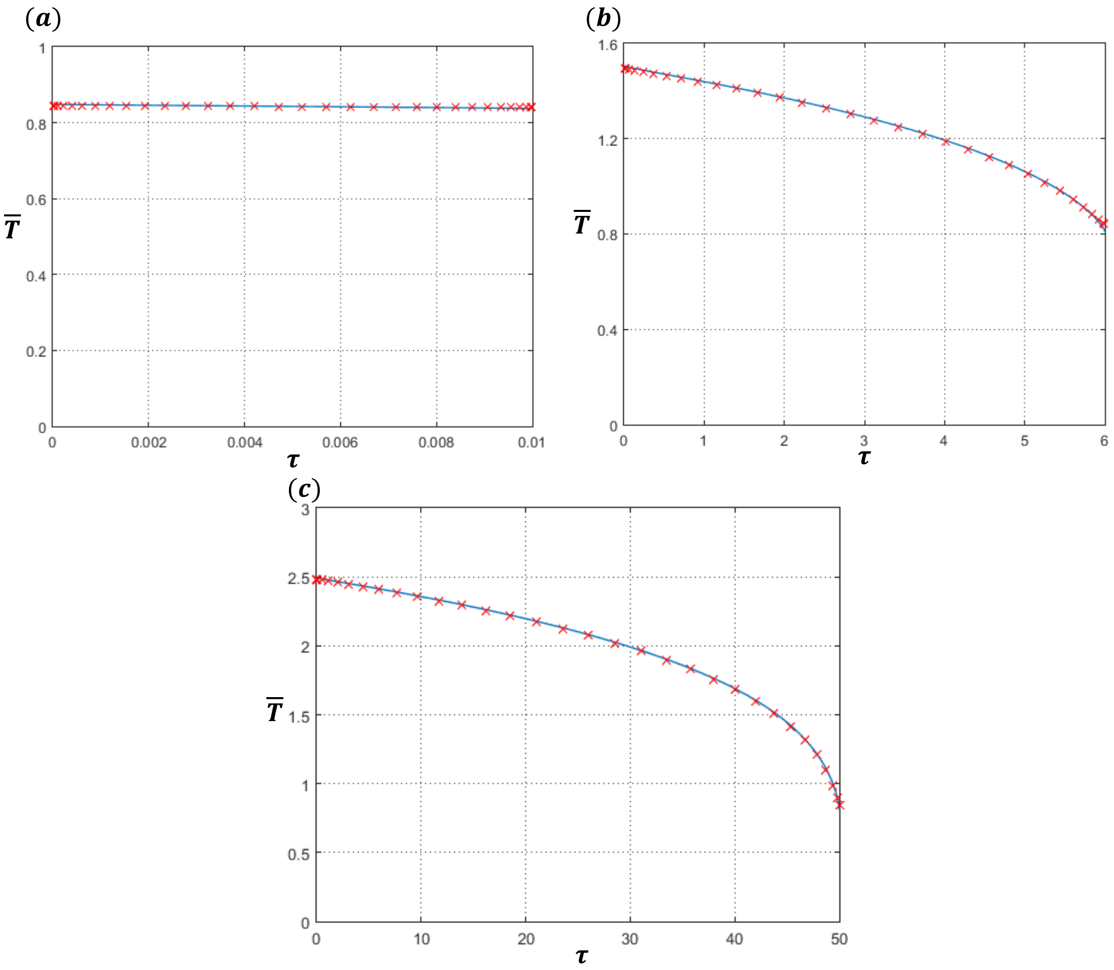

Figure 32: Comparison between results obtained by the numerical method (blue line) and those from Satoh (red crosses) for atmospheres in radiative equilibrium and uniform absorption coefficients. The values of the atmospheric optical thicknesses are **(a)** $\tau_0 = 10^{-2}$, **(b)** $\tau_0 = 6$ and **(c)** $\tau_0 = 50$.As one can observe, given solutions from the two different procedures are quite similar for the three cases.

3.3. Radiative atmosphere with variable absorption coefficient

The case of uniform absorption coefficient considered in the previous section is a very unrealistic one. In fact, the amount of radiation absorbed by the different layers of the atmosphere depends on its composition, especially on the distribution of absorbing constituents, such as CO_2, O_2, O_3 or H_2O. In this section a simplified atmospheric model with a height-dependent absorption coefficient will be analyzed by assuming that, as explained in section 3 of chapter 1, water vapor can be considered in good approximation as the sole absorber of infrared radiation in the troposphere. Thus, the absorption coefficient defined in the equation (1.48) will be used from now on in this chapter.

Using expressions (1.44) and (1.48), and differentiating respect to τ, equation (2.47) yields

$$\frac{D\overline{T}}{D\overline{t}} = \overline{p}^{\alpha} N_{cr} \frac{d}{d\tau}\left(\overline{\rho}\,\overline{p}^{\alpha}\frac{d\overline{T}}{d\tau}\right) - \overline{p}^{\alpha}(1-\omega)\left(\overline{T}^{4} - \frac{G(\tau)}{4\sigma T_e^4}\right) \tag{3.15}$$

where N_{cr} is defined as it was in chapter 2 but using β_e as the reference absorption coefficient. To close the problem, the hydrostatic equilibrium equation and the equation of state are used. It is easy to show that the hydrostatic equilibrium equation yields the pressure as a function of the optical depth as

$$\frac{\overline{p}^{\alpha+1}-1}{\alpha+1}=-\frac{\rho_e g}{p_s\beta_s}\tau \Rightarrow \overline{p}=\left(1-\frac{\tau}{\tau_0}\right)^{\frac{1}{1+\alpha}} \tag{3.16}$$

where the optical depth of the atmosphere in is given by

$$\tau_0=\frac{p_s\chi q_{as}R_g T_e}{g(1+\alpha)} \tag{3.17}$$

while the equation of state is

$$\frac{\overline{p}}{\overline{\rho}}=\overline{T} \tag{3.18}$$

In the previous equations the reference density, ρ_e, has been defined through the equation $p_s/\rho_e=R_gT_e$. Note that equations (3.15)-(3.16) and (3.19) permit to determine the temperature, pressure and density and, therefore, the absorption coefficient, as a function of τ. The relation between the height and the optical thickness is can be obtained by integration of the differential equation $dz=d\tau/\beta$.

The three cases represented in figure 33 show how the normalized absorption coefficient behaves with respect the normalised optical thickness for different kinds of atmospheres. As can be seen in the figure, the function tends to be linear for small values of τ_0 (transparent atmosphere), while for large values of opaque atmosphere, this linearity disappears, especially at the top of the atmosphere, where the presence of water vapour is negligible.

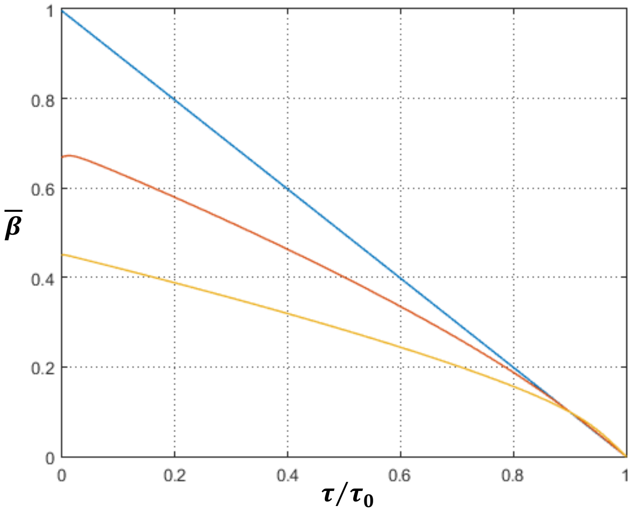

Figure 33: Representation of the normalized absorption coefficient for opaque atmosphere (yellow line), medium atmosphere (red line) and transparent atmosphere (blue line).

Figure 34 shows, for parameters values typical of the Earth's atmosphere ($\tau_0=4$ and $\alpha=4$), the temperature profiles obtained by the two-stream approximation [Satoh (2014)] and by using the numerical method developed in chapter 2 applied to equations (3.15)-(3.16) and (3.19). Observed the good agreement between the two solutions except in the outermost layers, which may be due to the approximate character of the two stream equations.

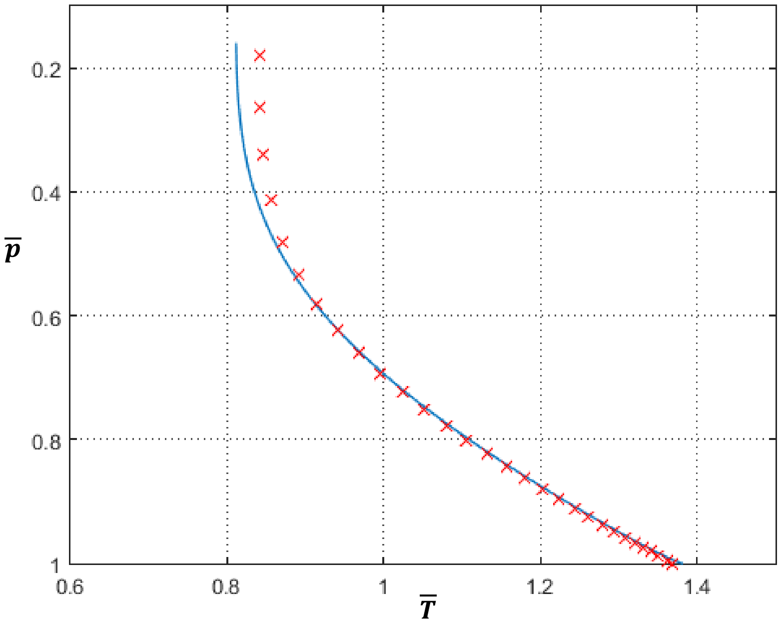

Figure 34: Comparison of numerical (blue line) and Satoh (red dashed line) solution for a variable absorption coefficient. The values of the parameter are characteristic of the atmosphere: $\tau_0 = 4$, $\alpha = 4$ and $N_{cr} = 0.1$.

Figure 35 shows the effects τ_0 and α have on the relation between the distributions of pressure and temperature. Observe that the larger α, the lower is the temperature for a given value of the pressure, except at the ground. This is due to the fact that as α increases the water vapor gets more concentrated near the surface, and so do the higher temperatures due to the absorption of radiation. On the other hand, the increase of τ_0 originates larger temperatures for a given pressure, even at the ground, due to the augmented radiation absorption. a similar effect, but it also affects to the ground values. Also note that none of these parameter affects the temperature at the top of the atmosphere as it only depends, according to equation (3.10), on the radiative flux, which remains constant for all cases.

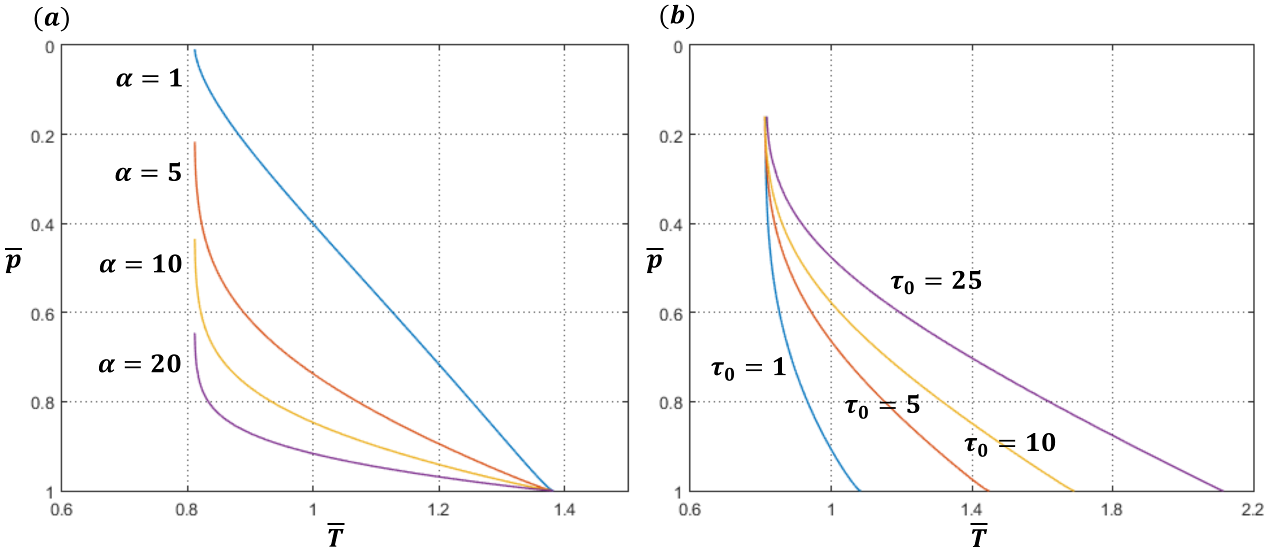

Figure 35: Pressure vs. temperature distributions for an atmosphere with a variable absorption coefficient. Parameters values are: **(a)** $\tau_0 = 4, \alpha = 1, 5, 10, 20$ and **(b)** $\alpha = 4, \tau_0 = 1, 5, 10, 25$.

Finally, we compare the temperature profiles for the variable and the constant absorption coefficient

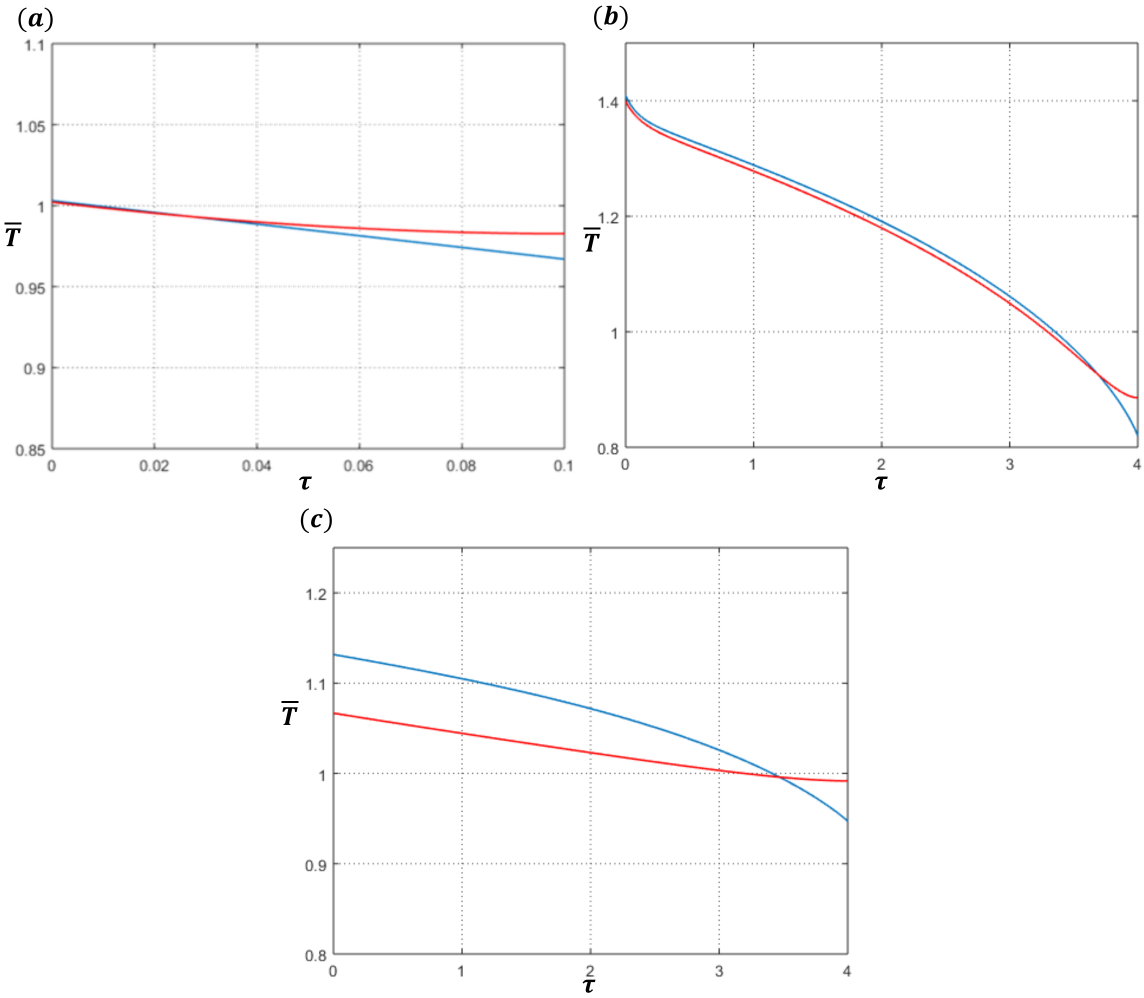

Figure 36: Temperature profiles for constant (blue line) and variable (red line) absorption coefficient. The parameter values are **(a)** $\tau_0 = 0.1$ and $N_{cr} = 0.1$, **(a)** $\tau_0 = 4$ and $N_{cr} = 0.1$ and **(a)** $\tau_0 = 4$ and $N_{cr} = 10$.

It can be observed that for the terrestrial case, the temperature profiles are quite similar independently of the absorption coefficient. However, for cases in which the radiation is less effective, that is, for higher values of τ_0 and N_{cr} the profiles tend to separate, so using a realistic absorption coefficient become quite important.

3.4. Time evolution of a radiative-conductive atmosphere

After having validated the numerical method with several known steady solutions, it will be applied in this section to analyse some unsteady situations for hypothetical radiative-conductive atmospheres. The analysis of the transient response is essential in a dynamical model of the atmosphere, as that solar radiative flux incident on a given portion of the planet's surface varies on a daily basis. Two kinds of model simulations will be carried out in this section. The first one –which will be called *heat impact*– analyses the transient response of the atmosphere of an initially very cold planet when the stellar radiative flux incident on the planet's surface suddenly increases from zero to a given value. The second simulation considers the more realistic and familiar situation in which the incident stellar radiative flux varies cyclically on a given area of the planet's surface.

3.4.1 Heat impact

The thermal atmospheric structures corresponding to different stages during the evolution of several transparent atmospheres under a heat impact are represented in figure 37. The atmospheres are characterized by the same, low value of the optical depth and by different values of the conduction-radiation parameter N_{cr} . It can be observed in figure 37.a that when thermal radiation is the only mechanism of energy transfer, the evolution of the outermost layers, where the absorption coefficient is very small due to the decrease of the concentration of the absorbing constituents, is much slower than that of the innermost ones, where the absorption coefficient is larger. Thus, the outer layers are the ones that control the time taken by the atmosphere to reach the radiative equilibrium. On the other hand, it can be observed in figures 37.b-37.d that, as expected, for increasing heat conduction the temperature profiles become more homogeneous within the whole atmosphere and the evolution towards the radiative-conductive equilibrium is faster.

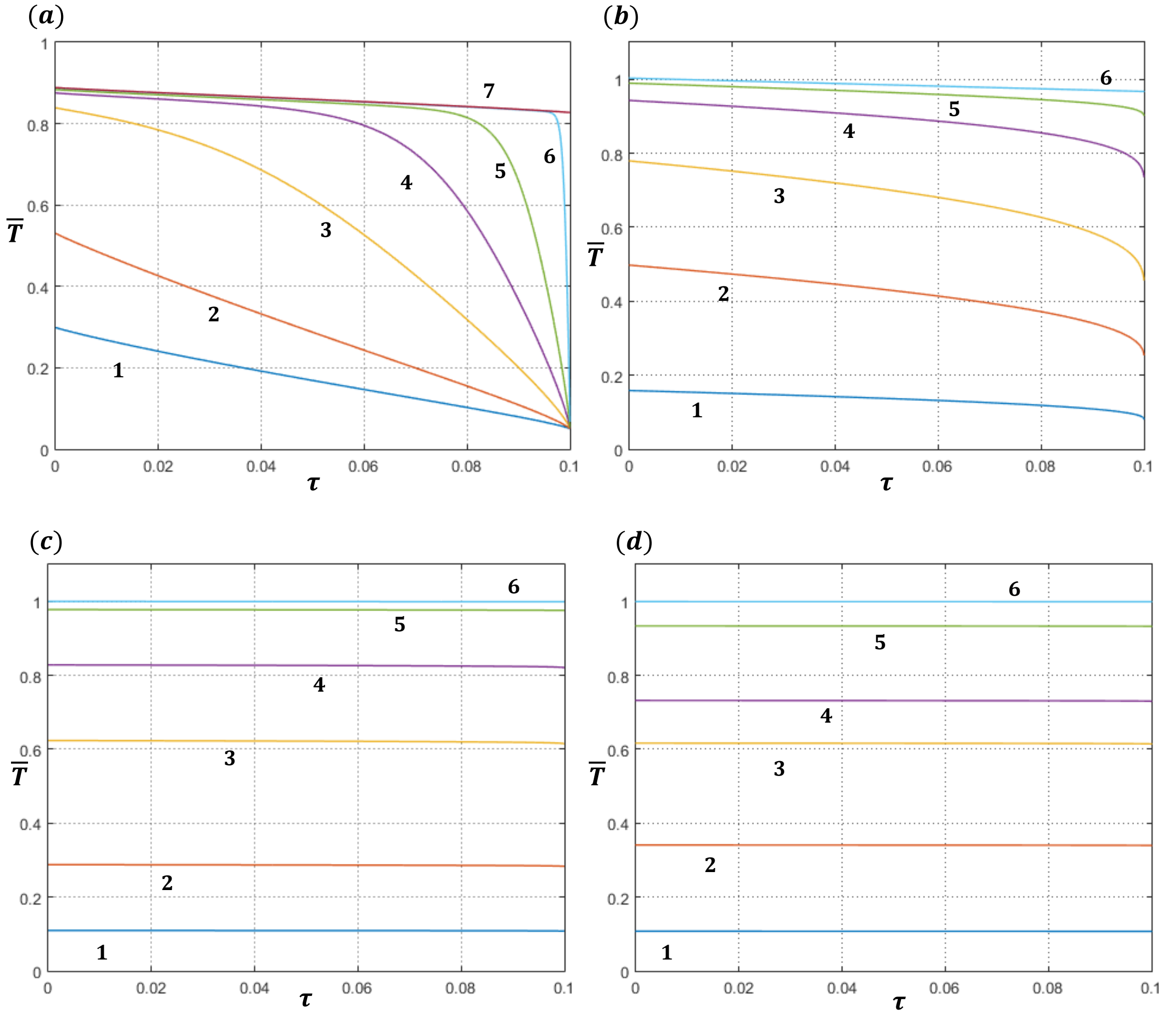

Figure 37: Temporal evolution of the temperature profiles for a transparent atmosphere ($\tau_0 = 0.1$) and $N_{cr} = 0$ **(a)**, $N_{cr} = 0.1$ **(b)**, $N_{cr} = 5$ **(c)** and $N_{cr} = 20$ **(d).** The numbers represent different stage of the evolution.

Figure 38 show the different stages of the response to a heat impact of different atmospheres with the same moderate value of the optical depth (semi-transparent atmosphere) and different values of N_{cr}. This case is especially interesting since the typical values of the optical depth for the Earth are in this range. It can be anticipated that, since the increasing of the optical depth reduces the effectiveness of the radiative energy transport, the times taken by the different atmospheres to reach the steady state will be longer than those corresponding to the previous, transparent case. In addition, this increase changes the way in which the temperature profiles evolve to the steady state, as can be seen by comparing figures 37.a and 38.a.

For the case of figure 37.a, in which radiation is very effective, the evolution begins with a linear temperature profile which deforms during de evolution but remaining smooth inside the atmosphere. However, at the optical depth increases (figure 38.a), also does the difference between the absorption coefficient between the inner and the outer atmospheric layers, which eventually leads to a large increase of the temperature of the inner layers which propagates outwards in the form of a heat wave. Although the case N_{cr}=0 is the most relevnt for the Earth's atmosphere, figures 38.b-38.c show that for increasing N_{cr} the effects of heat conduction in smoothing the temperature gradients and in shortening the characteristic time for the evolution also increase. However, this effects of the increase of N_{cr} are less pronounced than that in the case of a transparent atmosphere.

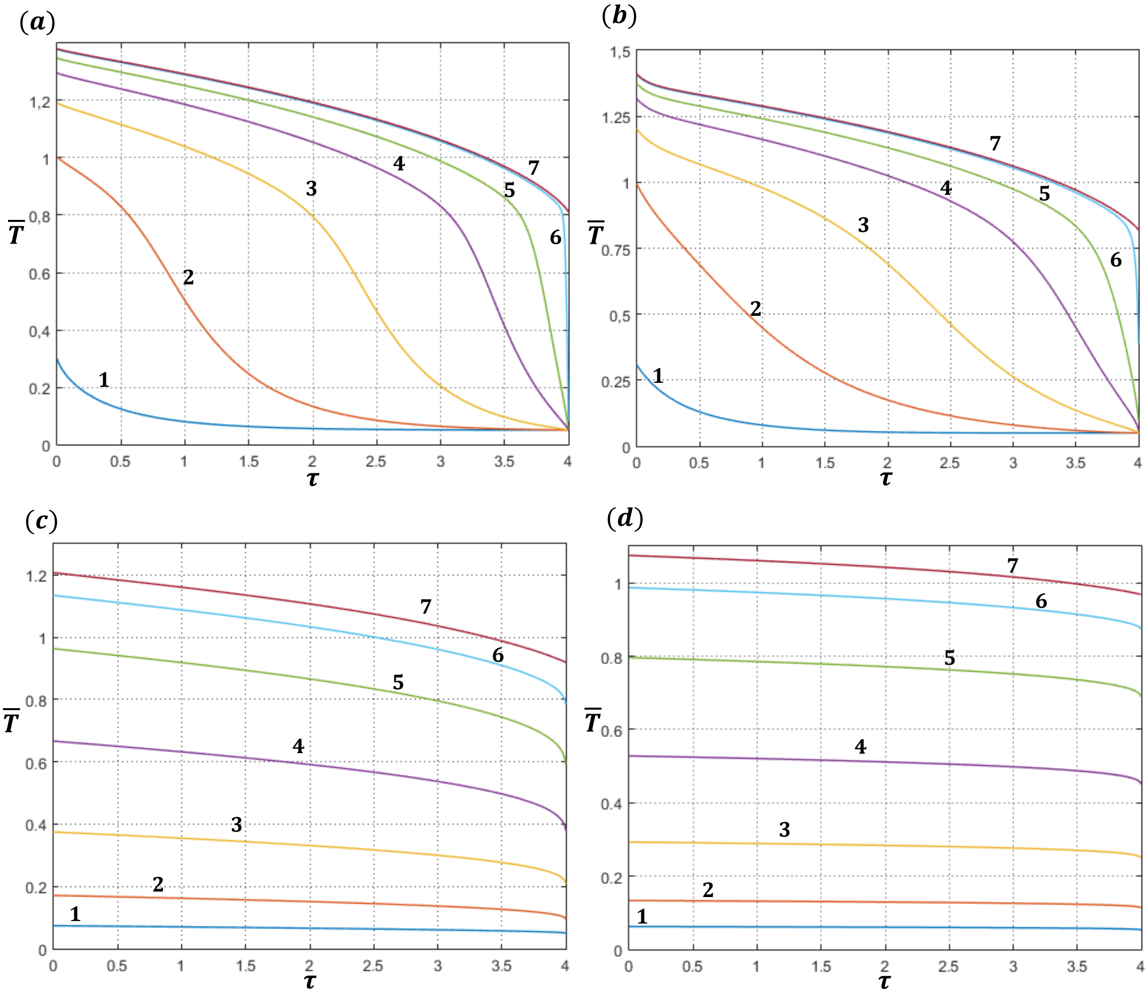

Figure 38: Temporal evolution of the temperature profiles for a transparent atmosphere ($\tau_0 = 4$) and $N_{cr} = 0$ **(a)**, $N_{cr} = 0.1$ **(b)**, $N_{cr} = 5$ **(c)** and $N_{cr} = 20$ **(d).** The numbers represent the order of the evolution.

Finally, as shown in figure 39, the features of the evolution of opaque atmospheres are qualitatively similar, but more pronounced, to those with an intermediate optical depth (figure 38) discussed in the previous paragraph.

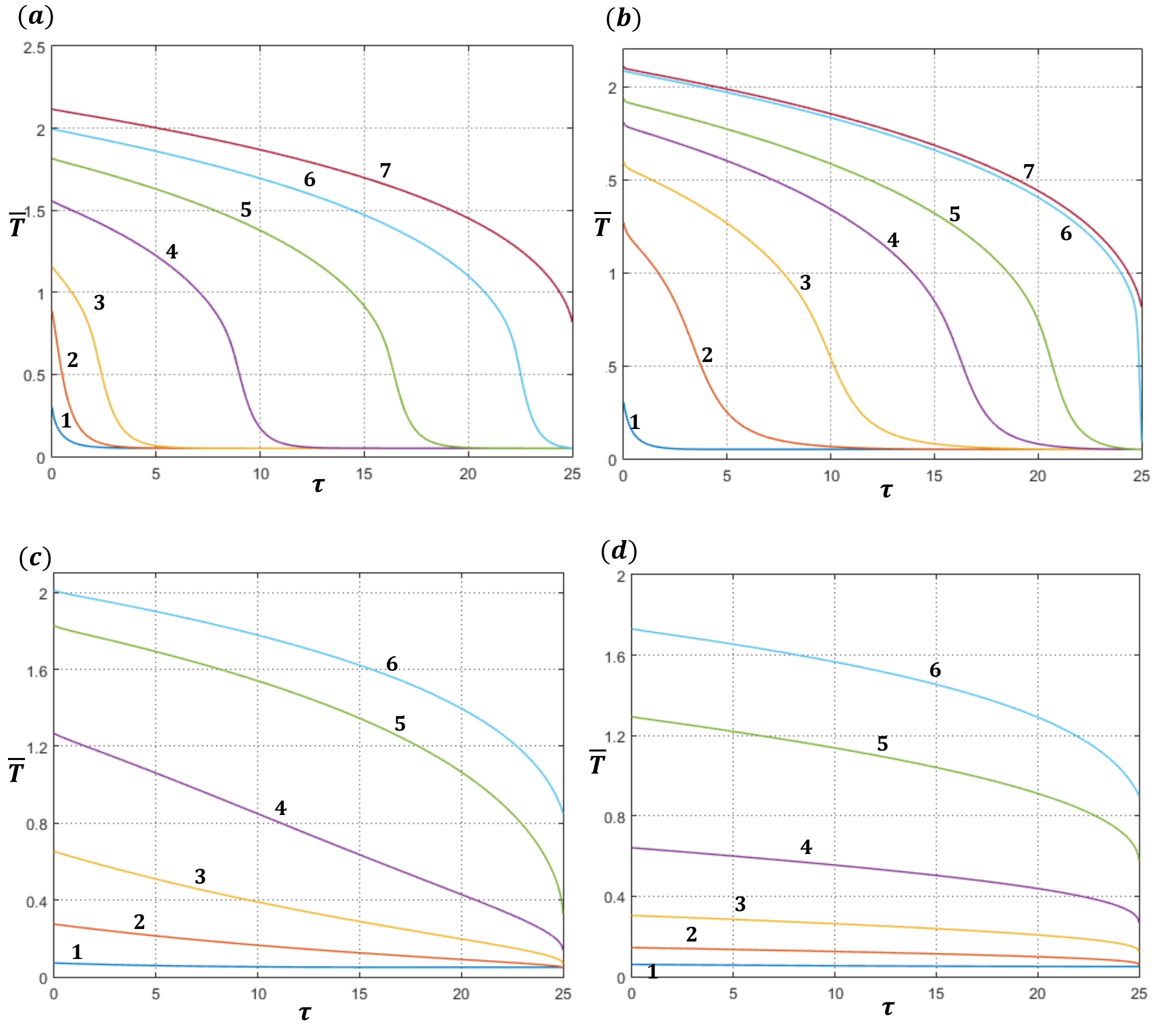

Figure 39: Temporal evolution of the temperature profiles for a transparent atmosphere ($\tau_0 = 25$) and $N_{cr} = 0$ **(a)**, $N_{cr} = 0.1$ **(b)**, $N_{cr} = 5$ **(c)** and $N_{cr} = 20$ **(d).** The numbers represent the order of the evolution.

The dimensionless times elapsed until the transient responses to a heat impact of the different atmospheres considered in this subsection reach almost the steady state are listed in the table of figure 40. It can be observed that, as discussed in the previous paragraphs, the effect of increasing heat conduction is to decrease the time for the evolution, while the increase of the optical depth has the opposite effect.

		N_{cr}			
		0	0.1	5	20
τ_0	0.1	6678.9	18.8	8.34	8.23
	4	7200.1	1332.3	303.7	269.45
	25	7425.8	4655.6	1789.5	1655

Figure 40: Value of the dimensionless time taken to reach the steady state, starting from a null temperature profile.

To end up this section, the time evolution of temperature profiles at different atmospheric heights will be analysed. We are especially interested in the Earth case, so the temperature time evolutions of an atmosphere with parameters values similar to those of the Earth will be compared with those of a more unrealistic one – higher value of real case and a more unrealistic one (with a higher value of N_{cr}). In figure 41, two differentiate time scales have been considered: that of the upper layers (figures 41.a and 41.c) and that of the lower and intermediate layers (figures 41.b and 41.d). As can be seen in the figures these scales differ by about two orders of magnitude for the case of the Earth ($N_{cr} = 0$ and $\tau_0 = 4$, figures 41.a and 41.b) and by one order of magnitude for the radiative-conductive atmosphere ($N_{cr} = 0.1$ and $\tau_0 = 4$, figures 41.a and 41.b). This figure also illustrates that the effect of heat is to increase the time for the lower layers to reach the state and to decrease that for upper layers.

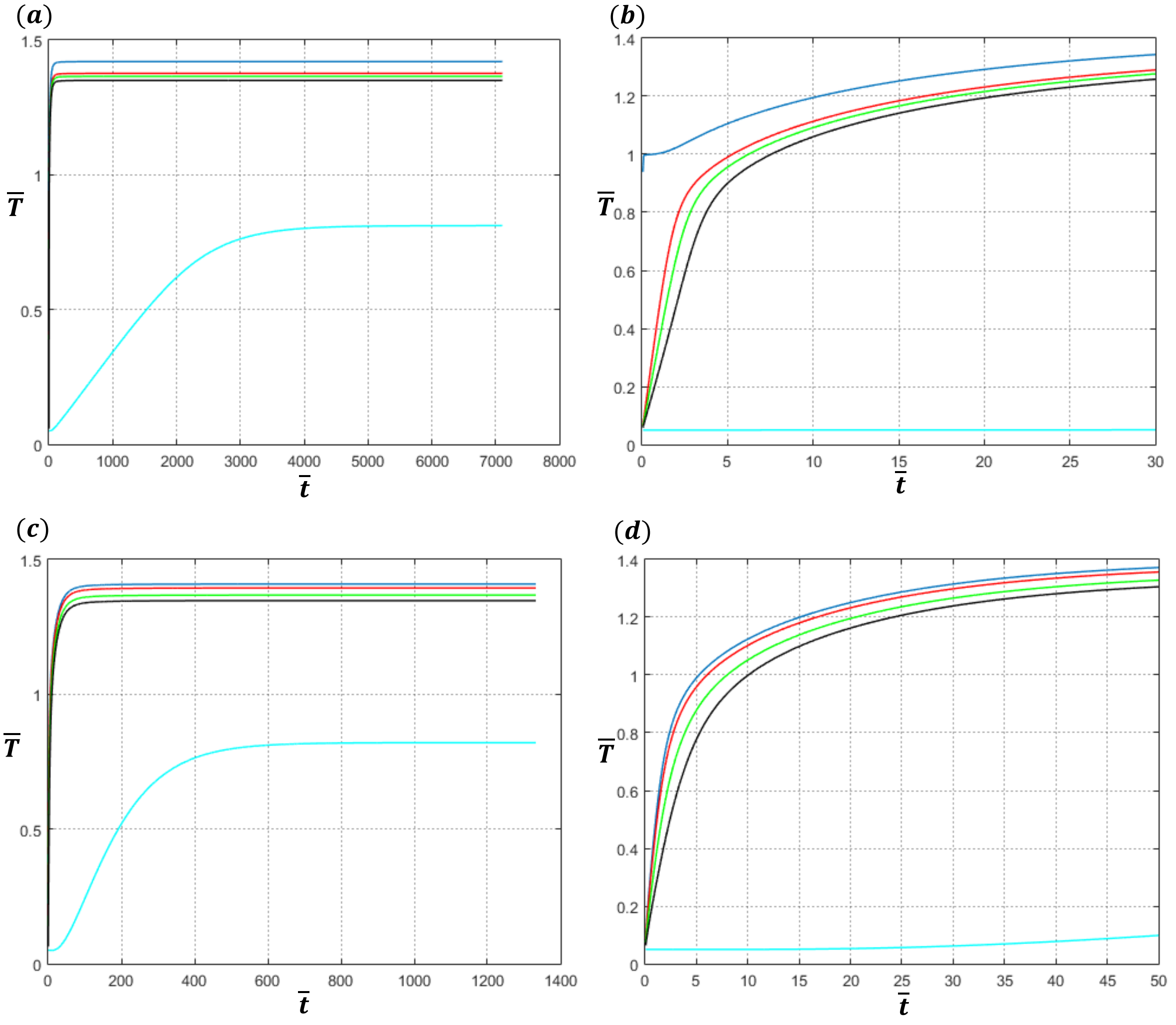

Figure 41: Evolution of the temperature with time for 0% of height (blue line), 25% of height (red line), 50% of height (green line), 75% of height (black line), 0% of height (cyan line). Figures **(a)** and **(c)** are represented in the characteristic scale of upper layers, and **(b)** and **(d)** in the scale of lower and intermediate layers.

3.4.2 Cyclical incident radiation

As was introduced is the first chapter, the main source of energy of the Earth is the incident solar radiation. Until now it has been assumed that this radiative flux is constant in time, although this is clearly a very unrealistic assumption. In fact, the radiative emission of the sun remains constant with time, but due to the terrestrial rotation the amount of it that arrives to a given point of the Earth's surface changes with time. For example, during the night the incident solar radiation is null, and reaches its highest value at midday.

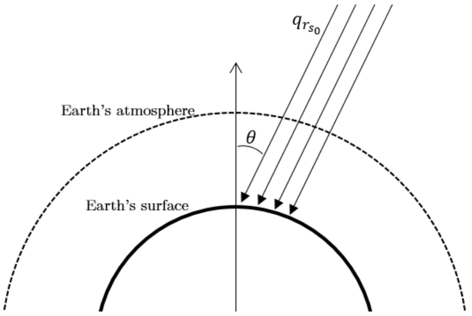

Figure 42: Schematic picture of the incident radiation to the Earth's surface.

In order to model properly the incident solar radiation, it is necessary to take into account several variables, such as the latitude of the point in which we are simulating the flux, the solar declination which depends on the season and, therefore, on the day of the year and, of course, the time of the day. Since taking into consideration all these factors lead to a cumbersome expression for the incident solar flux, it will be assume hear that it can be approximated by the following cyclic law which only consider the time of the day:

$$\begin{cases} q_{r_S} = q_{r_{S0}} \cos(\theta) & -\dfrac{\pi}{2} \leq \theta < \dfrac{\pi}{2} \\ 0 & \dfrac{\pi}{2} \leq \theta < \dfrac{3\pi}{2} \end{cases} \tag{3.19}$$

where $q_{r_{S0}}$ is the highest value of the solar flux, that is, the flux at midday, and θ is the angle rotated by the Earth (see figure 42). Due to its definition it is obvious that for the midday we have that $\theta = 0$. Thus, this angle can be written as $\theta = \Omega t$, where Ω is the angular velocity of the Earth, and t is the time elapsed from midday. Introducing the law for the time variation of the solar flux into the boundary conditions of the numerical model, the atmospheric profiles at each instant of time can be obtained.

Figure 43 shows the results of the simulation for the assumed solar law (3.19). The blue line represents the solution for a constant maximum flux (solar flux at midday), the red dashed line is the solution for a constant solar flux whose value is the mean value of (3.19) and the black lines represent the profiles with the highest and the lowest value of the temperature, respectively. In can be seen in the figure that the temperature profile oscillates around the mean-flux solution, that is, the dashed red line is between the two black lines. In addition, although during the cycle the maximum value of the solar flux, $q_{r_{S0}}$, is reached, the solution is very different

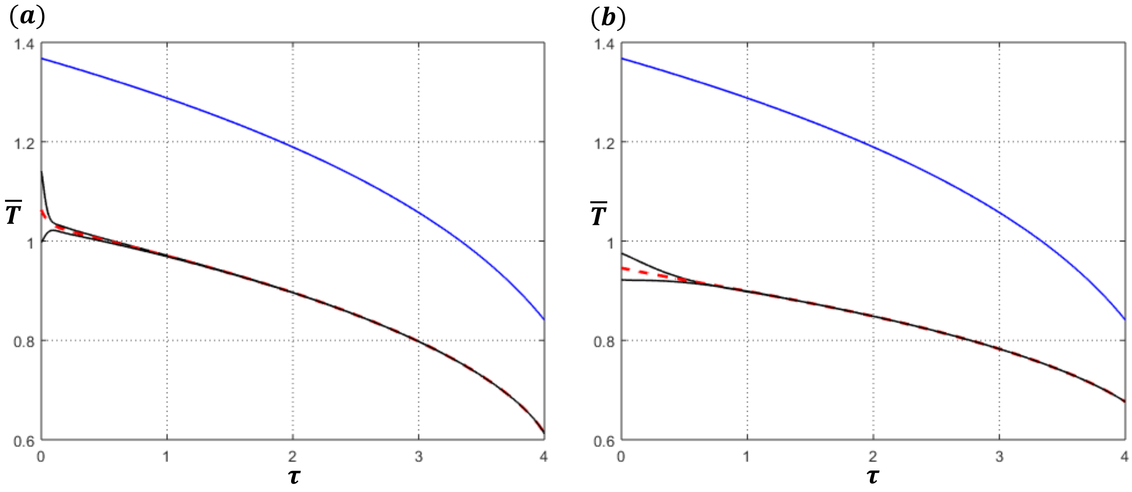

Figure 43:Temperature profiles for solar radiative flux. The **(a)** is for $N_{cr} = 0.01$ and **(b)** for $N_{cr} = 1$.

to that of a constant flux of that value (blue line). Thus, it may be concluded that a variable cyclic solar flux is almost equivalent to receive a continue flux whose value coincides with the average flux whose value coincides with the average of the cycle.

3.5. Radiative-convective-conductive atmosphere

The final step in the study of the atmosphere is the introduction of convection as another mechanism of energy transfer. Thus, in this section, the convective flux of energy will be described. In first place, the criterion for the onset convection will be investigated. After this, the convection term of the energy equation will be derived in terms of the magnitudes and parameters of the problem and introduced in the governing equations. Finally, the new equations will be solved using the numerical method developed in chapter 2 and results will be compared with those obtained in the absence of convection.

3.5.1 Onset of convection and convective flux

The phenomenon of convection appears as a consequence of an instability of the thermal structure of the atmosphere. The purposes of this subsection are to investigate what causes the onset of convection, to establish a mathematical criterion for its occurrence and, finally, to provide a plausible approximate expression to compute the energy flux carried by convection.

Consider a fluid particle initially located at a certain atmospheric layer, denoted by subscript 1, and in equilibrium with its surroundings, so that both have the same values of the state variables, $(T_{p1}, \rho_{p1}, p_{p1}) = (T_{s1}, \rho_{s1}, p_{s1})$. If the particle is then displaced upwards by some sudden perturbation up to a higher layer, denoted by subscript 2, it may be assumed that the particle evolves adiabatically and that its pressure equals that of the surroundings at every location of the particle. Thus, in the p-T diagram the evolution of the particle from the initial layer to the final layer, with pressure $p_{p2} = p_{s2}$, is along the red line shown in figure 44. Note that, as the evolution has been adiabatic, the densities of both particle and surroundings will differ at layer 2. Thus, if $\rho_{p2} < \rho_{s2}$, as happens if the temperature profile of the atmosphere (surroundings) is like the red one in figure 44 (where $T_{p2} > T_{s2}$) , the particle will continue raising due the buoyancy force, while if $\rho_{p2} > \rho_{s2}$, as happens if the temperature profile is like the blue one in figure 44 ($T_{p2} > T_{s2}$), the particle will return to its original position. In the first case, the atmosphere is unstable to convection, and is known as a

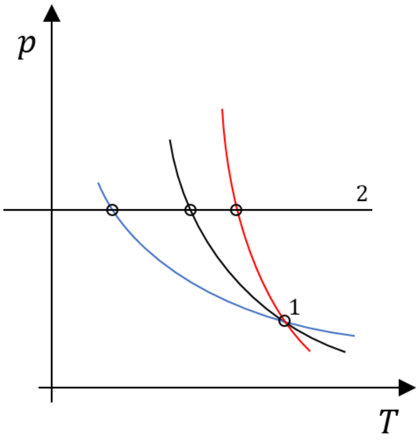

Figure 44: Schematic distribution of an adiabatic (black line), subadiabatic (red line) and superadiabatic (blue line) evolution.

superadiabatic atmosphere, while in the second one, it is stable to convection and is called a subadiabatic atmosphere.

This above physical reasoning leads to the well known Schwarzchild criterion, which permits to characterize mathematically the condition for the onset of convection. To derive it, it is first necessary to express the pressure and densities at layer 2 in terms of those at layer 1 by using Taylor series as

$$\rho_{p2} = \rho_{p1} + \left(\frac{\partial p}{\partial z}\right)\Delta z, \quad \rho_{s2} = \rho_{s1} + \left(\frac{\partial p}{\partial z}\right)\Delta z, \tag{3.20}$$

where derivatives are computed at layer 1 and higher order terms have been neglected. Since the stability condition requires

$$\rho_{p2} > \rho_{s2} \tag{3.21}$$

or, making use of the adiabatic evolution of the particle,

$$\rho_{s1}\left(\frac{p_{s2}}{p_{s1}}\right)^{\frac{1}{\gamma}} > \rho_{s2}\,, \tag{3.22}$$

insertion of (3.20) into (3.22) yields, after linearization,

$$-\frac{1}{\gamma}\frac{1}{p}\frac{\partial p}{\partial z} < -\frac{1}{\rho}\frac{\partial \rho}{\partial z} \tag{3.23}$$

where we have suppressed the subscripts in p and ρ . Considering an ideal gas, its equation of state can be differentiated to obtain

$$\frac{\partial p}{p} - \frac{\partial \rho}{\rho} = \frac{\partial T}{T}, \tag{3.24}$$

and combining equations (3.23) and (3.24) yields

$$-\left(1 - \frac{1}{\gamma}\right)\frac{T}{p}\frac{\partial p}{\partial z} > -\frac{\partial T}{\partial z}. \tag{3.25}$$

Taking into account that $R_g = C_p - C_v$ and $\gamma = C_p/C_v$, and using the hydrostatic equilibrium equation, dp/dz=- ρ g , one finally obtains from (3.25) the Schwarzchild criterion as

$$-\frac{dT}{dz} < \frac{g}{C_p}, \tag{3.26}$$

where $g/C_p = \Gamma$ is the adiabatic temperature gradient.

where $g/C_p = \Gamma$ is the adiabatic temperature gradient. It states that convection will take place if the local lapse rate is larger than the negative of the adiabatic temperature gradient or, in physical terms, if the temperature distribution decreases faster than the adiabatic one.

Once the criterion for the appearance of a convective energy flux has been determined, such a term can be introduced into equation (2.45) as

$$\rho c_p \frac{\partial T}{\partial t} = k\frac{\partial^2 T}{\partial z^2} + \frac{\partial q_c}{\partial z} - \beta(1-\omega)\big(4\sigma T^4(\tau) - G(\tau)\big), \tag{3.27}$$

where q_c is the heat flux due to convection.

where q_c is the convective energy flux. Since atmospheric convection is highly turbulent, the modelling of q_c in terms of the problem variables is not a trivial issue. In this work it will done be means of the so called *mixing length theory*, [Satoh (2014)] which assumes that the convective heat transport is due to eddies that have characteristic lengths much smaller that the characteristic length of the problem. The theory considers that the convective eddies are individual air parcels which may move up or down a distance l , the mixing length, before they mix with their turbulent surroundings and that the convective energy flux can be approximated by the heat transported per unit area and per unit time by those individual parcels. In this theory the convective heat flux can be expressed by

$$\begin{aligned} q_c &= -K_H\left(\frac{dT}{dz} + \Gamma\right) \quad && if \quad \frac{dT}{dz} + \Gamma \le 0, \\ q_c &= 0 && if \quad \frac{dT}{dz} + \Gamma > 0, \end{aligned} \tag{3.28}$$

where K_H is a turbulent thermal diffusivity which must be modelled in terms of the variables of the problem. According to [Ramanathan-Coakley (1978)], the thermal diffusivity takes the following expression

$$K_H = 1.32 z^2 \left(\frac{g\left|{}^{dT}/_{dz} + \Gamma\right|}{T}\right)^{\frac{1}{2}} \rho c_p. \tag{3.29}$$

In order to solve (3.27)-(3.29) it is convenient to nondimensionalize the variable z with a height related with the state variables of the problem, instead of the height of the atmosphere. In addition, as was done for the case of conductive-radiative equilibrium with variable absorption coefficient, the optical thickness will be taken as the independent spatial variable, which is related to z through equations (1.44), (1.46)-(1.47) and (3.17)-(3.18) as

$$d\tau = \tau_0(\alpha+1)\frac{g}{R_g T_e}\frac{\bar{p}^{\alpha+1}}{\bar{T}}dz. \tag{3.30}$$

According to (3.30), it is convenient express

$$z = H_e \bar{z} \tag{3.31}$$

where $R_g T_e/g = H_e$ is the scale height based on the effective temperature of the earth, and $\bar{z}$ is the dimensionless vertical coordinate. In terms of the dimensionless variables of the problem, and taking into account (3.28), the turbulent thermal diffusivity can now be expressed as,

$$K_H = 1.32\left(\frac{R_g T_e}{g}\right)^2 \rho_e c_p\, \overline{\rho}\beta_e^{\frac{1}{2}} g^{\frac{1}{2}} \overline{z}^2 \overline{\rho}\left|\frac{\overline{\rho}\,\overline{p}^{\alpha}}{\overline{T}}\frac{d\overline{T}}{d\tau} + \frac{\overline{\Gamma}}{\overline{T}}\right|^{\frac{1}{2}} \cdot \frac{1}{2}\left(1 - sg\left(\overline{\rho}\,\overline{p}^{\alpha}\frac{d\overline{T}}{d\tau} + \overline{\Gamma}\right)\right), \tag{3.32}$$

where sg denotes the *sign* function, and $\overline{\Gamma} = \Gamma/(T_e\beta_e)$, which can also be written in a more compact way as

$$K_H = 1.32\left(\frac{R_g T_e}{g}\right)^2 \rho_e c_p \beta_e^{\frac{1}{2}} g^{\frac{1}{2}} \widehat{K}_H, \tag{3.33}$$

where the expression of $\widehat{K}_H$ can be identified from (3.32). Introducing (3.28)-(3.33) in equation (3.27) and using the dimensionless quantities, there results:

$$\begin{aligned}\frac{\partial\overline{T}}{\partial\overline{t}} = \overline{p}^{\alpha}\Bigg[& N_{cr}\frac{\partial}{\partial\tau}\left(\overline{p}^{\alpha}\overline{\rho}\frac{\partial\overline{T}}{\partial\tau}\right) + \underbrace{\frac{1.32\left(\frac{R_g T_e}{g}\right)^2 \beta_e^{\frac{3}{2}}\rho_e c_p g^{\frac{1}{2}}}{4\sigma T_e^3}}_{N_{convr}}\frac{\partial}{\partial\tau}\left(\overline{K}_H\left(\overline{p}^{\alpha}\overline{\rho}\frac{\partial\overline{T}}{\partial\tau} + \overline{\Gamma}\right)\right) \\ & - \left(\overline{T}^4 - \frac{G}{4\sigma T_e^4}\right)\Bigg]\end{aligned} \tag{3.34}$$

which generalizes equation (2.47) by allowing for the presence of convection. The parameter N_{convr} is the convective equivalent to N_{cr}, since it measures the relative importance between the energy transport mechanisms of convection and radiation. In order to numerically solve (3.34), it is more appropriate write in the following form:

$$\begin{aligned}\frac{\partial\overline{T}}{\partial\overline{t}} = \overline{p}^{\alpha}\Bigg[& \left(\overline{p}^{\alpha}\overline{\rho}\frac{\partial^2\overline{T}}{\partial\tau^2} + \frac{\partial(\overline{p}^{\alpha}\overline{\rho})}{\partial\tau}\frac{\partial\overline{T}}{\partial\tau}\right)N_{cr} + N_{convr}\frac{\partial\overline{K}_H}{\partial\tau}\left(\overline{p}^{\alpha}\overline{\rho}\frac{\partial\overline{T}}{\partial\tau} + \overline{\Gamma}\right) \\ & + N_{convr}\left(\overline{K}_H\overline{p}^{\alpha}\overline{\rho}\frac{\partial^2\overline{T}}{\partial\tau^2} + \overline{K}_H\frac{\partial(\overline{p}^{\alpha}\overline{\rho})}{\partial\tau}\frac{\partial\overline{T}}{\partial\tau}\right) - \left(\overline{T}^4 - \frac{G}{4\sigma T_e^4}\right)\Bigg]\end{aligned} \tag{3.35}$$

3.5.2 Results for a convective-radiative-conductive atmosphere

In this final study of the thermal structure of the atmosphere, which, in general, involves the three mechanisms of heat transfer, equation (3.35) -instead of equation (3.15) - has been numerically solved using the method developed in chapter 2. The Matlab program for the numerical integration of (3.35) is included in the Appendix. The temperature profiles of the atmosphere will be computed for different conditions corresponding to different values of the governing parameters, N_{cr}, N_{convr} and τ_0 , and the results will be compared with those obtained for radiative-conductive atmospheres with the same N_{cr} and τ_0. Then, the vertical distributions of three types of heat fluxes will be represented. Lastly, the transient response to a heat impact of an initially cold atmosphere with terrestrial parameters will be numerically analized and the time evolutions of the potential and the thermal energy of the atmosphere computed

he temperature profiles for different atmospheres with and without convection are represented in figure 45

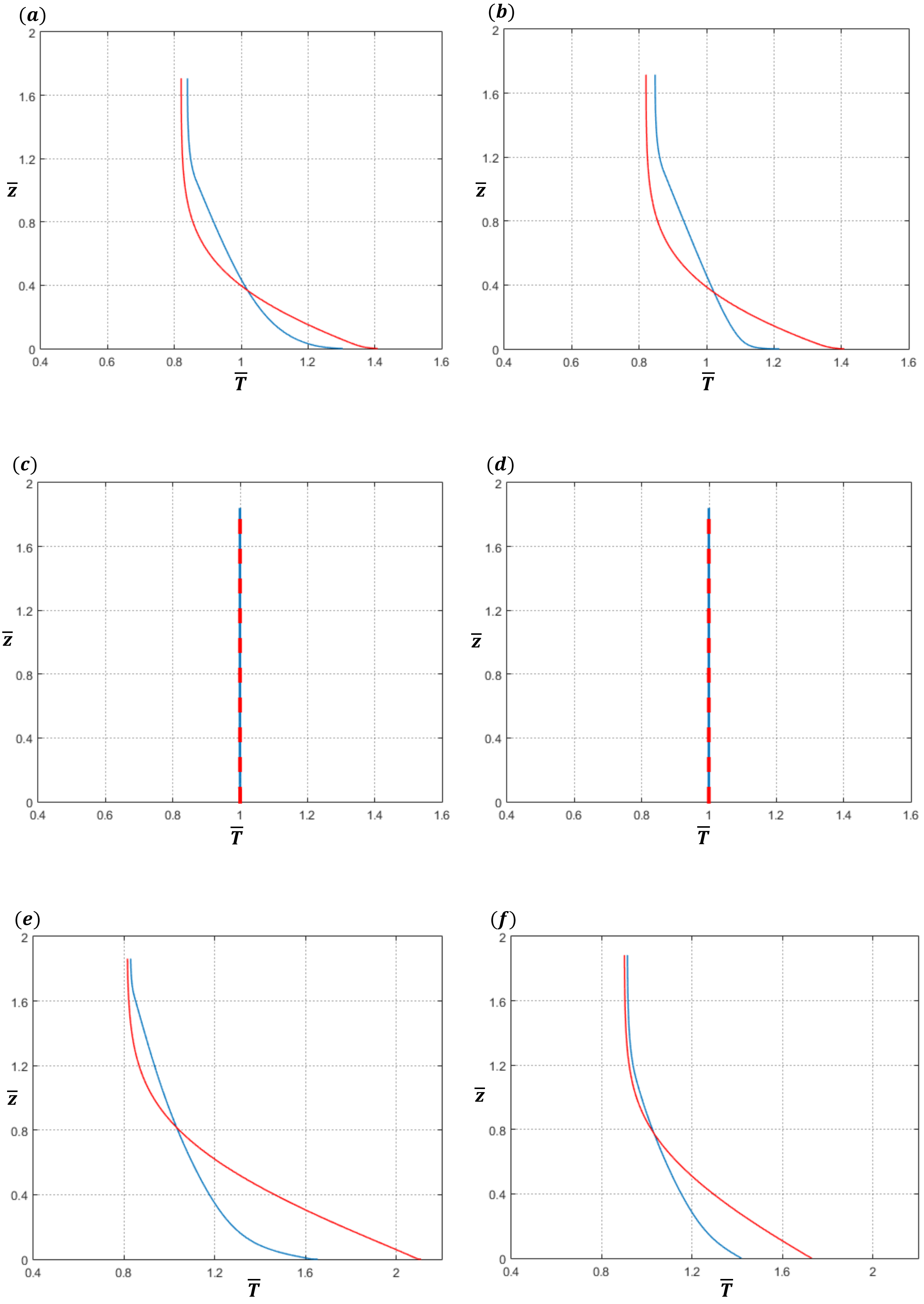
(a)
(b)
(c)
(d)
(e)
(f)
$\overline{z}$
$\overline{T}$
0
0.4
0.8
1.2
1.6
2
0.6
1
1.4

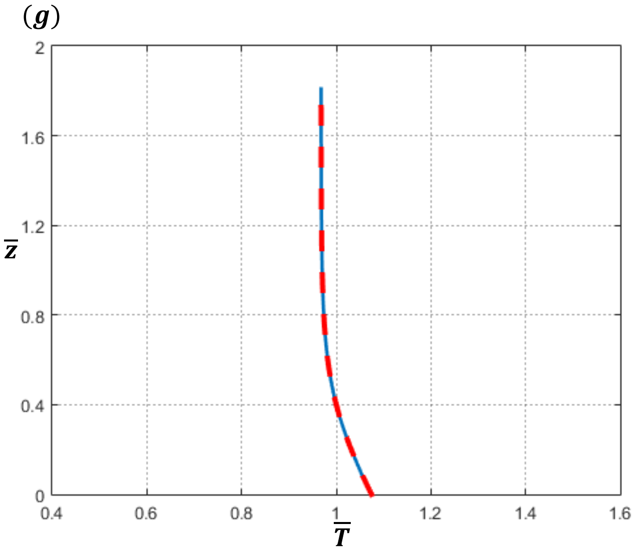

Figure 45: Temperature profiles considering convection (blue line) and neglecting convection (red line). The cases considered are **(a)** $N_{cr} = 0.1$, $N_{convr} = 10^3$ and $\tau_0 = 4$; **(b)** $N_{cr} = 0.1$, $N_{convr} = 10^4$ and $\tau_0 = 4$; **(c)** $N_{cr} = 0.1$, $N_{convr} = 10^4$ and $\tau_0 = 10^{-2}$; **(d)** $N_{cr} = 20$, $N_{convr} = 10^4$ and $\tau_0 = 10^{-2}$; **(e)** $N_{cr} = 0.1$, $N_{convr} = 10^4$ and $\tau_0 = 25$; **(f)** $N_{cr} = 20$, $N_{convr} = 10^4$ and $\tau_0 = 25$; **(g)** $N_{cr} = 20$, $N_{convr} = 10^4$ and $\tau_0 = 4$;

As can be observed the values of the parameters can change radically the solution of the problem. In particular, it can be seen in figures 45 (a) and (b) that convection makes the temperature profiles almost linear in the intermediate layers of the atmosphere. The region in which the temperature has a practically linear behaviour increases with N_{convr}, since convection becomes more important and its effects extend to layers closer to the surface.

In figures 45 (c) and (d) the optical depth has been decreased to a quite transparent value. The differences between these two pictures are unappreciable although in (c) the radiation is much more important in relation to conduction than in figure (d). This is a consequence of the tiny value of τ_0, which provokes that radiation is the main mechanism of energy transfer, and so conduction has very little effects in these kinds of atmosphere. Otherwise, if we compare the temperatures with and without convection, it can be seen convection increase their value because its efficient redistribution of energy.

Figures 45 (e) and 45 (f) correspond to an opaque value of τ_0. In this case, they are differences between the profiles. The relative importance of conduction has as a consequence an augmentation of the minimum temperature at the top of the atmosphere, and reduces the linear zone yielding a parabolic shape to the convective profile. Compared with the non-convective profile the main differences are the reduction of both the slope and the maximum temperature, due to the homogenising effect that convection has on the temperature distribution.

Finally, figure 45 (g) represents the same situation of figure 45 (b) but with conduction dominating over radiation. It can be seen that, as a consequence of the increase of N_{cr} , the linear zone has completely disappeared, and the minimum temperature has become higher while the maximum has become lower.

Is interesting to analyse how the different fluxes (radiative, conductive and convective) participate in the problem and affect to the final solution. To do this, each heat flux is represented separately in figure 46 for the same cases considered in figure 45.

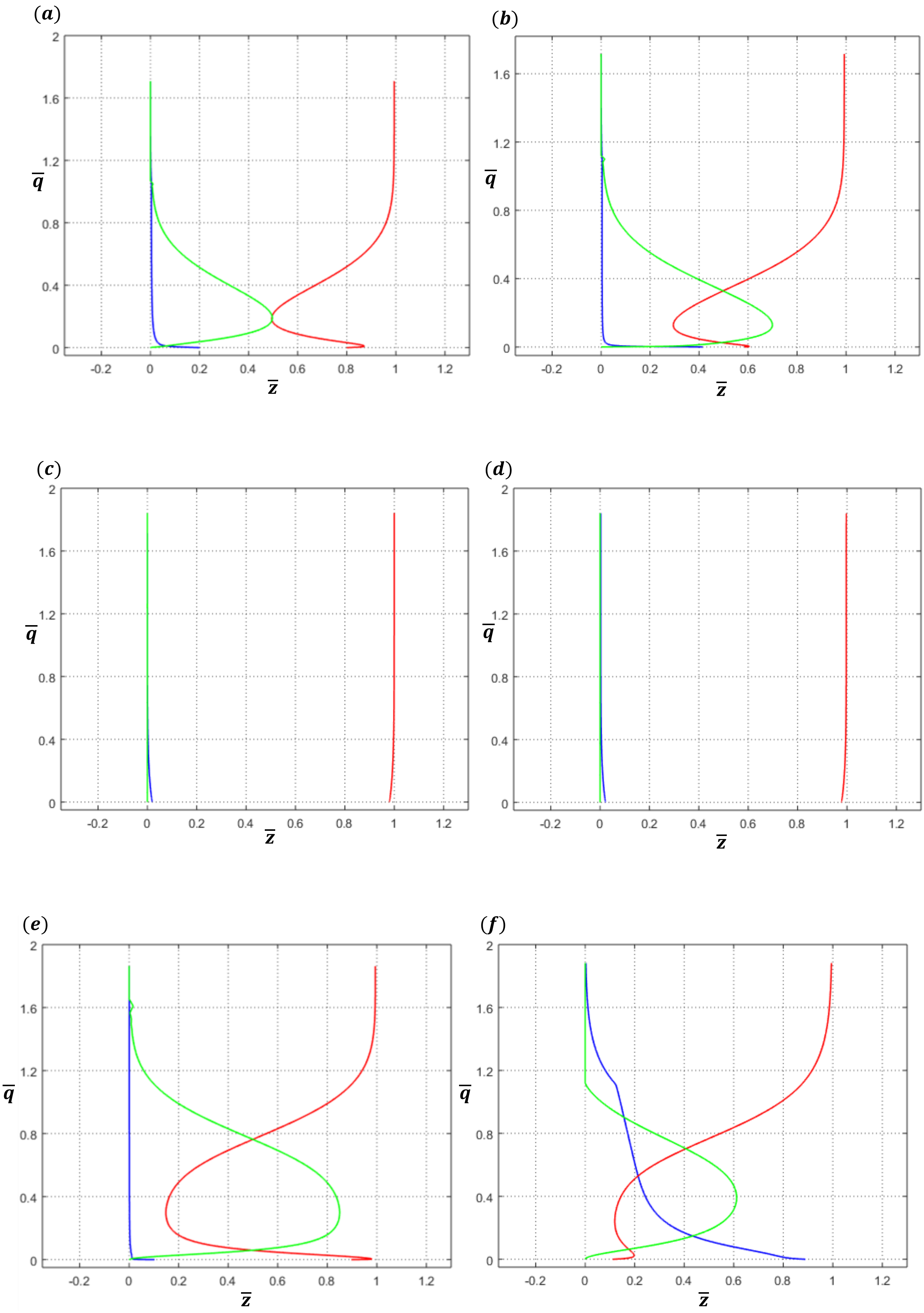
(a)
(b)
(c)
(d)
(e)
(f)
$\bar{q}$
$\bar{z}$
2
1.6
1.2
0.8
0.4
0
-0.2
0
0.2
0.4
0.6
0.8
1
1.2

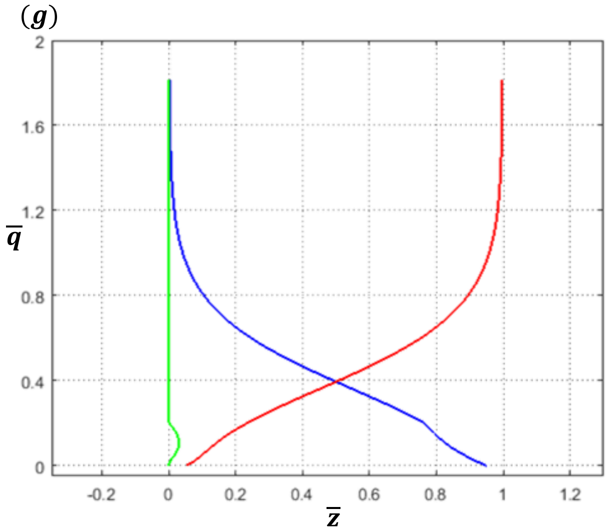

Figure 46: Heat fluxes of convection (green line), conduction (blue line) and radiation (red line). The cases considered are **(a)** $N_{cr} = 0.1$, $N_{convr} = 10^3$ and $\tau_0 = 4$; **(b)** $N_{cr} = 0.1$, $N_{convr} = 10^4$ and $\tau_0 = 4$; **(c)** $N_{cr} = 0.1$, $N_{convr} = 10^4$ and $\tau_0 = 10^{-2}$; **(d)** $N_{cr} = 20$, $N_{convr} = 10^4$ and $\tau_0 = 10^{-2}$; **(e)** $N_{cr} = 0.1$, $N_{convr} = 10^4$ and $\tau_0 = 25$; **(f)** $N_{cr} = 20$, $N_{convr} = 10^4$ and $\tau_0 = 25$; **(g)** $N_{cr} = 20$, $N_{convr} = 10^4$ and $\tau_0 = 4$;

In figures 46 (a) and 46 (b) can be observed that, since the main mechanisms of energy transfer are radiation and convection, there exists a kind of symmetry in the figure with respect to $\overline{z} = 0.5$ except in the lowest layers of the atmosphere where heat conduction acts in a small boundary layer near the surface. It can also be noticed that increasing N_{convr} augments the influence of convection in the lower and intermediates layers of the atmosphere and makes narrower the boundary layer where heat conduction is important in the boundary, but does not affect to the symmetry.

For the cases considered in figures 45(c) and 46(d), the high transparency of the atmosphere makes radiation the most important energy transfer process and predominates in the whole atmosphere for the two cases, even in the boundary layer, where the effect of conduction is very small compared to that of radiation.

Again, opaque atmospheres are represented in figures 46 (e) and 46 (f). In the first one the symmetry is maintained, but in the second one is not. The results of 46 (e) are quite similar to those of 46 (a), but as a consequence of the opacity, the convective flux reaches higher layer and layer values with respect to radiative heat flux, so that it predominates in a greater portion of the atmosphere. In figure 46 (f) it should be noticed that the radiative flux is more or less the same as in figure 46 (e) - except in the boundary layer because of the increase of N_{cr} and the consequent increment of the conductive flux -, but the convective flux has decreased in the intermediate layers and, consequently, the conductive one has increased. Thus, it may be concluded that when the atmosphere is opaque, conduction may acquire great importance in the bottom and the middle layers of the atmosphere.

Finally, in figure 46 (g) can be seen that convection has little effect in the atmosphere. Thus, it can be concluded that the diminution of the opacity leads to a decrease of the convective heat flux, and if it is not very low, an augmentation of the conductive heat flux as well as a reduction of the radiative one in the low atmosphere. Compared with the case of figure 46 (a), it can be noticed that conduction has gained importance, while both convection and radiation have lost it.

Lastly, the temperature profiles and the heat fluxes for the terrestrial atmosphere are represented for appropriate values of the three parameters in figure 47.

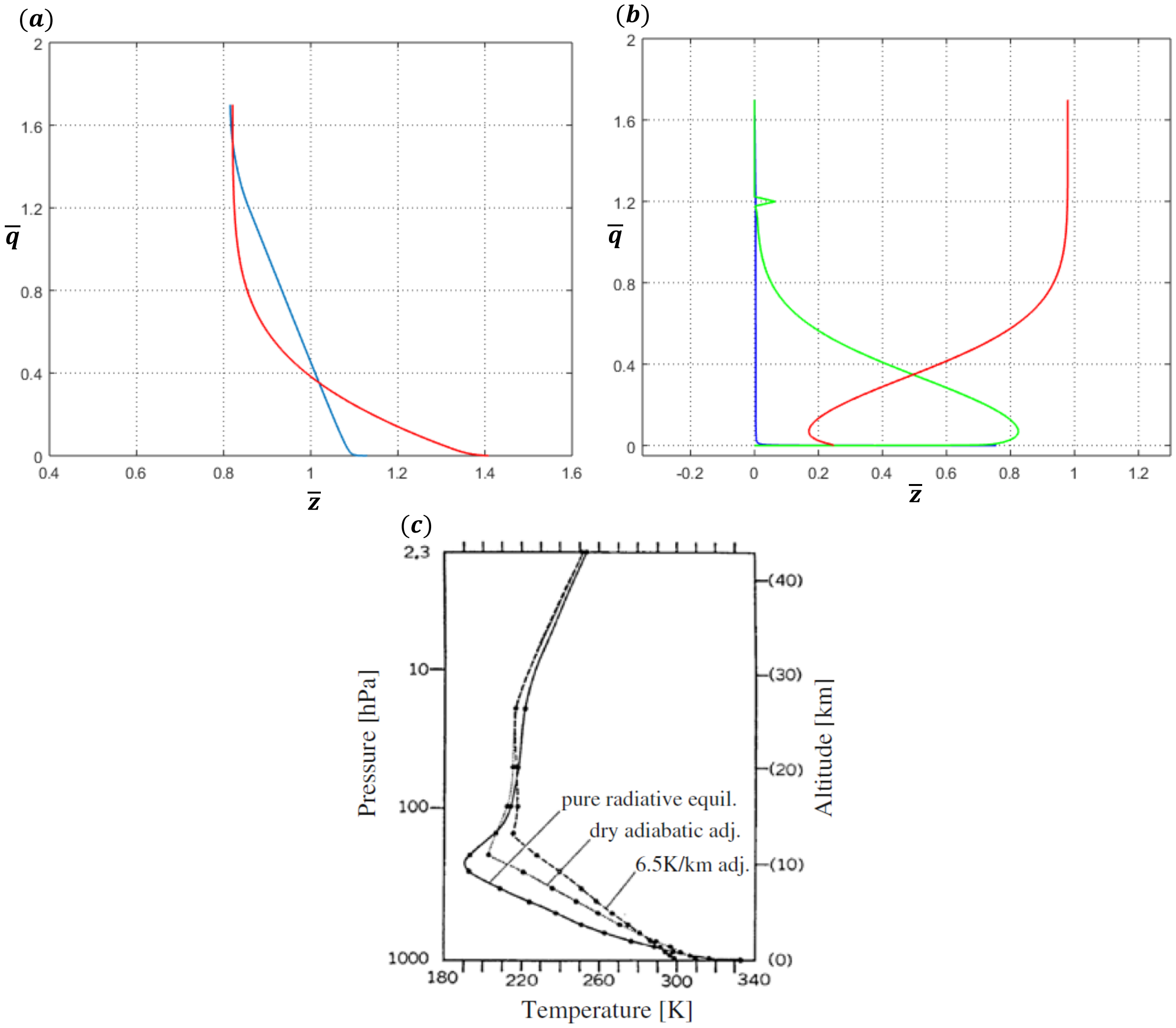

Figure 47: Temperature profile **(a)** and heat fluxes **(b)** for terrestrial atmosphere. The parameters used are $N_{cr} = 0.1$, $N_{convr} = 2 \cdot 10^5$ and $\tau_0 = 4$. Figure **(c)** taken [Manabe & Strickler 1964] shows the comparison of the temperature profile for pure radiative equilibrium, dry adiabatic adjustment, and the convective case with a lapse rate of $\Gamma = 6.5\, K/Km$.

It can be seen in figure 47 (a) that the effect described for figures 45 (a) and (b) has become accentuated, since almost all the temperature profile is linear except in the highest and lowest layers. In addition, the maximum temperature, that of the surface, has decreased. These effects appear as a consequence of the increased convection, which mixes upper and lower layers tending to homogenize the temperature.

Figure 47 (b) shows the effect predicted in figures 47 (a) and (b). In the very narrow boundary layer conduction has great importance, reaching values of $\overline{q} = 0.75$, and so have the convection, which has larger values of the flux. However, the increment of N_{convr} has not affected the heights up to which these fluxes have effect, since both conduction and convection have larger values only in the low atmosphere.

To conclude the section, the transient response of the atmosphere to a heat impact has been analysed and the time evolutions of the thermal and gravitational energy of the atmosphere computed. in order to see how the. The atmospheric energy is divided into two main contributions: thermal energy and gravitational energy

$(E = E_T + E_g)$. Their expressions are respectively given by

$$E_T = \int_0^H \rho c_v T \, dz, \qquad E_g = \int_0^H \rho g z \, dz. \tag{3.36}$$

Taking into account (1.44), equations (3.36) can be written in dimensionless variables as

$$\overline{E_T} = \frac{E_T}{\left(\frac{\rho_s c_v T_e}{\beta_e}\right)} = \int_0^{\tau_0} \frac{\overline{T}}{\overline{p}^{\alpha}} d\tau, \qquad \overline{E_g} = \frac{E_g}{\left(\frac{\rho_s R_g T_e}{\beta_e}\right)} = \int_0^{\tau_0} \frac{\overline{z}}{\overline{p}^{\alpha}} d\tau. \tag{3.37}$$

These two magnitudes are represented in figure 48, as well as the total energy.

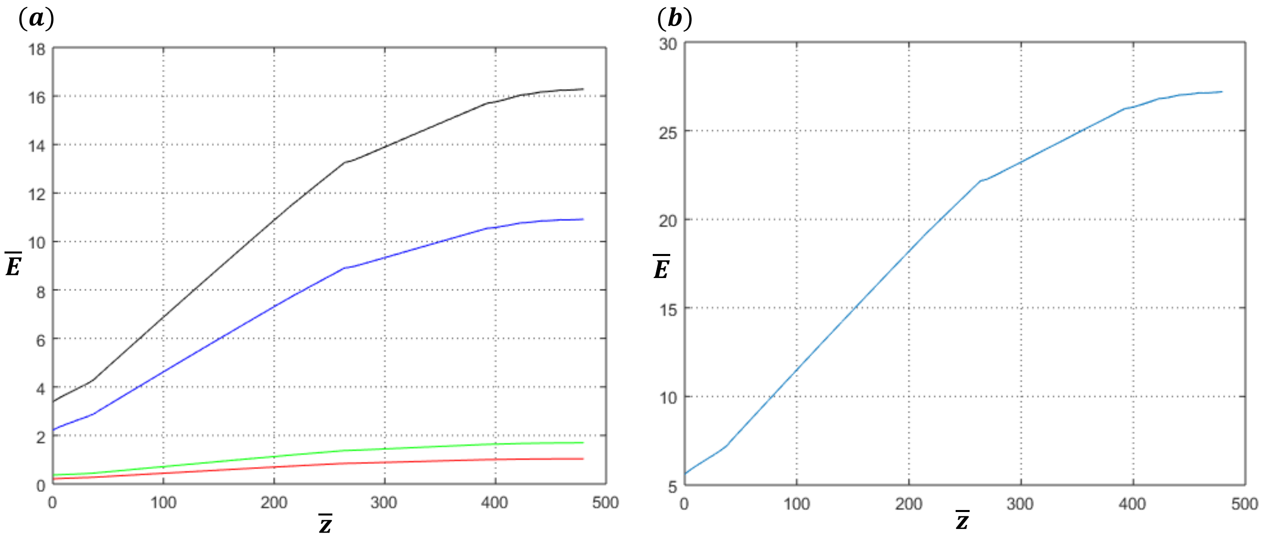

Figure 48: Evolution of atmospheric potential energies. Figure (a) represents the thermal energy (black line) and the gravitational energy (blue line), as well as the nondimensionalized height with respect to the effective temperature (red line) and the mean temperature of the atmosphere (green line). Figure (b) shows the total energy evolution.

It can be observed how both energies grow with time, as the height and the mean temperature of the atmosphere grow too. However, it can be noticed that their time evolutions slowly separate as the mean temperature grows faster than the height of the atmosphere.

4 CONCLUSION AND FUTURE LINES

Along this document we have intended to achieve two main objectives. The first one was to give a concise and a practical approach to the physics of radiation - especially that related with atmospheric problems -, while the second one was to develop a numerical method which allows to solve unsteady, one-dimensional radiation problems in a simple way and not only for limit cases such as radiative equilibrium, or the approximations of optically thin or optically thick medium, but for a great variety of situations, including the transient state.

In the first chapter, the general principles of the physics of radiation were presented as a theoretical base for the derivation of the governing equations. In addition, a simplified model of the atmosphere was described, as well as some of the phenomena which happen in it.

After this, in chapter 2 the governing equations were derived, and written in an appropriate form to solve them numerically. A numerical method was then developed based on these equations, which consists on a combination of a finite difference discretization of the radiation equations and the use of a Newton-Rapson's method for solving the energy equation. The method was verified by comparing the results obtained with those of the literature, giving very similar solutions. The unsteady state was tested by proving that, as the theory predicts, the method yields a unique steady state solution for given conditions independently of the initial state.

Finally, in chapter 3 the implementation of the atmospheric model in the numerical method was checked and validated with results of the literature. Next, the method was used to study the evolution and steady state of different kinds of atmospheres by comparing the time taken to reach the final state. Lastly, to have a complete model of the energy transfer, convection was included and, again, results for different atmospheres were calculated.

We may conclude that the numerical method developed in this project is both compact and functional, allowing to obtain a first approximation of the atmospheric thermal structure, and can be used as starting point for more complex methods and to calculate variables of interest such as the heat fluxes, which help to understand how the atmosphere evolves and behaves under certain conditions.

As future objectives, it would be interesting to relax some of the assumptions made. For example, for the absorption coefficient, instead of considering the water vapour as the only constituent, other gases, such as ozone and CO_2 could be taken into account. In addition, the absorption bands of figure 15 may be considered in order to have a more complete model of the thermal structure of the atmosphere.

With the same purpose, the vaporization and the latent heat of the vaporization could be included in the energy budget of the atmosphere considered here, as well as how the heating of the atmosphere gets fed back from this vaporization.

Otherwise, in the atmospheric model presented here, only the troposphere has been studied for simplicity. Other layers of the atmosphere may be also taken into account, such as the stratosphere and the mesosphere, including the different processes that take place in those areas. This will improve and complete the vertical thermal structure, because, in addition to increment the height considered, some of the boundary conditions which were imposed in order to simulate the existence of these zones can be deleted if the zone itself is considered.

Finally, about convection, the movement induced by a nonuniform heating can be taken into account to study the dynamic behave of the convective atmosphere. Additionally, convective models different from the mixing length can be used. These models could be tested and compared with experimental or theoretical data of the literature, and determinate which model fulfil best the structure of the terrestrial atmosphere.

APPENDIX: MATLAB CODE

```
function RadSparrowConvSimple
clear all; clc; close all;
%Governing parameters of the problem
tau0=4; emiss1=1; emiss2=1;
alpha=4; Ncr=0.1; omega=0;
Nconvr=200000;
Gamma=(1-1/1.4)/tau0/(alpha+1)*6.5/9.8; %lapse rate

%Calulation of tau as spatial variable
Ntau=500;
taumin=0; taumax=0.9999*tau0;
pmin=(1-0.9999)^(1/(alpha+1));
tauv(1:Ntau)=(taumax+taumin)/2-(taumax-taumin)/2*cos(((1:Ntau)-1)*pi/(Ntau-1));
htau(1:Ntau-1)=tauv(2:Ntau)-tauv(1:Ntau-1); htau(Ntau)=htau(Ntau-1);
traptau(2:Ntau-1)=(tauv(3:Ntau)-tauv(1:Ntau-2))/2; traptau(1)=(tauv(2)-tauv(1))/2;
traptau(Ntau)=(tauv(Ntau)-tauv(Ntau-1))/2;

%Matrix for the first and second derivate with respect to tau
[D_tau, D_tau2]=FinDiff(tauv,Ntau);

%Calculation of the exponential functions
tauH=tau0;
NX=3*10^3; Nmu=10^5;
Xv=linspace(0,tauH,NX);
mu=linspace(10^-10,1,Nmu);
E2v(1)=1;
trapmu(2:Nmu-1)=(mu(3:Nmu)-mu(1:Nmu-2))/2; trapmu(1)=(mu(2)-mu(1))/2; trapmu(Nmu)=(mu(Nmu)-
mu(Nmu-1))/2;
muinv=1./mu;
for iX=2:NX,
    X=Xv(iX);
     E2v(iX)=trapmu*exp(-X.*muinv)';
end
E3_H=trapmu*(mu.*exp(-tauH.*muinv))'; % Value of E3(tauH), needed for radiosities

% Matrix A:
Mtau=tauv'*ones(1,Ntau)-ones(Ntau,1)*tauv; % Matrix of dicretization of tau_i-tau_j de tau-tau'
Mabtau=abs(Mtau); % Matrix of dicretization of |tau_i-tau_j| de |tau-tau'|
ME2=interp1(Xv,E2v,Mabtau); % Matrix of dicretization of E2(|tau-tau'|)
Mstaup=sign(Mtau+10^-10); Mstaum=sign(Mtau-10^-10);
g(1:Ntau,1:Ntau-1)=Mstaup(:,2:Ntau).*ME2(:,2:Ntau)-Mstaum(:,1:Ntau-1).*ME2(:,1:Ntau-1);
A(1:Ntau,1)=0.5*g(:,1); A(:,2:Ntau-1)=0.5*(g(:,1:Ntau-2)+g(:,2:Ntau-1)); A(:,Ntau)=0.5*g(:,Ntau-
1);

% Vectors a and b:
vE2(1:Ntau)=interp1(Xv,E2v,tauv); vE2(1)=1;
vE2H(1:Ntau)=interp1(Xv,E2v,abs(tau0-tauv)); vE2H(Ntau)=1;
a(1:Ntau)=0.5*[vE2(1:Ntau-1).*(tauv(2:Ntau)-tauv(1:Ntau-1)) 0]+0.5*[0
vE2(2:Ntau).*(tauv(2:Ntau)-tauv(1:Ntau-1))];
b(1:Ntau)=0.5*[vE2H(1:Ntau-1).*(tauv(2:Ntau)-tauv(1:Ntau-1)) 0]+0.5*[0
vE2H(2:Ntau).*(tauv(2:Ntau)-tauv(1:Ntau-1))];
```

```
% Matrices LGJ and RIb:
LGJ(1:Ntau,1:Ntau)=eye(Ntau)-omega/2*A; LGJ(1:Ntau,Ntau+1)=-2*vE2(1:Ntau)'; LGJ(1:Ntau,Ntau+2)=-
2*vE2H(1:Ntau)';
LGJ(Ntau+1,1:Ntau)=-omega*(1-emiss1)/2*a; LGJ(Ntau+1,Ntau+1)=1; LGJ(Ntau+1,Ntau+2)=-2*(1-
emiss1)*E3_H;
LGJ(Ntau+2,1:Ntau)=0; LGJ(Ntau+2,Ntau+1)=0; LGJ(Ntau+2,Ntau+2)=1; %J2=0
RIb(1:Ntau,1:Ntau)=2*pi*(1-omega)*A;
RIb(Ntau+1,1:Ntau)=pi*emiss1*[1 zeros(1,Ntau-1)]+2*pi*(1-emiss1)*(1-omega)*a;
RIb(Ntau+2,1:Ntau)=0; %J2=0%
LGJiRIb=LGJ\RIb; MG=LGJiRIb(1:Ntau,1:Ntau); aJ1=LGJiRIb(Ntau+1,1:Ntau);
aJ2=LGJiRIb(Ntau+2,1:Ntau);

% Advance in time:
dt=0.001;

% Relation between the pressure and the optical thicness (independent of t)
gamma=alpha/(alpha+1);
pn(1:Ntau,1)=(1-tauv'/tau0).^(1/(alpha+1));
pnalpha(1:Ntau,1)=(1-tauv'/tau0).^gamma;
pnalphamat=spdiags(pnalpha,0,Ntau,Ntau);

%Matrix C of the Newton-Raphson method
C=dt*(1-omega)*spdiags(pnalpha,0,Ntau,Ntau)*(eye(Ntau,Ntau)-MG/4/pi);
C(1,:)=(aJ1-2*pi*(1-omega)*a-omega/2*a*MG)/pi;
C(Ntau,:)=0;
ftau2=log(1-tauv'/tau0).^2;
dermax=0; %Set the derivate of the temperature with time to 0

%Solving loop
for it=1:100000,
    t=dt*it; %Dimensionless time
    tv(it)=t; %Dimensionless time vector
    if it==1,
        Tnm1(1:Ntau,1)=0.2; %Initial value of temperature profile
        rhonm1=pn./Tnm1; %Initial value of densit profile
    end

    % Calculation of the dimensionless absorption coefficient
    rhopna=rhonm1.*pnalpha; drhopna=D_tau*rhopna;

    %Calculation of the height nondimensinalized with effective temperature
    zad(1,1)=0;
    for k=2:Ntau,
    zad(k,1)=zad(k-1,1)-0.5/(alpha+1)*(Tnm1(k,1)+Tnm1(k-1,1))*(log(1-tauv(k)/tau0)-log(1-tauv(k-
1)/tau0));
    end
    zad2=zad.*zad;

    % Calculation o convection parameters
    dTpGam=rhopna.*(D_tau*Tnm1)+Gamma;
    KHaux=(1-exp(-zad.^2./(Tnm1.^2*0.3))).*pn.*Tnm1.^.5.*abs(dTpGam).^(1/2);
    KH=0.5*(1-sign(dTpGam)).*KHaux;
    dKH=0.5*(1-sign(dTpGam)).*(D_tau*KHaux);

    % B matrix of the Newton-Raphson method
    BT=eye(Ntau)-dt*pnalphamat*(spdiags((Ncr+Nconvr*KH).*rhopna,0,Ntau,Ntau)*D_tau2+...
        spdiags((Ncr+Nconvr*KH).*drhopna,0,Ntau,Ntau)*D_tau);
```

```
    BT(1,:)=-4*Ncr*rhonm1(1,1)*pnalpha(1,1)*D_tau(1,:);
    BT(Ntau,:)=D_tau(Ntau,:);

    % b vector of the Newton-Raphson method
    bnm1=[1; ...
        Tnm1(2:Ntau-1,1)+dt*Nconvr*pnalpha(2:Ntau-1,1).*dKH(2:Ntau-1,1).*dTpGam(2:Ntau-1,1);...
        -3/16/(1/2*(3/2*(tau0-taumax)+1)).^(3/4)];

    % Newton-Raphson iteration
    Tk=Tnm1;
    for k=1:100,
        Tk3=Tk.*Tk.*Tk; Tk4=Tk3.*Tk;
        Fk=BT*Tk+C*Tk4-bnm1;
        Hk=BT+4*C*spdiags(Tk3,0,Ntau,Ntau);
        dTk=-Hk\Fk;
        if max(abs(dTk)) <= 10^-12,
            break
        else
            Tk=Tk+dTk;
        end
    end
    Tn=Tk;
    Tn4=Tk4;

    %Condition to considerd that the Newton-Raphson is good enogh
    dermax=max(abs((Tn-Tnm1)/dt));
    if dermax <= 10^-7,
        break;
    end

    %Actualization of the state variables
    Tnm1=Tn;
    rhon=pn./Tn;
    rhonm1=rhon;

    % Dimensionless magnitudes of interest (referred to sigma*Teff^4)
    J1=aJ1*Tn4/pi; %Lower radiosity
    J2=aJ2*Tn4/pi; %Upper radiosity
    G=MG*Tn4/pi; %Radiant intensity
    S=(1-omega)*Tn4/pi+omega/4/pi*G; %Source function
    qR_H=2*J1*E3_H-J2+2*pi*b*S; %Upper downward radiative flux
    qR_0=aJ1*Tn4/pi-2*pi*(1-omega)*a*Tn4/pi-omega/2*a*MG*Tn4/pi; %Lower upward radiative flux
    qcond_0=-4*Ncr*rhonm1(1,1)*pnalpha(1,1)*D_tau(1,:)*Tn; %Upper downward conductive flux
    qcond_H=-4*Ncr*rhon(Ntau,1).*pnalpha(Ntau,1)*D_tau(Ntau,:)*Tn; %Lower upward conductive flux
    qcond=-4*Ncr*rhonm1.*pnalpha.*(D_tau*Tn); %Conductive flux
    qconv(1:Ntau,1)=-4*Nconvr*dTpGam.*KH; %Convective flux
    dqrad_tau=(1-omega)*(4*Tn4-G); %Radiative flux
    qrad(1,1)=qR_0;
    for k=2:Ntau;
        qrad(k,1)=qrad(k-1,1)+0.5*(dqrad_tau(k,1)+dqrad_tau(k-1,1))*(tauv(k)-tauv(k-1));
    end
    Tnrad(1:Ntau,1)=(1/2*(3/2*pn(1:Ntau,1).^(alpha+1)*tau0+1)).^(1/4); %Radiative equilibrium
analitycal distribution of the temperature
    Ts_satoh=(1/2*(3/2*(tau0-0)+2)).^(1/4); %Surface temperature for radiative equilibrium
analitycal solution
end
```

```
%Finite differences function to calculate the first and second derivate
%with respect to tau
function [D1x, D2x]=FinDiff(x,N)

D1x=sparse(N,N);
D2x=sparse(N,N);

for i=1:N,
    xc=x(i);
    if i==1,
        kv(1)=i; kv(2:7)=2:7;
    end
    if i==2;
        kv(1)=1; kv(2)=i; kv(3:7)=3:7;
    end
    if i==3;
        kv(1:2)=1:2; kv(3)=i; kv(4:7)=4:7;
    end
    if i >= 4 && i <= N-3
        kv(1:3)=(i-3):(i-1); kv(4)=i; kv(5:7)=(i+1):(i+3);
    end
    if i==N-2,
        kv(1:4)=(N-6):(N-3); kv(5)=i; kv(6:7)=(N-1):N;
    end
    if i==N-1,
        kv(1:5)=(N-6):(N-2); kv(6)=i; kv(7)=N;
    end
    if i==N;
        kv(1:6)=(N-6):(N-1); kv(7)=i;
    end
        xk(1:7)=x(kv(1:7));
        [d1x]=deriv1(xk,xc);
        [d2x]=deriv2(xk,xc);
        D1x(i,kv(1:7))=d1x;
        D2x(i,kv(1:7))=d2x;
end

function[d1x]=deriv1(xk,xc)
Nst=7;
for j=1:Nst,
    for jj=1:Nst
        if abs(jj-j)> 0,
        a(jj)=(xc-xk(jj))/(xk(j)-xk(jj));
        ap(jj)=1/(xk(j)-xk(jj));
        else
            a(jj)=0;
            ap(jj)=0;
        end
    end
    d1x(j)=0;
    for k=1:Nst,
        prodk=ap(k);
        for ip=1:Nst,
            if abs((ip-k)*(ip-j))> 0,
                prodk=prodk*a(ip);
            end
        end
```

```
        d1x(j)=d1x(j)+prodk;
    end
end

function[d2x]=deriv2(xk,xc)
Nst=7;
for j=1:Nst,
    for jj=1:Nst
        if abs(jj-j)> 0,
        a(jj)=(xc-xk(jj))/(xk(j)-xk(jj));
        ap(jj)=1/(xk(j)-xk(jj));
        else
            a(jj)=0;
            ap(jj)=0;
        end
    end
    d2x(j)=0;
    for k=1:Nst,
        for ele=1:Nst,
            if abs(ele-k)>0,
            prodk=ap(k)*ap(ele);
            for ip=1:Nst,
            if abs((ip-j)*(ip-k)*(ip-ele))> 0,
                prodk=prodk*a(ip);
            end
            end
            d2x(j)=d2x(j)+prodk;
            end
         end
    end
end
```

REFERENCES

Aston, J.A.G., Chan, W-L., Moore, D.R. and Walton, I.C., 2000, “Radiative Transfer in a Static Model Atmosphere”, Geophysical & Astrophysical Fluid Dynamics.

Cengel, Y.A., 2002, “Heat Transfer: A Practical Approach”, 2nd Edition, McGraw-Hill, N.Y.

Coakley, J., Yang, Ping 2014, “Atmospheric Radiation: A Primer with Illustrative Solutions”, 1st Edition, Wiley-VCH.

Howell, John R., Siegel, Robert, Mengüç, M. Pinar 2010, “Thermal Radiation Heat Transfer”, 5th Edition, CRC Press

Lillesand, T.M., Kiefer, R.W and Chipman, J.W, "Remote sensing and image interpretation", Wiley, N.Y. 2008

Manabe, S., Strickler, Robert F., 1963, “Thermal Equilibrium of the Atmosphere with a Convective Adjustment”, American Meteorological Society.

Matsuda, Y., Matsuno T., 1977, “Radiative-Convective Equilibrium of the Venusian Atmosphere”, Journal of the Meteorological Society of Japan

Ramanathan, V., Coakley, J.A., JR., 1978, “Climate Modelling Through Radiative-Convective Models”, Reviews of Geophysics.

Satoh, M., 2004, “Atmospheric Circulation Dynamics and General Circulation Models, 2nd Edition, Springer, Published in association with Praxis Publishing.

Sparrow, E. M. and Cess, R.D., "Radiation heat transfer", Hemisphere Publishing Corporation, N.Y. 1978.

Vincenti, Walter G., Kruger Jr., Charles H., 1965, “Introduction to Physical Gas Dynamics”, Krieger Publishing Company.

Visconti, G. 2001, “Fundamentals of Physics and Chemistry of the Atmospheres”, 2nd Edition, Springer.